NON-DESTRUCTIVE SOIL TESTING USING X-RAY COMPUTED TOMOGRAPHY

by

Brent Daniel Nielsen

A thesis submitted in partial fulfillment
of the requirements for the degree

of

Master in Science

in

Civil Engineering

Montana State University
Bozeman, Montana

November 2004

APPROVAL

of a thesis submitted by

Brent Daniel Nielsen

This thesis has been read by each member of the thesis committee and has been found to be satisfactory regarding content, English usage, format, citations, bibliographic style, and consistency, and is ready for submission to the College of Graduate Studies

Robert L. Mokwa

Approved for the Department of Civil Engineering

Brett W. Gunnink

Approved for the College of Graduate Studies

Bruce R. McLeod

STATEMENT OF PERMISSION TO USE

In presenting this thesis in partial fulfillment of the requirements for a master's degree at Montana State University, I agree that the Library shall make it available to borrowers under rules of the Library.

If I have indicated my intention to copyright this thesis by including a copyright notice page, copying is allowable only for scholarly purposes, consistent with "fair use" as prescribed in the U.S. Copyright Law. Requests for permission for extended quotation from or reproduction of this thesis (paper) in whole or in parts may be granted only by the copyright holder.

Brent Daniel Nielsen

Table of Contents

Table of Contents, Continued

List of Figures

Figure Page

List of Figures, Continued

List of Figures, Continued

List of Tables

Abstract

The mechanical behavior of soils is highly dependent on the particle microstructure. Traditional geotechnical engineering soil tests generally do not measure soil properties on a micro-scale; instead, macro scale properties are commonly used as estimates of microstructure properties in determining soil engineering behavior. Additionally, traditional geotechnical engineering soil tests are destructive in nature, and many test methods destroy the same soil properties they intend to measure. The goal of this research was to develop non-destructive soil test methods using x-ray computer-aided tomography (CT) scanning techniques to determine soil index properties. The CT scanning process provides a promising method for examining soil microstructure in a non-destructive manner.

This research had two main objectives. The first was to configure the Montana State University Civil Engineering Department's computer-aided tomography scanner to perform CT scans on soil samples. The second objective was to use the CT scanner to develop non-destructive test procedures to determine geotechnical index properties of soils. Test methods were developed in this study to determine porosity, grain size distribution, and pore size distribution.

The results from the first objective showed that the MSU CT scanning equipment is capable of producing high quality CT scans of soil materials. Resolution limitations of the scanner define the smallest soil grain size that is detectable in a CT scan, but the scan resolution may be improved by using smaller sample sizes for small particle soils.

The results of the second portion of the study show that the non-destructive CT scanning test methods compare favorably with traditional geotechnical laboratory mechanical test methods. CT-measured porosity values and grain size distributions compared well with mechanical testing results, which were used to validate the new test methods. In addition, the CT-measured pore size distributions were in good agreement with an accepted pore size mathematical model. Since traditional pore size distribution tests are time-consuming, labor-intensive, and destructive in nature, the non-destructive x-ray CT scanning test methods developed in this study show strong promise as a means for measuring an elusive soil property that cannot be accurately measured using traditional geotechnical testing procedures.

CHAPTER 1

INTRODUCTION

The research described in this thesis is part of a larger project funded by the Western Transportation Institute to investigate the frost heave phenomenon in soils. This study involved the use of x-ray computed tomography (CT) scanning techniques to measure the microstructure of soil, including porosity, particle properties, and void space properties.

This research had two main objectives. The first was to configure the Montana State University Civil Engineering Department's computer-aided tomography scanner to perform CT scans on soil samples. The second objective was to use the CT scanner to develop non-destructive test procedures to determine geotechnical index properties of soils. Test methods were developed in this study to determine porosity, grain size distribution, and pore size distribution.

The mechanical behavior of granular soils is highly dependent upon the soil microstructure. Soil microstructure includes the shape, distribution, and arrangement of particles and void space within a soil. Historically, micro properties of soil have been difficult to measure, so geotechnical engineers commonly use soil macroscopic properties to estimate soil behavior. In the past, the observation and measurement of soil microstructure has been a time consuming and destructive process. Traditional methods to measure soil microstructure involve impregnating soil specimens with a hardening agent such as resin or Wood's metal that replaces air and water in the soil's void space. Once the specimen is cooled and hardened, it is cut into thin coupons and polished. These thin slices are then

measured with image analysis techniques (Jang 1999). This procedure is extremely time consuming and may alter the microstructure of the soil – the actual properties being measured.

X-Ray CT scanning has been shown to be useful for measuring soil microstructure (Phillips 1997, Alshibli 2000). An x-ray image is a picture of the x-ray linear attenuation coefficient of an object, which is related to the density of an object (Phillips 1997). A material with high density will attenuate more x-rays than will a low-density material; therefore, two materials of different densities will appear differently in an x-ray image. The digital image created during the x-ray CT process provides an internal cross-section, in which different materials can be distinguished. The field of CT scanning in geotechnical engineering is in its infancy, but it is showing growth as the technology continues to develop and its use is encouraged. Over the last decade, researchers have experimented with the use of x-ray CT scanning technologies to measure physical density, void ratio, and soil aggregate size distribution (Phillips 1997, Alshibli 2000, Tollner 1998).

The advantages of x-ray CT scanning include time savings and minimal sample disturbance. Tollner (1998) noted that x-ray CT scanning can provide aggregate size data consistent with traditional testing methods but without the time-consuming sample preparations involved with traditional tests. In particular, CT scan testing provides significant savings in time and effort when compared to sample coupon preparation techniques. The non-destructive nature of CT scanning allows the same soil sample to be scanned many different times. Since the sample is not affected by the testing, CT scanning provides an opportunity to investigate particle and pore interactions at any time and location

within the sample. With the proper test equipment, CT scans could even be taken as a sample is loaded or experiencing changes in stress state or environment.

The research described in this thesis was designed to develop non-destructive soil testing methods using x-ray CT scan techniques. The first objective of the research was to perform high quality CT scans on soil samples using the Montana State University Civil Engineering Department's custom-built CT scanner. The scanner was originally purchased to study snow and ice formations, and experiments indicated that the scanner had the capability to produce high quality CT scans of granular soil samples. The second objective of this research was to develop testing methods to determine geotechnical index properties from the CT scan images of the soil materials. The methods developed in this research would draw from established image processing techniques and mathematical morphology topics.

The soil index properties determined from CT scans in this research include porosity, grain size distribution, and pore size distribution. The results from the CT testing techniques were compared with results from traditional geotechnical laboratory tests. Results from the porosity and grain size distribution tests were used to validate the CT scan testing methods, since the mechanical laboratory tests to determine these index properties are simple and straightforward. Traditional geotechnical test methods for determining pore size distribution in soils are typically difficult to perform and require significant time and effort. However, it is recognized that pore size and pore size distribution are directly and fundamentally related to the three most important engineering characteristics of soils: permeability, compressibility,

and strength. Therefore, the pore size distribution CT testing methods developed in this study are of particular interest to researchers and practitioners.

The CT testing techniques developed in this research may be used in future studies to measure the effects of microstructure properties on freezing behavior of soils. In particular, CT testing may be utilized to easily and non-destructively measure pore structure parameters such as porosity and pore size distribution and how those structures behave under freezing conditions. Frost heave behavior in soils has been shown to be related to pore size distribution; however, pore size distribution has historically been difficult to measure experimentally (Gaskin 1973). The CT testing methods developed in this research may provide simpler and more non-destructive means to measuring pore size distributions than current experimental techniques.

CHAPTER 2

BACKGROUND CONCEPTS

Introduction

The primary objective of this study has been the development of non-destructive testing methods for determining geotechnical properties of soil using the Montana State University Civil Engineering Department's custom-built Computer-Aided X-Ray Tomography (MSU CT) scanner. The use of CT scanning equipment is commonplace in the medical radiology field; however, the application of this technology in the civil engineering discipline is relatively untried. This chapter presents an overview of the fundamental concepts used to develop geotechnical test methods for examining soil microstructure using a CT scanner. These topics include the steps to performing a CT scan, stereology theory and calculations, and pore size distribution modeling techniques. The concepts described herein were collected from the fields of medical radiography, image processing, and soil physics, and have been modified for geotechnical applications. The use of CT scanning for geotechnical applications is a growing field, and recent studies have experimented with CT technology to determine physical density, void ratio, and aggregate size (Phillips 1997, Alshibli 2000, Tollner 1998).

CT Scanning Overview

CT scanning has been used in medical fields for several decades, and the term "CAT scan" is well known to the public. But, what does a CAT scan, or CT scan entail? From start to finish, a CT scan consists of two main processes: data collection and image reconstruction.

During the data collection stage, a specimen is digitally photographed from multiple angles as it is exposed to x-rays. During the reconstruction phase, many individual x-ray photographs are superimposed in such a way that their resulting image describes the interior structure of the specimen. The complete process is described in greater detail in the following paragraphs.

X-Ray Science

The first main phase of a CT scan involves taking photographs of a specimen from multiple angles while it is exposed to x-ray beams. X-Rays are invisible, high-energy electromagnetic waves that are able to pass through many objects. As a beam of x-rays penetrates an object, some of the x-rays are absorbed by the object's matter; dense matter (e.g., rock and wood) and some heavy materials (e.g., steel and lead) absorb more x-rays than less dense materials (e.g., plastic and water). X-Rays that penetrate through the object hit an x-ray sensitive screen within the CT scanning equipment and cause it to illuminate. A digital camera is used to capture the image on the screen, which replicates the x-ray penetration pattern of the object.

A single image is generally not sufficient to describe the internal structure of an object. An x-ray image from only one location provides a two-dimensional look into an object, but the internal structures are stacked on top of each other in the image. A dark spot in the x-ray image (resulting from low penetration, implying dense material) can result from a single dense region within an object, or from multiple dense regions that are in alignment with the x-ray trajectory. X-Ray images taken at different angles around the object will show

different alignments of the same dense regions, and a general description of the regions' locations can be made. For example, a radiologist diagnosing a bone fracture will use x-ray images from multiple angles around the injury to develop an accurate description of the injury's location and extent. For simple objects, only a few different images are required, but complex objects containing a large number and variety of internal features may require many more viewing angles to obtain a complete internal description of the object.

CT Data Collection

The data collection phase of a CT scan occurs after the object is viewed with x-rays from many different directions. In traditional two-dimensional CT scanning, the object is scanned through a single "slice," and each of the individual images consists of the object's x-ray penetration pattern through the location of the slice. Some three-dimensional CT scanning techniques use individual images consisting of broad sections of the object's x-ray penetration pattern. In either case, the object must be photographed as it rotates at least one-half of a full rotation relative to the x-ray trajectory and detector screen (Russ 2002). Views around at least one-half of a rotation are necessary to capture all possible dense region alignments. Rotating the specimen more than a half rotation is possible, but views beyond 180° are redundant because the interior features of an object align in all possible combinations within a half of a rotation. Additionally, using more closely-spaced views around the rotation will result in a finer image resolution. A CT scan that uses a one-degree increment of rotation between individual views will capture only 180 different views of the object as it rotates 180° through the x-ray beam. As the interval spacing decreases, the

number of views increases, and the resolution of the final image improves dramatically. An example of this is shown in Figure 2-1.

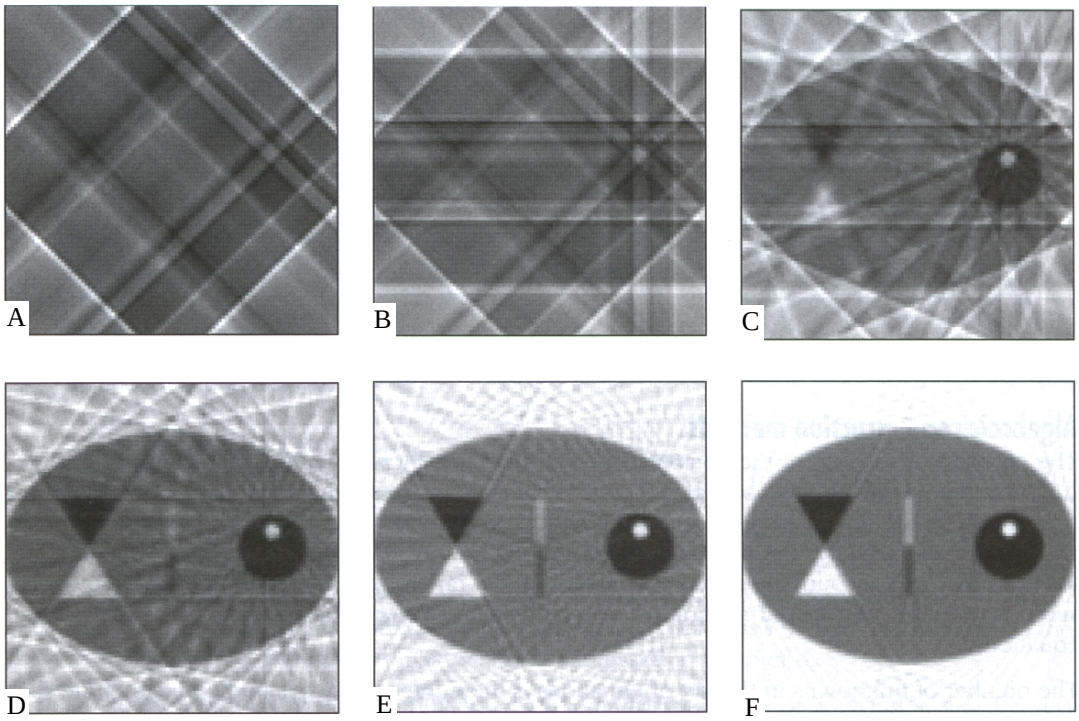

Figure 2-1: Examples of reconstructed images using A) two views, B) four views, C) eight views, D) 16 views, E) 32 views, and F) 64 views (Russ 2002).

This research involved the two-dimensional CT scanning approach to develop images of the internal structure of soils. The data collection phase of the CT scanning process for the soil scans involved using 1/4-degree increment scans with a full rotation of the soil sample relative to the x-ray. The 1/4-degree increment was chosen as an adequate balance between scan resolution and expediency. The MSU CT equipment is capable of performing scans with 1/8-degree increments, but those scans require a significant amount of time to complete and do not provide a substantial improvement in resolution compared to the1/4-degree scans. For soil materials, the time required for a 1/4-degree scan is approximately two hours; the

duration of a scan is based on the degree increment and the camera exposure time, which is also dependent upon specimen density. Using a full 360° rotation for each scan was unnecessary, but the equipment controls were designed to complete full rotations. When the last rotation increment is completed and the final x-ray image has been captured, the CT scan is ready to be reconstructed.

Image Reconstruction

Reconstructing a CT scan produces a representation of the interior features of an object. A regular single x-ray image can also show the same features, but accurate locations of interior features cannot be determined from a single view. The CT process uses x-ray images from many different views through a thin section of an object to pinpoint the locations of internal features. When the scan is reconstructed, the resulting image is a cross-sectional view of the object as if it had been cut through the plane at the scan location.

As the many thin images of a CT scan are collected, they can be stacked on top of one another to produce a graphical description known as a sinogram. An example of a sinogram is shown in Figure 2-2. The scan shown in Figure 2-2 is of a test object known as the Shepp-Logan phantom, which is used to calibrate medical CT scanners. The internal features of the phantom are meant to represent parts of a human brain, and their densities are approximately the same as brain structures. Each horizontal line in a sinogram describes a single x-ray image of the object through the scan "slice" location. A sinogram allows the user to visually detect features within the scanned object as it rotates. The sinogram image is useful for detecting possible errors in a CT scan before the final reconstructed image is created.

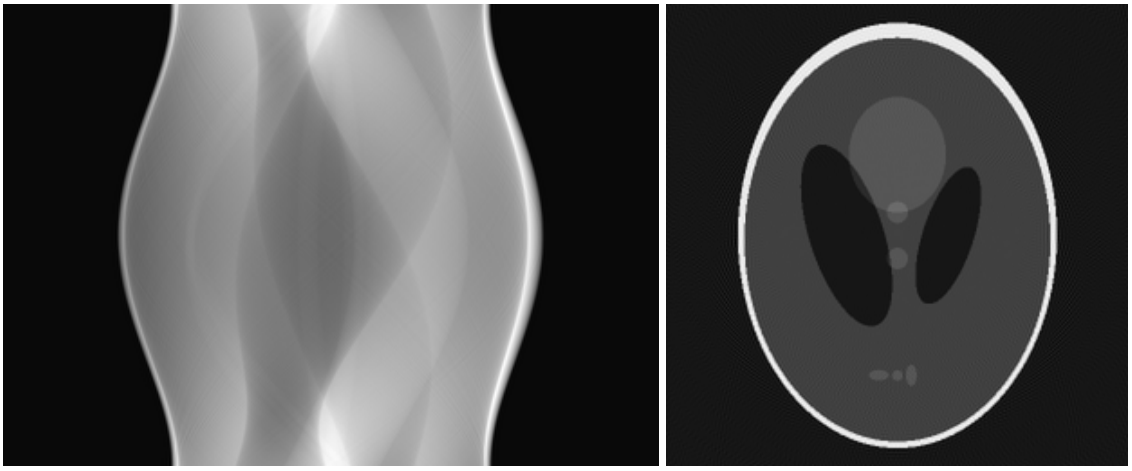

Figure 2-2: The sinogram and reconstructed image of the Shepp-Logan phantom test object (Biomedical Imaging Group 2000).

Each line in the sinogram corresponds to a single x-ray view of a thin slice of the object. If the object rotation is known for each line in the sonogram, then each line can be projected into and out of the screen and then rotated to its correct angle. This produces a stack of x-ray image planes, with each plane rotated slightly relative to its neighbors above and below. Imagine each plane as a transparent piece of glass with colored lines on it, and consider looking down through the stack of planes from the top. Figure 2-3 shows a graphical representation of this process for a theoretical CT scan. The theoretical object in Figure 2-3 contains three circular and concentric internal features. These internal regions are shown as gray, pink, and blue sections in Figure 2-3-A. Part B shows the projection of the slice from A. If each plane is a projection of a one-dimensional x-ray image through the object, then each plane has parallel colored streaks through it that correspond to the low- and high-density regions in the x-ray image. When the stack of planes are viewed from above, the black streaks add together to produce a view of the interior of the object. Figure 2-3 parts C and D are the reconstructed images of the scan using 6 and 18 views (corresponding to

180°-rotation scans with 30° and 10° increments). Note that when the projections are aligned correctly, the concentric internal features can be located. This is a simple description of the reconstruction process, and a more detailed and mathematical analysis of the process is given by Russ (2002).

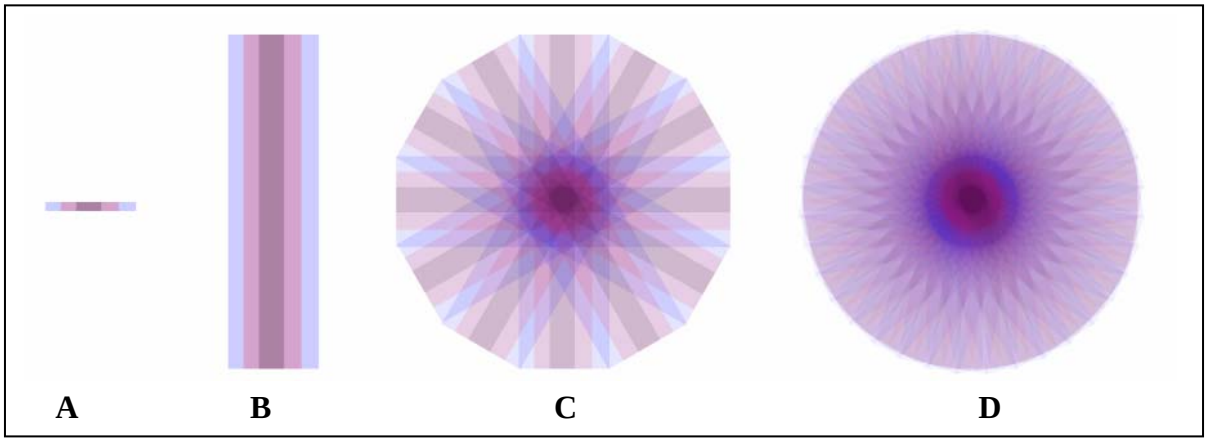

Figure 2-3: The reconstruction process: A) a theoretical x-ray slice image, B) the projection of A, C) the reconstructed image using 30° increments, and D) the reconstruction using 10° increments.

Stereology Methods

CT scans provide a means of projecting internal features of a specimen onto a two-dimensional cross-section. CT scans are commonly used to measure three-dimensional features, but traditional CT scans produce two-dimensional cross-section views of objects. Therefore, a method to determine three-dimensional properties from a two-dimensional image must be used. One common method to achieve this goal is known as stereology, which can be defined as the science of determining three-dimensional properties from two-dimensional images. Classical stereology uses a process known as unfolding to determine the size distribution of particles from an image. The unfolding process utilizes relationships

in geometry and counting statistics to develop a matrix of probability values that enable the calculation of the size distribution of spheres that could contribute to a given cross-sectional distribution of circles (Russ 2002).

A CT scan image of soil is not only a cross-section of the soil sample as a whole, but it also contains images of cross-sections of the individual soil particles. Some of the particles in the scan may have been sectioned at their largest diameter, while others may have been sectioned near their edge. Therefore, using the two-dimensional granulometry size distribution alone is not sufficient to measure the three-dimensional particle size distribution or the related pore size distribution. Stereological unfolding allows calculation of the three-dimensional size distribution using approximations in regards to the shape of the particles. The easiest assumption to make about particle shape is that every particle is spherical. This assumption may work well for some soil particles (such as well-rounded sand particles) but not for others (highly angular and elongated particles). Other possible shapes that are commonly assumed in the unfolding process include prolate and oblate ellipsoids, cubes, disks, cylinders, and others. A closed-form solution for unfolding is only available for spherical particles; other shapes require the use of approximate solutions.

Stereological methods employ geometric and statistical relationships to represent original three-dimensional particle sizes based on two-dimensional cross-section images. Geometry is used to determine the cross-section sizes that are possible from a certain size particle. Statistics are used to determine the probability that a given cross-section size came from a certain class of particle sizes. The diameter of a cross-section circle defines the smallest particle size that could have contributed to that cross-section, since the largest

possible cross-section from a given particle is through its diameter. However, the same cross-section could have been produced by a larger particle cut near its edge, as shown in Figure 2-4. Thus, a cross-section image alone cannot accurately describe the particles contained within a sample. Statistics are used to examine the probabilities of all possible cross-section sizes resulting from a single particle. The cross-section size probabilities are summed for each particle size class to determine the size distribution of the particles shown in a CT scan (Russ 2002). A detailed description of the calculations follows.

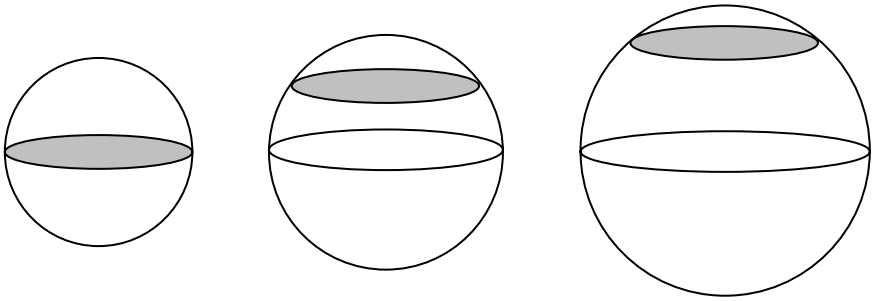

Figure 2-4: A single cross-section size may result from many different particle sizes.

Stereology Calculation Steps

There are five main calculation steps necessary to develop a size distribution using the stereological unfolding method.

1. Calculate a two-dimensional circle size distribution using granulometry.
2. Group the particle sizes into geometric classes and determine the cross-section size frequency for each geometric class.

3. Calculate the probabilities of all 2-D cross-sections produced by cutting the largest particles through various cross-sections.
4. Determine conversion coefficients α for each geometric size class (this step is only to make the calculations more expedient)
5. Calculate the three-dimensional size distribution and correct it for physical impossibilities.

Grouping the cross-sections sizes into geometric class sizes is important because the successive calculations are made much simpler when geometric classes are used. The granulometry procedure provides the two-dimensional cross-section size distribution, but it is given in terms of linear size classes. Converting the circle size distribution from linear classes to geometric classes is a counting procedure.

The boundaries of the geometric size classes are defined using normalized sizes. The sizes of the linear class boundaries are normalized by the largest cross-section size in the image. If there are ten linear classes that encompass the cross-section sizes, the first (largest) size class includes normalized sizes from 1.00 to 0.90, the second comprises sizes from 0.90 to 0.80, and so on. The upper and lower boundaries of the normalized geometric classes are defined using equations 2-1 and 2-2 (Sahagian 1998):

$$UB_i = 10^{\frac{-(i-1)}{10}} \tag{2-1}$$

$$LB_i = 10^{\frac{-i}{10}} \tag{2-2}$$

where UB and LB are the normalized upper and lower bounds of geometric size class i. For example, the first (largest) geometric class includes normalized cross-section sizes from 1.00 to 0.794, and the fifth geometric class has sizes 0.398 to 0.316.

The first geometric size class includes more circle sizes than the first linear class. Therefore, the first geometric class includes some particles from the first, second, and possibly more linear classes. The circles in the linear classes must be correctly assigned to the appropriate geometric sizes. The re-distribution procedure was automated in this study using a Visual Basic function, shown in Appendix B. The next step is to calculate the fraction of all 2-D cross-sections produced by the particles that are cut through their largest diameter.

The stereological unfolding process is at its core a method that sums the probability that a certain particle was cut to produce a shape shown in a two-dimensional cross-section. These probabilities are based on the geometry of the particle shapes and their aspect ratios, and are independent of the absolute particle size. Transect probabilities define the fraction of the entire set of cross-sections that falls into the particle size classes. Figure 2-5 shows a graphical representation of the cross-section probability. If geometric class sizes are used, the first (largest) few classes contain a larger proportion of the possible cross-section sizes than the remaining classes, so the chance of these classes containing cross-sections from the largest size of particles is relatively high.

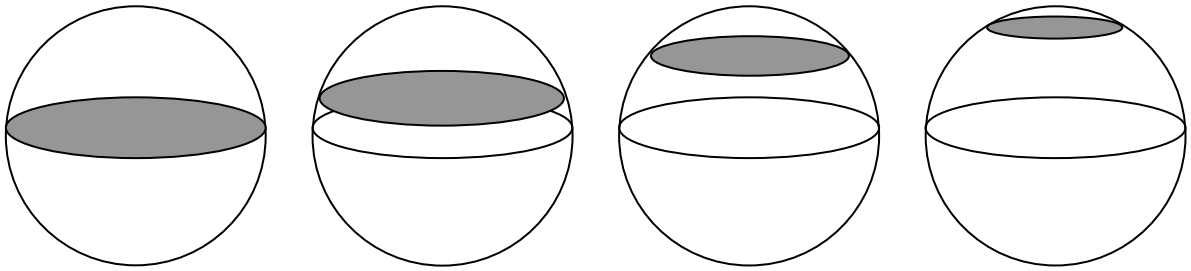

Figure 2-5: Possible cross-sections through a spherical particle.

The transect probability for each particle size class can be determined analytically for spheres, and has been approximated for many other particle shapes (Sahagian 1998). For spheres, the frequency $\phi(r)$ of cross-sections with radius *r* through a particle of radius *R* in a certain class size is given by:

$$\phi(r) = \frac{r}{\sqrt{R^2 - r^2}} \tag{2-3}$$

The probability of the cross-section with radius r falling into the particle size class defined by the lower and upper limits r_1 and r_2 is found by integrating the frequency equation:

$$P(r_1 < r < r_2) = \frac{1}{R}\left(\sqrt{R^2 - r_1^2} - \sqrt{R^2 - r_2^2}\right) \tag{2-4}$$

The cross-section probability for each particle size class is used to calculate the conversion coefficients for the classes. The particle size distribution of each class is dependent upon those of all the preceding (larger) classes, and calculating conversion coefficients eliminates the need for multiple steps in the computations. The coefficient for the i-th class is calculated by:

$$\alpha_i = \frac{1}{P_1}\left[\alpha_1 \cdot P_i - \sum_{j=1}^{i-2}\left(\alpha_{j+1} \cdot P_{i-j}\right)\right] \tag{2-5}$$

where a_i and P_i the conversion coefficient and transect probability for class i, and α_1 is calculated with:

$$\alpha_1 = \frac{1}{P_1} \tag{2-6}$$

The final step in calculating a size distribution with the stereological unfolding method is to calculate the number of particles that contribute to the cross-section sizes. For the *i*-th class, this is accomplished with:

$$N_{Vi} = \frac{1}{\overline{H_i}'}\left[\alpha_1 \cdot N_{Ai} - \sum_{j=1}^{i-1}\left(\alpha_{j+1} \cdot N_{A(i-j)}\right)\right] \tag{2-7}$$

where N_{Vi} is the proportion of particles in size class i, $\overline{H_i}'$ is mean projected height of the particle (for spheres, $\overline{H_i}'$ is equal to 1.0), and N_{Ai} is the proportion of cross-sections in the i-th size class.

The series of N_{Vi} values describes the number of particles with radius r_i and defines the particle size distribution. One illogical characteristic of the classical unfolding procedure described here is that it can result in negative N_{Vi} values, which are not physically possible (i.e., negative numbers of particles in a sample). One suggestion for dealing with such anomalies is to absorb the negative errors into the next largest particle class size (Yi-Hua Xu 2003). Small negative values (close to zero) that occur in a single particle size class are generally neutralized by the next larger class, but significantly negative values (far from

zero) accumulate and may neutralize the positive values of multiple larger classes. This procedure was automated in this study using a Visual Basic program, which is shown in Appendix B.

The particle radii calculated with the stereology calculations are normalized to the largest particle size, so they must be returned to their original state before they can be used in a size distribution. Additionally, if the original radii values were measured in pixels, they should be converted to units of length (millimeters, inches, etc) using the scale of the digital image as a final step.

The calculations described above can be summarized as a series of sums, and are described graphically in Figure 2-6. The particles in the first (largest) size class can be cut through cross-sections that fall into any of the smaller size classes, and the fraction of the smaller cross-sections that are produced by the largest particles is determined by the transect probability for each class. The two-dimensional size distribution calculated with granulometry determines how many total cross-sections are in the image. The fraction of these cross-sections that comes from the largest particles is subtracted, leaving those cross-sections that are from smaller particles. Since the cross-section probabilities are dependent only on particle shape and not size, the fraction of remaining cross-sections that comes from the second-largest class can be calculated. Again, the second-class cross-sections are removed, and the number of third-class cross-sections can be calculated from the remainder. Therefore, the cross-sections remaining after each step are dependent upon all the preceding (larger) classes.

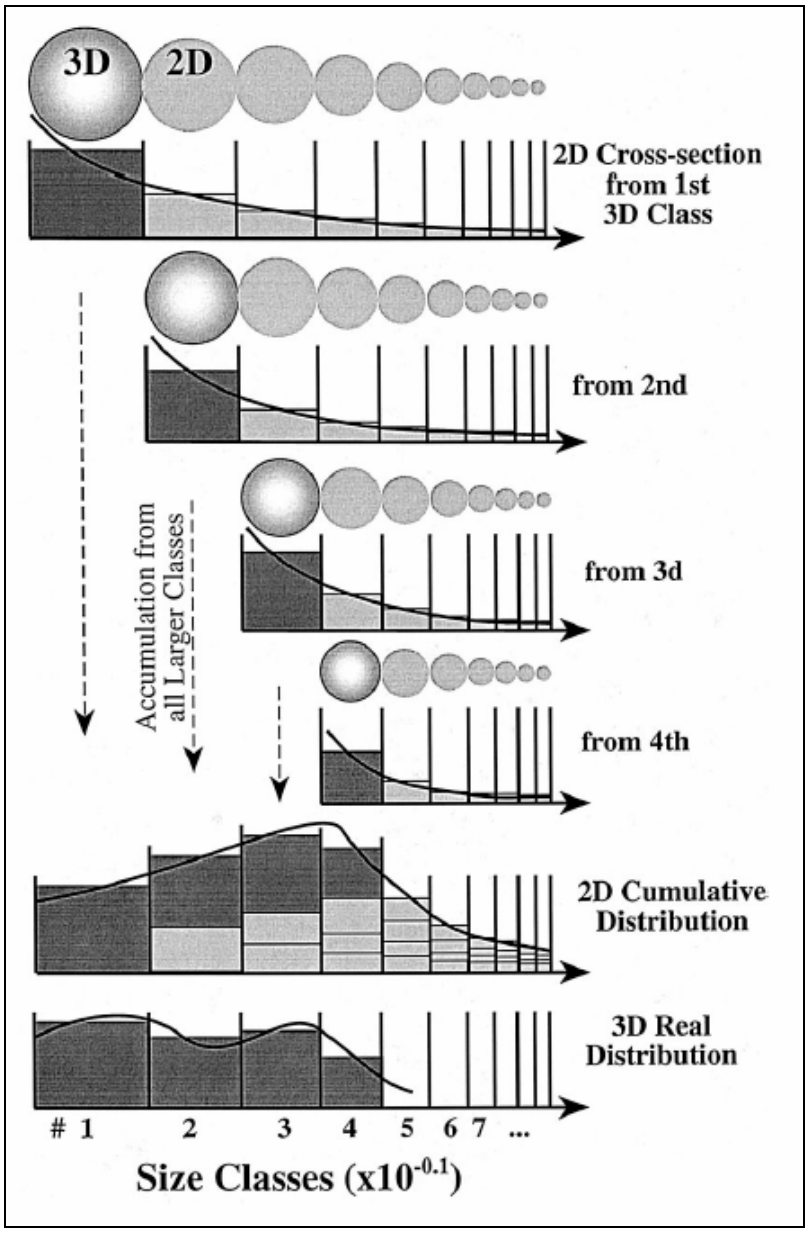

Figure 2-6: Graphical description of the stereology process (Sahagian 1998).

Pore Size Distribution Modeling

The grain size distribution of a soil is easy to measure in the geotechnical laboratory using simple equipment including a stack of sequentially smaller screens and sieves, a

shaking device, and a scale. On the other hand, determination of the pore size distribution of a soil has traditionally been a difficult task for soil scientists and engineers. Soil pores are difficult to visually inspect and measure, so tests are often used that relate pore characteristics to other more easily measured properties. Two of the biggest problems with measuring pores are tortuosity and connectivity. For example, a long, straight (low tortuosity) pore will have different physical properties than a very twisted (high tortuosity) continuous pore, and a soil with low pore connectivity will measure differently than a soil with high connectivity, even if the pores in all four cases have the same characteristic size (Vervoort 2003). If the complex shapes of pores have not been taken into account, pore size results can include very significant errors. Dullien (1992) suggests using the definition of a pore as "a portion of pore space bounded by solid surfaces and by planes erected where the hydraulic radius of the pore space exhibits minima, analogously as a room is defined by its walls and the doors opening to it." Figure 2-7 shows an example of a typical pore as described by this definition.

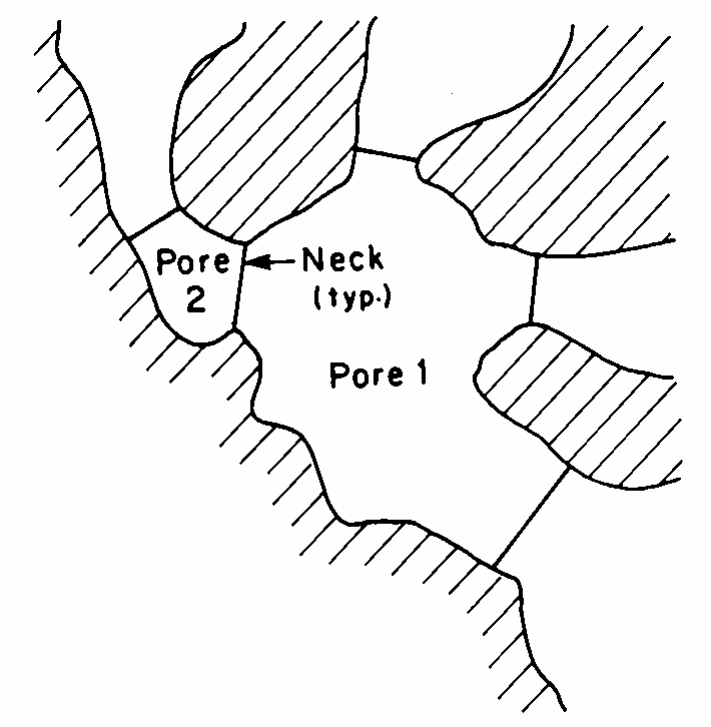

Figure 2-7: Common definition of the shape of a pore as a “room” within several pore “necks”.

Two traditional testing methods for pore size distribution include mercury intrusion and pressure plate suction (Gaskin 1973). These test methods essentially work on the fundamental principles of capillary pressure and related pore suction pressures.

Mercury intrusion testing involves saturating a soil sample with mercury under various levels of suction pressue. After the sample has equilibrated at each suction level, the mass of the mercury soaked into the soil is measured, a characteristic curve is created after several measurements, and a pore size distribution can be computed. This method is no longer in practice because of the hazards associated with mercury exposure.

The second traditional method, pressure plate suction (also known as laboratory tensiometry), measures pore suction as the soil dries. Saturated soil samples are placed

between two semi-permeable ceramic tensiometer plates. Varying levels of suction are applied to the plate and the soil samples are allowed to equilibrate (Cassel 1986). Capillary pressure within the soil pore space varies as a function of the pore size, thus water from large pores will be removed at low suction and water in small pores will require high suction to be removed. The water content of the soils is measured after each suction level, and a drying suction curve can be plotted after several measurements. The suction data can be converted to a pore size distribution using approximate capillary pressure relationships.

Pressure plate testing is still in use today, but it is not appropriate for granular materials such as the soils used in this research. The suction levels in this test are determined by the permeability of the ceramic plates, and different plates are used for different suction levels. The suction levels applied to the soils during testing are suitable for fine-grained materials that have high capillary pressure potential (small pores), but even the lowest-level plates produce suction that is too high for granular materials, which lose all their water very quickly under suction. For this reason, water retention curves of granular materials are not generally developed. Tensiometry is primarily suited for fine-grained soils, and pressure plates are generally designed for testing water-retaining agricultural soils rather than permeable granular materials.

Gaskin and Raymond noted significant difference in the pore size distribution results between the mercury intrusion test and the pressure plate suction (tensiometry) test. They found that the mercury intrusion test was the more accurate when compared with field performance during freezing (1973). There is no benchmark test for pore size distribution, and the majority of the tests are destructive to the soil structure. The test procedures destroy

or alter the same parameters they are supposed to measure. Therefore, a need exists to develop non-destructive pore testing methods so that pores can be viewed and measured without altering their structure.

Pore size distributions can be estimated using correlations to other more readily measurable soil parameters such as cumulative grain size distribution. Two approximate methods include the Arya and Paris method (1981) and the Haverkamp and Parlange method (1986). These two methods are based on physical properties of soils and generally work on a similar hypothesis involving water retention. This hypothesis uses the similarity between the shapes of the cumulative grain size distribution of a soil and its water retention curve (Haverkamp 2002). The water retention curve for a soil can be quickly converted to the pore size distribution by using approximate capillary pressure relationships. The Arya and Paris and the Haverkamp and Parlange models are based on the same fundamental hypothesis of shape similarity, but they arrive at a water retention curve (and therefore a cumulative pore size distribution) using different routes. The Arya and Paris model is generally more widely used than the Haverkamp and Parlange model because it is more user-friendly and applicable to a wide variety of soil types. The shape factor required for the Arya and Paris model is considered constant or based on soil type and cumulative grain size distribution, and the shape function for the Haverkamp and Parlange model is typically determined experimentally. Additionally, the Arya and Paris model is not restricted to certain soil types, but the Haverkamp and Parlange model is limited for use only with clean sands (Haverkamp 2002). The Arya and Paris model was chosen to model the pore size distributions of the soil materials used in this study because of its ease of use and more widespread acceptance.

The Arya and Paris Model Procedure

The Arya and Paris model can be used to calculate the water characteristic curve and the cumulative pore size distribution curve of a soil by utilizing the shape similarity between the grain size and pore size distribution curves. The grain size distribution is divided into several classes of soil particle sizes, and a pore volume is calculated for the pores between the particles in each particle size class. The procedure can then be used to calculate point values on the water retention curve for points on the grain size curve. The steps required to develop a pore size distribution using the Arya and Paris model are presented here as described by Haverkamp (2002).

1. Divide the cumulative grain size distribution curve into several fractions, starting with the smallest particles. Twenty classes are suggested, and an average particle diameter (D_i) is assigned to each grain size fraction.
2. Calculate the fraction weights (W_i) from the grain size distribution curve. The W_i values correspond to the percentages of total weight from each class of particle sizes, and the sum of the W_i values is unity.
3. Calculate the number of particles n_i in each class based on the class weight, average class diameter, and soil grain density:

$$n_i = \frac{6 \cdot W_i}{\pi \cdot D_i^3 \cdot \rho_s} \qquad (2\text{-}8)$$

where D_i is the grain diameter of the particles in class i, and ρs is the solid density of the soil particles.

4. Calculate the mean pore radius by using the shape function factor α:

$$R_i = \frac{1}{2} \cdot D_i \cdot \left(\frac{2 \cdot e \cdot n_i^{1-\alpha}}{3} \right)^{0.5} \qquad (2\text{-}9)$$

where e is the soil void ratio. It is common to use a constant α value of 1.38, but a soil-specific α can be determined.

5. Calculate the pore volume fraction of each particle class using the mean pore radius and the effective pore length from each particle class:

$$dVp_i = \pi \cdot R_i^2 \cdot Le_i \qquad (2\text{-}10)$$

where the effective pore length of class i is defined as

$$Le_i = n_i^{\alpha} \cdot D_i \qquad (2\text{-}11)$$

6. Accumulate the pore volume fractions for the classes to calculate the cumulative pore size distribution curve.

Shortcomings of the Arya and Paris Model

The Arya and Paris model does have some limitations, including: unaccounted trapped air, problems with determining the shape factor α, hysteresis, and compatibility between two inherent assumptions used in the model. First, the model does not account for trapped air in the pores (Arya and Paris 1982). Entrapped air within a pore would cause different saturation and water content than if the same pore was filled entirely with water. The presence of trapped air tends to introduce errors on the small-pore end of the pore distribution curve (Soil Physics Handbook).

The second main problem with the Arya and Paris model is the determination of the shape factor α. The original model (1982) proposes using a constant α-value of 1.38 for all soils. It was noted however, that large deviations from experimental results are created for particles with diameters larger than 100 μm (Arya and Paris 1982). The authors later suggested a method to use a variable α value calculated for each particle class (Arya 1999). Using variable α-values for the soil materials in this study resulted in very minor adjustments to the pore size distribution curves calculated using $\alpha = 1.38$ as recommended by Arya and Paris (1982); therefore, a constant value of α was used here.

Third, the Arya and Paris model does not account for hysteresis (Arya and Paris 1982). Hysteresis in the water retention curve causes a slight difference between the drying and wetting curves. The original Arya and Paris model does not explicitly account for hysteresis, but it can be paired with a hysteresis model in order to accommodate this phenomenon (Soil Physics Handbook). Since the soils in this study were measured at constant water content, it is difficult to determine whether the drying or wetting curve is more appropriate, so the affect of hysteresis is unknown.

Finally, the Arya and Paris model uses a non-linear relationship between pore radius and particle diameter. The relationship used in the model is a power function, which forces the use of non-constant partial porosities for the individual particle classes. However, the model also makes the assumption that the partial porosity from each particle class is constant over the sample. The assumption of constant partial porosity should be incompatible with a non-linear pore radius function, but the Arya and Paris model uses the two together (Soil

Physics Handbook). In spite of the limitations of its assumptions and shortcomings, and that no accurate way to experimentally verify the model, the Arya and Paris model is still considered appropriate in most cases.

CHAPTER 3
MATERIALS AND METHODS

Introduction

The purpose of this research was to develop a non-destructive method of soil measurement using x-ray computer assisted tomography. To do this, a testing procedure was developed using a custom-built digital radiography and computer-aided tomography (CT) scanner. The scanner was first calibrated by scanning objects of known shapes and sizes, such as plastic beads. The CT scanner was used to measure three geotechnical soil properties: porosity, grain size distribution, and pore size distribution. A single CT scan image provides the data needed to calculate each of these three properties, but different image processing steps are needed to determine each property. In addition, traditional soil tests were performed to compare the CT scanning process results. This chapter describes the experimental materials and methods used to complete this research.

Soil Materials

There were five soil materials used in these experiments, which have been termed Gravel, Coarse Sand, Medium Sand, Fine Sand, and Concrete Sand. The Gravel, Coarse Sand, Medium Sand, and Fine Sand materials were uniformly-graded soils manufactured to test the resolution of the CT scanner and each consisted of similarly-sized particles. The Concrete Sand material was used to test the CT scanning procedure using a soil that

consisted of a wide variety of particle sizes. These materials are described in more detail in the following sections.

Gravel

The Gravel soil material was manufactured by isolating soil particles between the #4 (4.75 mm) and #6 (3.35 mm) sieve sizes. The particles in the Gravel material are shown in Figure 3-1. In general, the Gravel particles are somewhat angular and are slightly elongated.

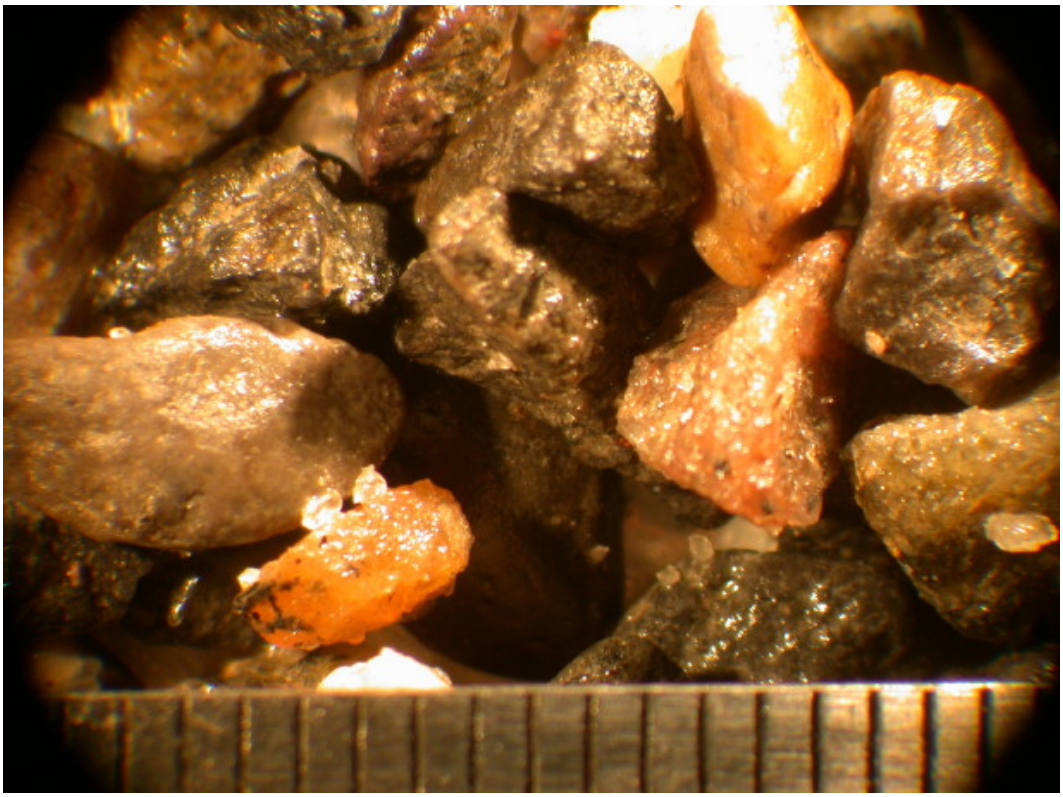

Figure 3-1: Microscopic photograph of the Gravel soil material (scale in millimeters).

Coarse Sand

The Coarse Sand is a uniformly-graded soil with particles smaller than the Gravel material. The Coarse Sand was manufactured by isolating soil particles between the #10 (2.0

mm) and #20 (0.85 mm) sieves. Figure 3-2 shows a microscopic photograph of the Coarse Sand material. The particles in the Coarse Sand material are generally sub-angular to rounded and are elongated to spherical in shape.

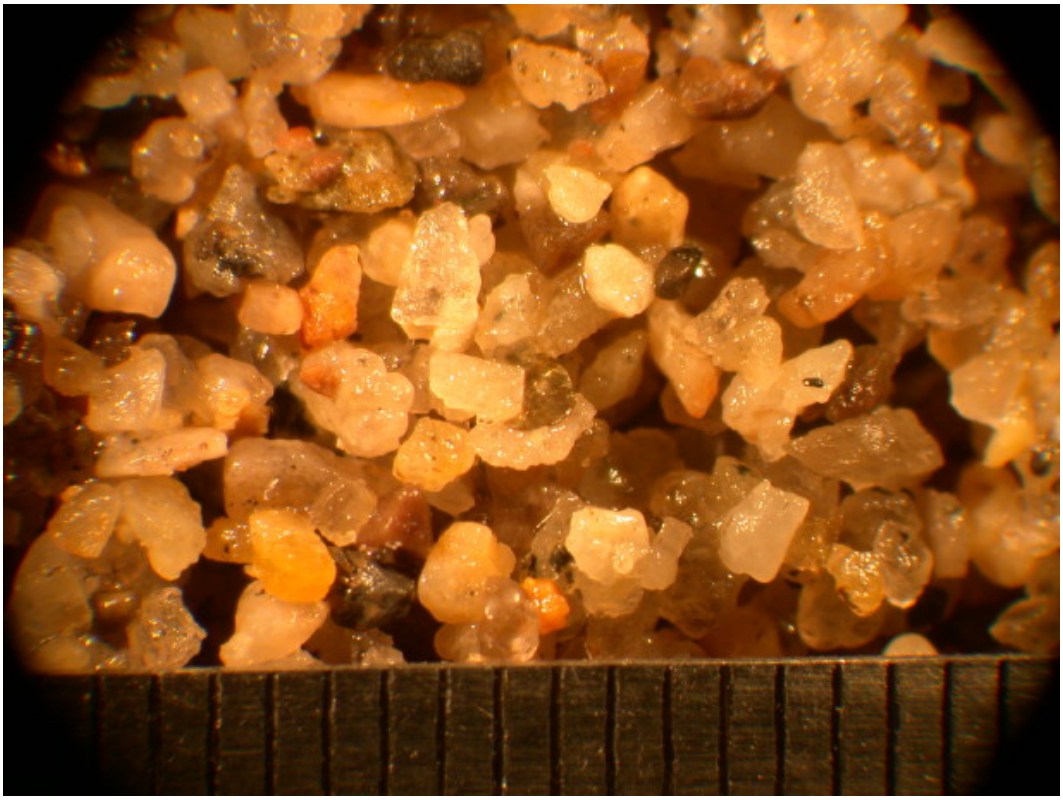

Figure 3-2: Microscopic photograph of the Coarse Sand material (scale in millimeters).

Medium Sand

The Medium Sand material is a uniformly-graded soil consisting of particles sized between the #20 (0.85 mm) and #40 (0.425 mm) sieves. The particles are generally sub-rounded and nearly spherical. A microscopic photograph of the Medium Sand material is shown in Figure 3-3.

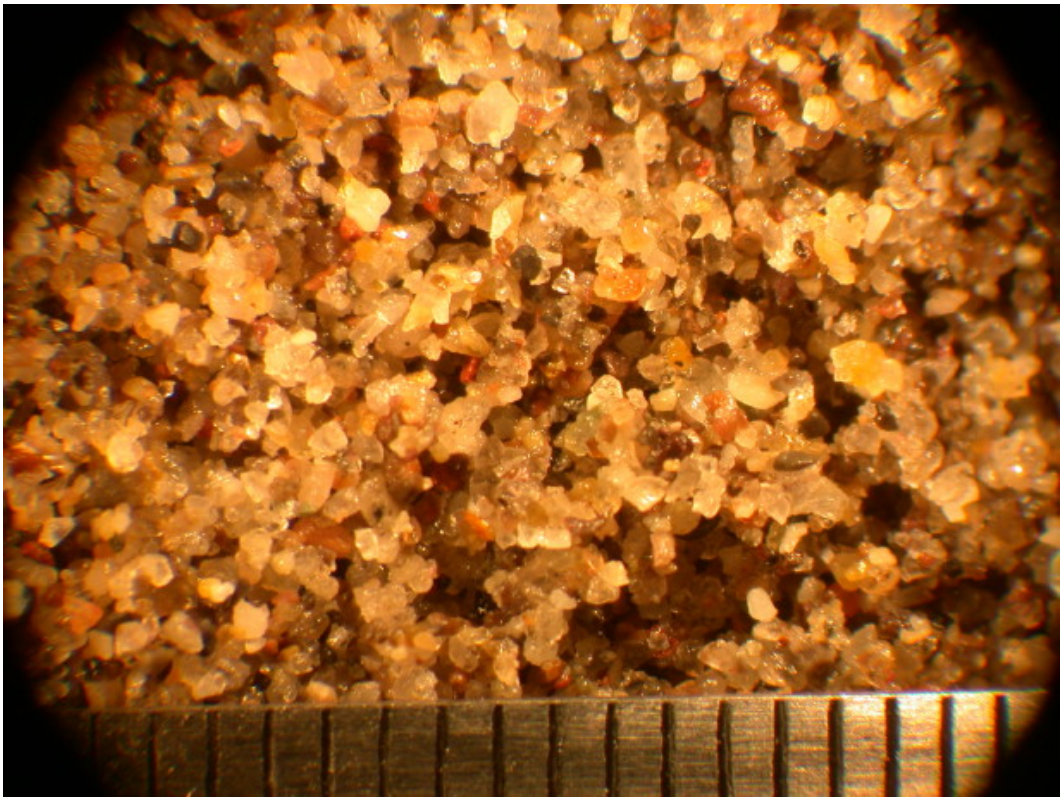

Figure 3-3: Microscopic photograph of the Medium Sand material (scale in millimeters).

Fine Sand

The Fine Sand material was the smallest uniformly-graded soil manufactured to test the CT scanning resolution. The particles in this material are sized between the #40 (0.425 mm) and #80 (0.177 mm) sieves and are generally sub-rounded and spherical. A microscopic photograph of the Fine Sand material is shown in Figure 3-4.

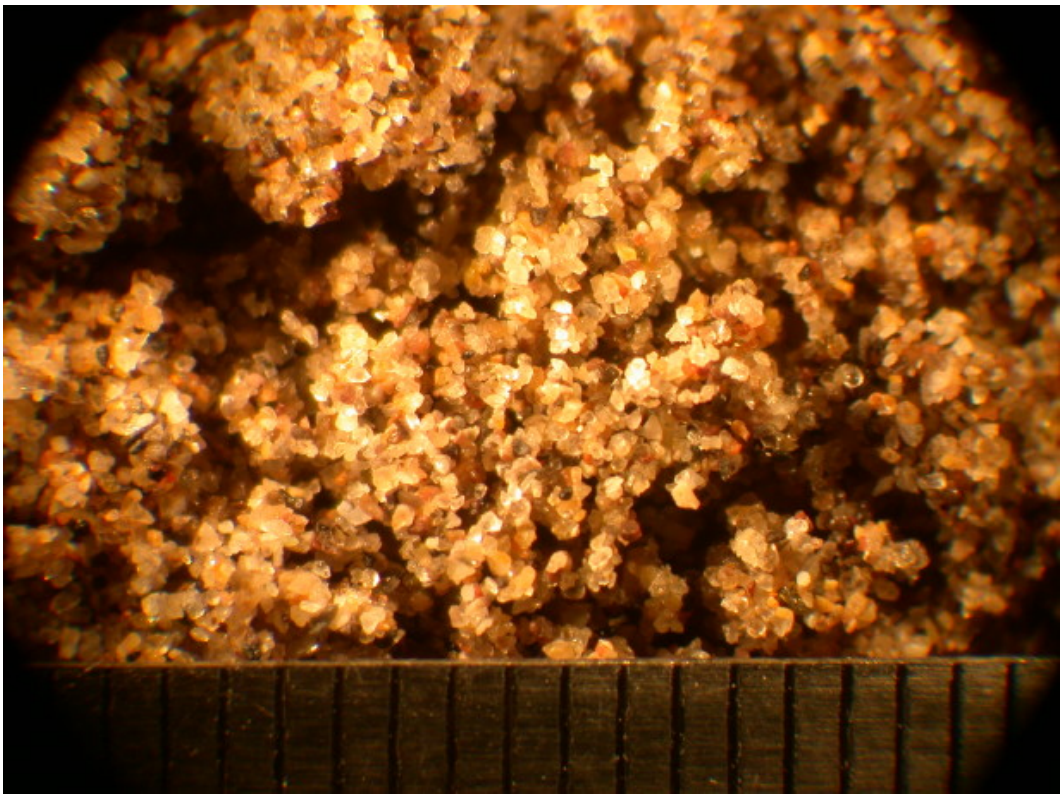

Figure 3-4: Microscopic photograph of the Fine Sand material (scale in millimeters).

Concrete Sand

The Concrete Sand material was the only soil used in this research that consisted of a wide variety of particle sizes. The Concrete Sand material was taken from a batch of soil commonly used as small aggregate for structural concrete mix designs. Figure 3-5 shows a microscopic photograph of the Concrete Sand material. The largest particles in the Concrete Sand soil are retained on #4 (4.75 mm) sieve, and the smallest particles pass a #200 (0.075 mm) sieve. Details of the Concrete Sand grain size distribution are discussed in later sections.

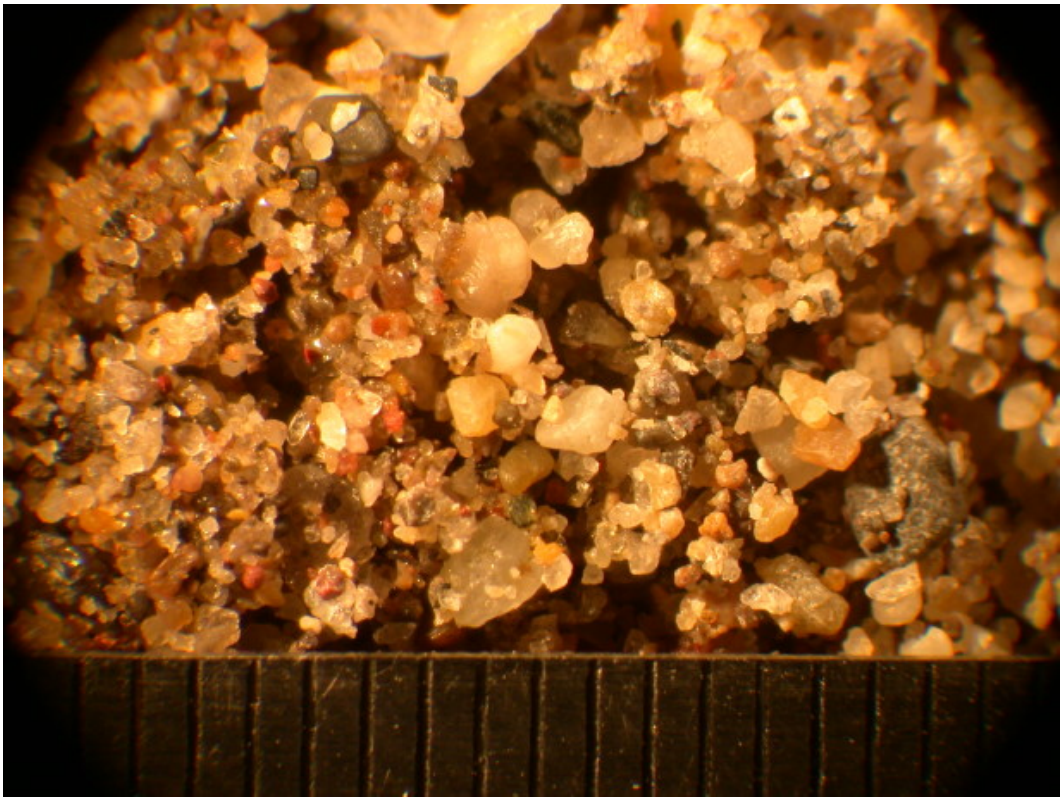

Figure 3-5: Microscopic photograph of the Concrete Sand material (scale in millimeters).

Traditional Geotechnical Laboratory Testing

Soil characteristics were quantified using CT scanning procedures developed in this study, and the results were compared to traditional geotechnical index tests. The parameters measured using the CT scanner include porosity, grain size distribution, and pore size distribution. Several geotechnical index tests are required in order to compare the values calculated with the new CT scanning procedure to values measured with accepted testing methods. These tests include specific gravity, water content, and sieve analyses tests. Each of these tests was performed in general accordance with ASTM standards.

The procedure to determine soil porosity is based on the definition of bulk density:

$$\rho_m = G_s \cdot \frac{1 + w}{1 + e} \cdot \rho_w \qquad (3\text{-}1)$$

where ρ_m = soil bulk moist density, G_s = soil specific gravity, w = soil water content, e = soil void ratio, and ρ_w = density of water (0.998 gm/cm^3 at 25°C). Thus to calculate the void ratio (and subsequently, the porosity) of a soil, lab tests are required to determine the following parameters: specific gravity (ASTM D854-92), water content (ASTM D2216), and bulk density. The density of water is a relatively constant value of 0.998 gm/cm^3 for atmospheric pressure and near-room temperatures. To minimize the effects of random testing errors, five specific gravity and five water content tests were performed on each material. The values used in later portions of the research were based on average values of these five tests.

The bulk moist densities of the soils in this study were measured using the following simple procedure.

1. The mass of a two-inch nominal diameter, 8-inch long PVC testing container was measured and recorded.
2. The container was filled completely with water, and the mass was measured again.
3. The mass of the water was found by subtracting the mass in Step One from the mass in Step Two. The volume of the water was calculated by dividing the mass of water by the density of water. Since the container was completely filled with water, this volume corresponds to the volume of the PVC container.

4. The soil was prepared and compacted until it completely filled the PVC container. The mass of the container and soil was measured. The mass of the soil was calculated by subtracting the mass of the container, from Step One.
5. Since the volume (V) of the container and the mass (M) of the soil are known, the bulk density is easily calculated as:

$$\rho_m = \frac{M}{V} \tag{3-2}$$

With all the parameters known or measured, the void ratio can be calculated by rearranging the definition of moist bulk density:

$$e = \left[G_S \cdot (1 + w) \cdot \frac{\rho_w}{\rho_m} \right] - 1 \tag{3-3}$$

The porosity is directly related to the void ratio by:

$$n = \frac{e}{1 + e} \tag{3-4}$$

where n = porosity and e = void ratio.

The technique described above to determine the bulk porosity of a soil sample requires the bulk density of the entire sample. It is expected that the density across the entire height of the soil sample would vary slightly. Precautions were taken during sample preparation to minimize the porosity variations through the sample. Each sample was compacted into its 8-inch tall, 2-inch diameter PVC container in four to five lifts, with each lift receiving ten 6-inch hammer drops from a standard proctor hammer. The nondestructive CT testing method developed in this research measures the soil porosity at a single cross-section through the soil, and this value must be compared to the entire sample's bulk

porosity. Therefore, some discrepancy between the individual porosity values from the CT technique and the laboratory tests is unavoidable.

The other laboratory test required for this study is used to determine soil particle size gradation. This test, designated in two parts as ASTM D421 and D422, involves sieving dry soil over consecutively smaller sieves to segregate the soil particles by size. The portions retained on each sieve are weighed to characterize the particle size distribution for that particular soil. This test was performed in this study on the Concrete material. The uniform soils used in this study were manufactured using sieves; consequently their grain sizes were quite uniform. Figure 3-6 shows the measured grain size distributions for the five soil materials used in this research. Since the grain sizes for these soils are in between two consecutive sieves, the grain size distributions for the uniformly-graded soils were estimated using a normal distribution of particle sizes between the known minimum and maximum grain sizes for each soil.

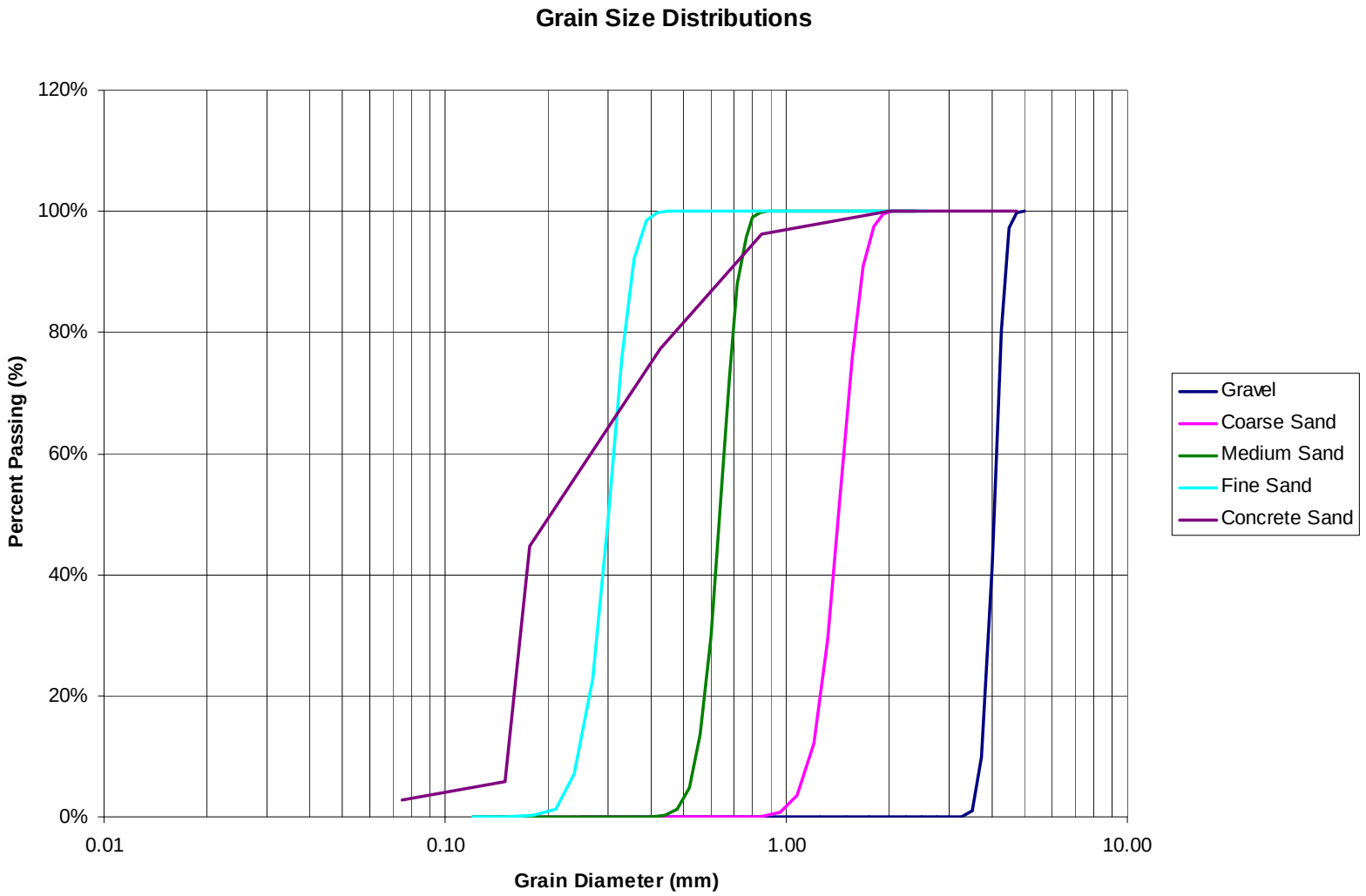

Figure 3-6: Grain size distributions for the five soil materials.

Computed Tomography Testing Methods

PVC Testing Containers

Two-inch diameter, 8-inch long PVC containers were manufactured to hold the soil samples during the CT scan process. Each container was attached to a wooden base to stabilize it in the vertical position. A picture of the containers is shown in Figure 3-7.

Figure 3-7: PVC soil containers (2-inch diameter, 8-inch height) ready for CT scan testing.

Location and Spacing of CT Scans

Several options are available for the choice of where to test a soil sample with CT scanning. Multiple tests should be run on each sample to increase the accuracy of the results. The selection of scan locations depends primarily on the intended applications of the results.

One option would be to completely randomize the process; this approach would be applicable for a study in which the testing methodology was established and the research involved a qualitative evaluation of materials, such as a comparison of different soil treatments. Another option is to equally space the scans along the length of the sample. This approach would be applicable for research examining soil parameters that may change based on location, such as compaction or saturation. A third option for determining scan locations would be to space the scans very close together to examine the local effects of soil particle shape, size, and orientation. This option would be useful in examining the particle interaction that occurs along failure surfaces during shearing.

In this study, a combination of the second and third scan spacing methodologies was employed. Three groups of closely-spaced scans were performed on each sample; one scan group each near the top, center, and bottom of the sample. This scan spacing scheme is shown diagrammatically in Figure 3-8. Tests were not performed within the top and bottom 1-1/2 inches of the sample to minimize potential edge effects from the PVC canister. Each scan group consisted of three individual scans spaced between fifty percent and seventy-five percent of the maximum sample particle size. For example, for the Coarse Sand material, which had a maximum particle size of 2.00 mm, the intra-group scan spacing was chosen as 1.25 mm. The MSU CT controller's precision is limited to a tenth of a millimeter; consequently, intra-group scan spacings were rounded to 0.1 mm.

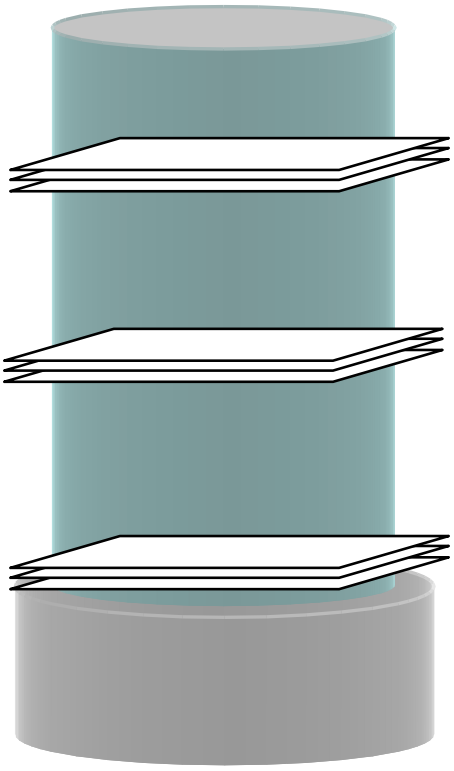

Figure 3-8: Diagram of the clustered scan spacing scheme.

Scan Resolution and Camera Field-of-View

The CT scanner is capable of scanning objects of a variety of sizes and composed of many different materials. The digital camera that photographs the x-ray absorption pattern as x-rays pass through the specimen has a fixed field of view; consequently, if the size of the testing container is changed, the camera settings can be adjusted to maintain the accuracy and resolution of the scans.

The resolution of the CT scanner is affected by two main mechanical settings within the scanner cabinet. The first parameter is the quality of the phosphor screen that converts the x-ray absorption pattern to visible light. As with photographic film, high sensitivity and resolution are both desired with most applications. Unfortunately, the two are mutually

exclusive – a highly sensitive film (able to record images quickly in low light situations) does not have high resolution (the ability to distinctly display features), and a high-resolution film does not have high sensitivity. Most phosphor screens used in radiography have been developed for use in medical settings, and short x-ray exposures are desired to minimize tissue damage and other medical complications. The short exposure times result in decreased resolution. However, in the arena of CT scanning of non-organic specimens, longer x-ray exposures can be used to achieve greater resolutions, because damage from x-rays is not usually an issue.

The second parameter that affects the resolution of CT scan images is the location of the digital camera. Digital cameras capture images of the visible light that travels through a lens and impacts a charge-couple device (CCD). A CCD is a wafer of silicon that acts similarly to a frame of film in a traditional camera with a fixed maximum resolution. Much like a human eye reading a newspaper, the CCD is able to discern small features when they are closer. If you try to read newsprint from across the room, large headline letters may be clear, but the small text letters will likely be blurry. As you bring the newspaper closer to your eye, such as arm's length away, the small text becomes clear enough to distinguish individual letters and words, even in small font. As you bring the newspaper closer to your eye, you may even be able to distinguish individual print dots that make up the letters.

The CCD in the CT scanner's digital camera performs in a similar fashion to the newspaper analogy. The digital camera must be moved far enough from the phosphor screen to capture the entire specimen. The entire specimen may be seen at this setting, but the smallest distinguishable detail may actually be quite large because of the inherent resolution

limitation of the CCD camera. However, like the newspaper page, if the camera is placed closer to the specimen, smaller details can be accurately recorded. As the focal distance is further decreased, it may be possible to observe micro-scale details in the captured image.

Now, we can apply the newspaper analogy to CT scanning of soil samples. The PVC canister holding the soil becomes the newspaper, the soil particles are the small-font text, and micro-scale variations of the particles are the newsprint dots. The digital camera must be positioned appropriately to accommodate the large size (two inches in diameter in this case) of the PVC canister, and at the same time record the smallest detail possible. As the soil particles get smaller, they get closer to the lower limit of the camera's resolution. It is possible that finer grained soils may contain particles smaller than the smallest detail the camera can distinguish. One option to overcome this problem with small particle sizes would be to use a smaller PVC canister; the camera could be moved closer to the phosphor screen, and smaller particles could be viewed clearly. Unfortunately, all canisters exert influence on the soil particles, especially near the sides and edge of the canister. So called "edge effects" are unavoidable, but they can be reduced by using large canisters compared to the soil particles. For this study, edge effects were reduced by using 2-inch diameter PVC pipe for the soil canisters, and the scan resolution was adjusted accordingly. Canisters for the small-particle soil materials could have been smaller, but it was decided for consistency to use identically-sized canisters for each of the scans.

X-Ray Power and Camera Exposure

One important step when performing CT scans is preventing saturated pixels in the digital image. Saturated pixels occur because a digital camera assigns pixel intensity based on the amount of light that hits its detector. If too much light reaches a certain point on the detector, the pixel intensity value is maximized, resulting in a white spot in the image. This is equivalent to over-exposing traditional film, which results in washed-out white regions in the film. In digital radiography, saturated pixels can be prevented by two scan parameters: x-ray power and camera exposure.

The x-ray power used for a scan determines the strength of x-rays that reach the phosphor screen and therefore determines the brightness of the resulting image. When high x-ray power is used, x-rays that pass from the x-ray source to the phosphor screen still have high power when they hit the phosphor screen. The screen converts high power x-ray hits into bright spots, and the digital camera detects these bright spots. If very high x-ray power is used, the parts of the screen beyond the edges of the scanned object receive very strong x-ray hits, and consequently transmit very bright spots to the camera, which can saturate the pixels along the edge of the image.

Problems can arise from low x-ray power as well. If too low of a power is used, some materials will absorb a large portion of the emitted x-ray's power and only a small portion of the x-rays will travel to the phosphor screen. Consequently, the CT scan images are very dim and there is little contrast between high- and low-density materials.

Camera exposure time also affects the quality of CT scan images. The resolution of images is increased with long exposure times because the digital camera is able to detect

more light. With long exposures, objects in the scan appear brighter, and those materials that are dim with short exposures become visible. The use of long exposure times is one solution to the resolution-versus-sensitivity compromise inherent in the phosphor screen. The use of long exposure times can effectively increase the apparent resolution of otherwise poor resolution screens. Unfortunately, the trade-off with long exposures is that too much light may reach the digital camera detector. Pixels may then become saturated, and the CT scan quality is ruined.

Therefore, a balance between x-ray power and camera exposure time should be achieved for highest-quality CT scans. The desired balance is to use a high x-ray power with a long exposure time. The CT scanner used in this research is able to produce x-rays with up to 160 kilovolts of power, and there is no maximum camera exposure time. The appropriate combination of x-ray power and camera exposure is determined primarily by the materials being scanned. Low-density materials such as water, air, and ice will not absorb high amounts of x-ray power, and low x-ray powers may be used with these materials. Conversely, high-density materials such as metals, soil, and minerals will require much higher x-ray power. Once an appropriate x-ray power is found, a trial-and-error process should be used to find the corresponding camera exposure time that maximizes the quality of the CT scan images. Generally, the scans produced in this study were created using a 140-kV x-ray beam and a camera exposure time of approximately two seconds. The x-ray beam power is held constant throughout the entire CT scanning process, and the camera exposure corresponds to the time the camera shutter is open for each of the x-ray images that makes up a CT scan.

Reconstruction Parameters

After completing a CT scan, the x-ray images are compiled into a quality two-dimensional view of the interior of the scanned specimen. This process is known as reconstruction, and the most important parameter in the process is called the image center of rotation. The process of reconstruction is essentially an overlaying procedure, where the individual x-ray images are aligned and laid on top of each other to form the final image. The center of rotation parameter defines the center pixel at which the x-ray images are rotated and stacked. Its location is not the same for all scans and can change dramatically when adjustments are made to the CT equipment including the camera, lens, and x-ray source location.

Determination of the center of rotation for a scan is a trial and error procedure. The goal of this procedure is to match the CT image reconstruction center of rotation used to compile the x-ray images into a cross-section view and the center of rotation of the scanned object as it rotates within the cabinet. The user first assumes an arbitrary center of rotation value and reconstructs the scan. Changing the center of rotation parameter does not change the data contained in x-ray images themselves, but only adjusts the center point at which they are reconstructed. If the assumed center of rotation was not the true center of rotation, the user chooses a new center, either higher or lower, and reconstructs again. If the resulting image is clearer than the first, then the change was in the right direction; if the image is of poorer quality, then the change was incorrect. Eventually, the quality of the reconstructed images will maximize with a certain center of rotation value. This value defines the best pixel location at which to center the reconstruction process. The minimum and maximum

center of rotation values for image reconstruction correspond to the extreme left and right pixel locations in the original x-ray images, which are equal to zero and 1023 for full-size scans.

As mentioned above, the center of rotation changes dramatically with adjustments to the CT equipment. Also, the center point can move on a series of scans where no adjustments are made. This occurs most often when the rotating specimen table is out of vertical alignment. Instructions for leveling the table are given in Appendix A. If the table is tilted, the bottom of the specimen moves less side-to-side with respect to the x-ray beam than does the top. Therefore, scans of the top of the sample will have a slightly different center of rotation than those at the bottom. Typically, the centers of rotation along the sample vary linearly with the height of the scan. If the user can determine the centers of rotation at the bottom and top of the sample, the centers for scans at intermediate points can be approximated by linearly interpolating between the top and bottom center of rotation values.

It is possible to pinpoint the center of rotation of a scan to a tenth of a pixel or smaller, but this accuracy is not necessary. Minor changes to the center of rotation parameter result in minor adjustments in the reconstructed scan images. It was found that for the images in this study, determining the center of rotation to the nearest one pixel was sufficient. In general, the CT scan images produced in this research were reconstructed satisfactorily with a center of rotation value of approximately 505. If the sample containers had been placed directly on the cabinet's center of rotation, the reconstruction center of rotation would correspond to the center pixel of each x-ray image, which is located at pixel

512. The center of rotation value of 505 implies that the containers were not placed exactly at the cabinet's center of rotation.

Image Processing Methods

Porosity Calculation

Porosity is defined as the ratio of void volume to total volume in a soil sample. The CT scanning process provides a description of the solid and void spaces shown in cross-sections through soil samples. The steps to calculate the porosity of a soil pictured in a CT scan image are: 1) despeckling, 2) thresholding, 3) selecting the region of interest, and 4) measuring the image. The image processing steps were completed for this research using the ImageJ image analysis software, developed by the National Institutes of Health. These steps are described in detail in the following.

Despeckling removes much of the "noise" that occurs in CT images. The despeckle process is a median filter that reduces isolated high-intensity pixels in a digital image. For each pixel in a digital image, the despeckle filter measures the intensities of the pixel's neighboring pixels within a 3x3 grid and assigns the center pixel the value of the median pixel intensity (Russ 2002). In the ImageJ software, the despeckle function is found in the Process – Noise menu.

Soil particles appear in a CT scan as many different shades of gray that correspond to each particle's density. In order to calculate porosity from the image, these shades of "solid space" gray must be distinguished from the shades of darker "void space" gray. Solid and void spaces in the image can be separated using a threshold filter. The threshold filter takes

an image with many pixel intensity values and replaces its pixels with either white or black pixels. In an 8-bit grayscale digital image, each pixel is assigned a color intensity ranging from 0 (white) to 255 (black). For a given threshold value, the filter replaces each pixel's intensity with white (pixel value 0) if it is below the assigned threshold, and black (pixel value 255) if it is above. The result is an image that consists only of white and black pixels instead of varying grayscale pixels. An example of the results from a threshold step is shown in Figure 3-9. The two histograms correspond to the pixel counts of the two images. Notice that the original image includes a wide variety of shades, whereas the thresholded image includes only black and white pixels. In the ImageJ software, the threshold function is found in the Image – Adjust menu.

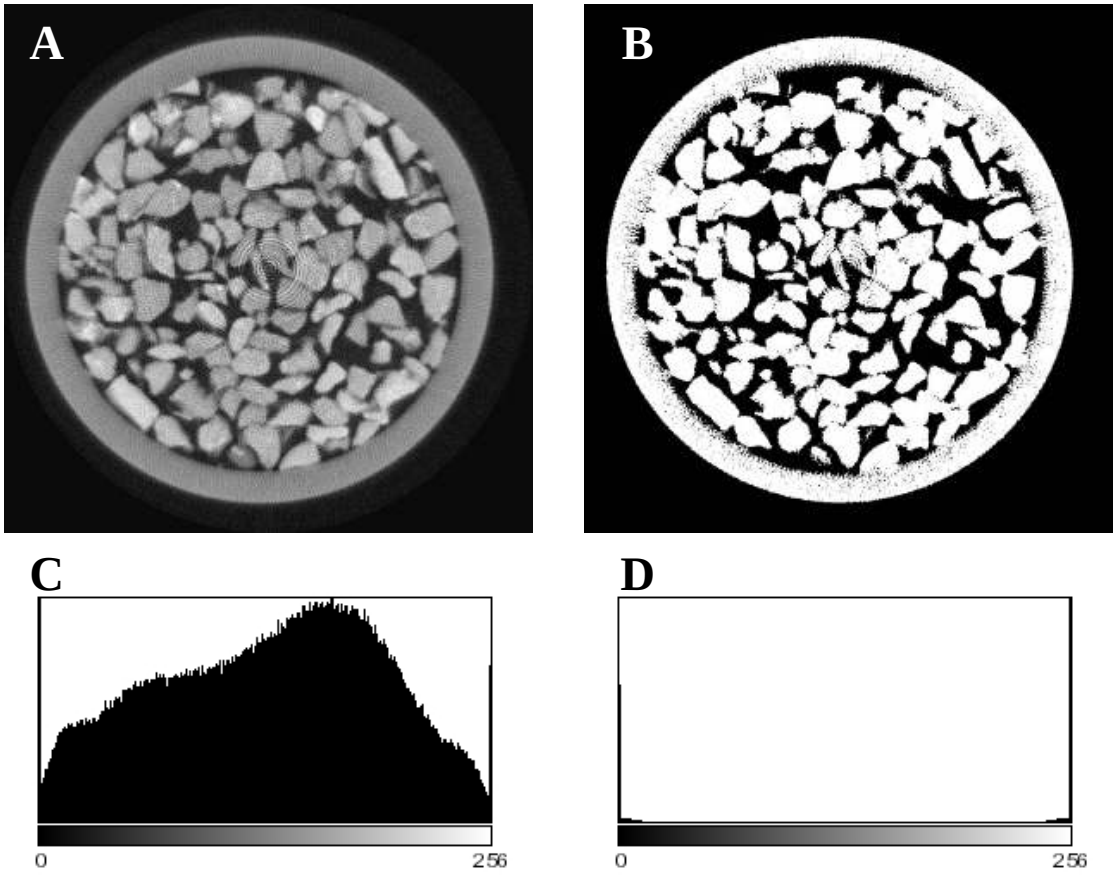

Figure 3-9: An example of porosity determination from a digital CT scan image of the Gravel material: A) the original image, B) the image after thresholding, C) the pixel histogram of the original, and D) the histogram of the thresholded image.

The number of remaining white pixels is dependent on the threshold value. If too low a threshold is used, an excessive number of pixels will be above the threshold level, leading to an abundance of black pixels. Conversely, a high threshold value results in an excessive number of white pixels. The void ratio of the soil pictured in a CT scan image is calculated by dividing the number of black (solid) pixels by the number of white (void) pixels. Therefore, the void ratio determined from each image is highly dependent on the threshold level used. Each CT scan image will have a different threshold level based on the parameters

of the scan and the properties of the material being scanned. For this study, the threshold level for each image was subjectively set at the point where the centers of visible solid particles were filled with black space. For scan images of the finer-grained materials, this level was difficult to set because the particles often appeared to blend together, and visible void space was not obvious at first glance.

At this stage in the process, the CT scan image contains white and black groups of pixels, which correspond to solid and void space in the soil. In order to count the number of pixels in the image, a region of interest must first be selected. The PVC testing container appears in the image as a ring of white pixels, but these "solid" pixels should not be counted as solid soil space. Therefore, the region of interest for CT scans here should be the space within the PVC ring. Once the inside edge of the PVC is selected as the region of interest, the final step is to count the pixels with a histogram function.

The histogram function counts the number of pixels within the region of interest and organizes them according to their color intensity value. A histogram of a grayscale image may look like a common bell curve, with a wide distribution of pixel values, as shown in Figure 3-9-C. The histogram of a thresholded image appears as two spikes at the zero and 255 color intensity values (for black and white images) with no pixels having other intensity values, as shown in Figure 3-9-D. The void ratio of a soil shown in a CT scan image histogram is found by simply dividing the number of white (void) pixels by the number of black (solid) pixels. Similarly, the porosity is calculated by dividing the number of white pixels by the total number of pixels. For example, the histogram of the thresholded image of the Gravel material CT scan shown in Figure 3-9 tells that the image contains 197,703 void

space (black) pixels and 298,674 solid space (white) pixels. The void ratio and porosity are found by:

$$e = \frac{\text{void}}{\text{solid}} = \frac{197703}{298674} = 0.662 \tag{3-5}$$

$$n = \frac{\text{void}}{\text{total}} = \frac{197703}{197703 + 298674} = 39.8\% \tag{3-6}$$

Grain Size Determination

Particle size can be determined in a digital image using a process known as opening. Opening is performed on a binary image containing only black and white pixels (this is achieved during the thresholding step described in the preceding section) and consists of two steps: erosion and dilation. The result of one opening is that large groups of white pixels are smoothed, and small isolated groups of pixels are removed. The intermediate steps of an opening include first removing pixels from the edges of white pixel groups (erosion) and then adding pixels back on to the remaining white pixel groups (dilation) (Serra 1982). For each opening, a reference shape of characteristic size λ is used to remove pixel groups smaller than size λ. The size λ is the characteristic length of a reference shape; it may be the diameter of a circle, the edge length of a square, or the characteristic length of an arbitrary shape. Erosion is defined as the intersection of image elements with given size elements (Serra 1982). The result of an erosion step is that image elements smaller than the reference shapes of size λ are removed, and elements larger than λ are shrunken but remain. Dilation is defined as the union of elements in a digital image with elements of a given size (Serra

1982). The result of a dilation step is that small features (small grains, narrow lines, etc) in an image are enlarged and smoothed.

By following an erosion (removal) step with a dilation (expansion) step, small features in an image can be removed without affecting larger features. The combination of erosion and dilation steps is known as an opening procedure. Figure 3-10 shows an example of an image after both erosion and dilation steps. Notice in Figure 3-10 how the smallest features in the original image have been removed by the opening. By counting the foreground pixels in an image before and after an opening, the number of pixels that were removed can be calculated. Since the removed features were smaller than the reference size λ, the total area of small features can be determined.

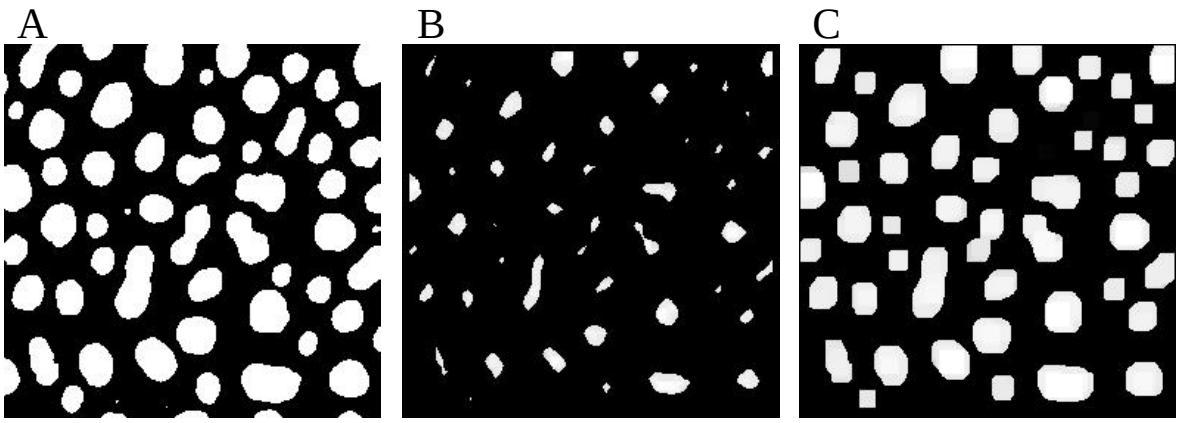

Figure 3-10: Results of an opening iteration: A) the original image, B) after erosion, and C) after dilation.

A series of openings will provide the number of features that are smaller than a series of reference shapes. Thus, the size distribution for features in a digital image can be described as:

$$G_1(\lambda) = 1 - \frac{P_B(-\lambda)}{P_B(0)} \qquad (0\text{-}7)$$

where $G_1(\lambda)$ is the cumulative number of pixels removed for size λ, λ is the diameter of a circular reference shape, $P_B(-\lambda)$ is the number of pixels removed in the opening step from size λ-1 to size λ, and $P_B(0)$ is the original number of pixels in the image (Serra 1982). This process of additive openings is known as granulometry and can provide a size distribution of objects from a digital image in terms of pixels. The particle sizes in pixels can be then scaled to traditional units of length (such as millimeters) if the scale of the CT scan image is known. Figure 3-11 shows the intermediate results of a granulometry calculation procedure on a digital image. In each successive step of the granulometry procedure, larger pixel groups are removed and counted. The resulting size distribution is shown in Figure 3-12.

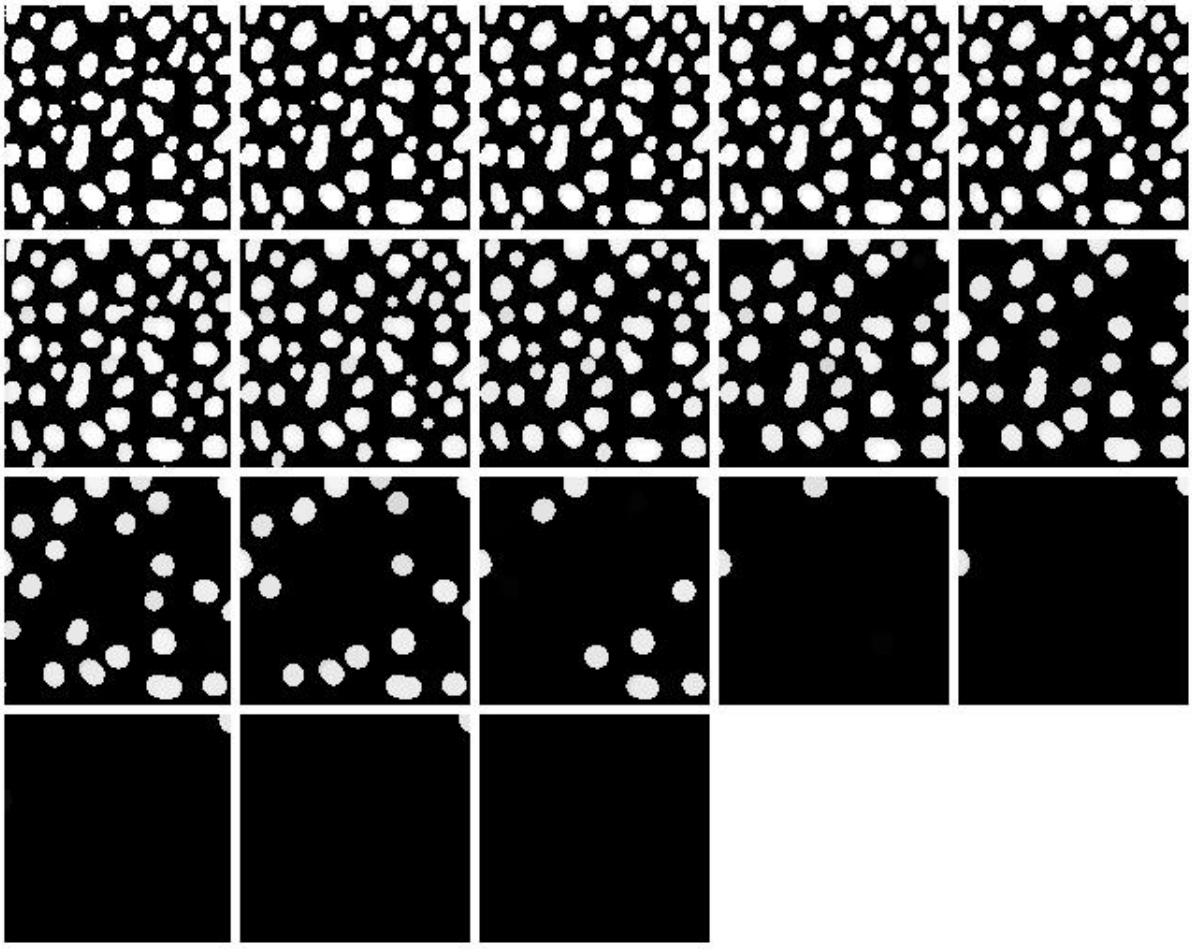

Figure 3-11: Resulting images after successive opening iterations in the granulometry process.

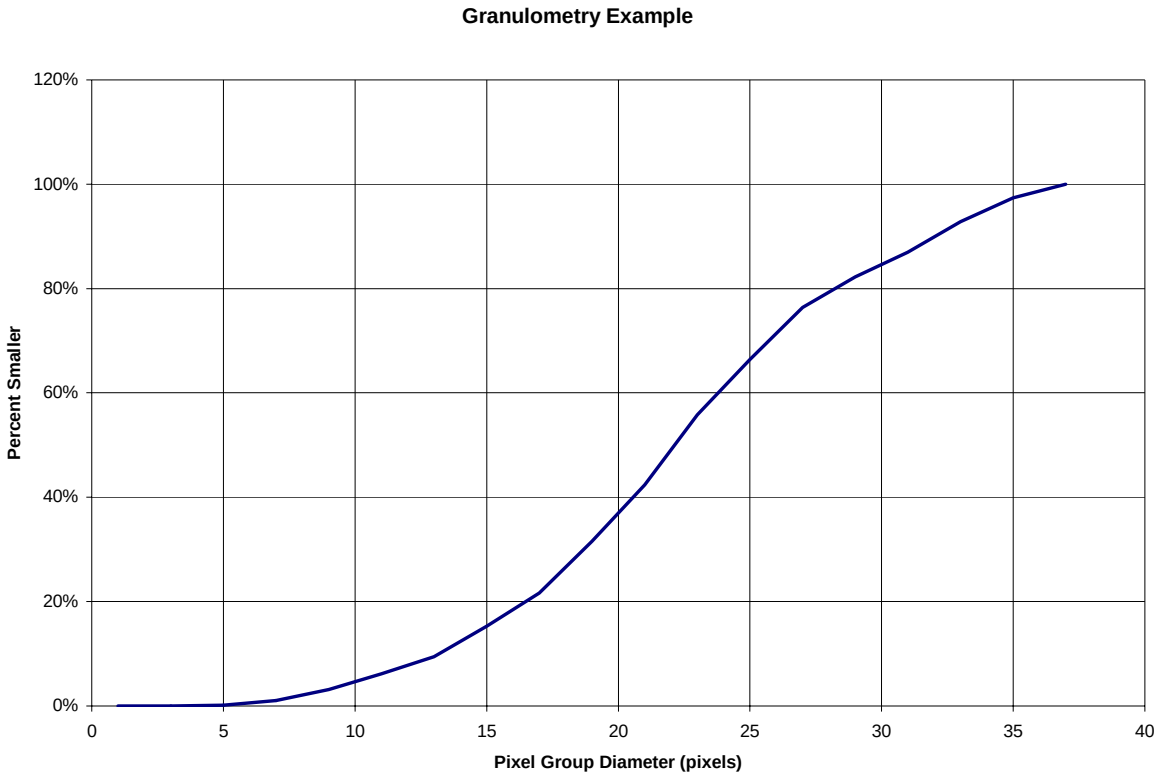

Figure 3-12: Cumulative size distribution of the example image.

CHAPTER 4

EXPERIMENTAL RESULTS

Introduction

The goal of this research was to develop x-ray CT methods to non-destructively test granular soil materials. The MSU CT scanner was used to produce CT scans, and image processing methods were used to determine soil index properties from the CT scan images. The soil properties determined with the new CT testing methods included porosity, grain size distribution, and pore size distribution. Traditional geotechnical laboratory mechanical tests were used to verify the CT-measured results. This chapter presents the results of this study.

CT Scan Images

The first step of this project was to adjust the MSU CT scanner so it was capable of producing quality CT scans of soil materials. The CT scans done during this research were two-dimensional, “slice” style scans that produce a cross-sectional view of the soil materials. The scan images of the soil materials are shown in Figure 4-1 through Figure 4-6. Each soil sample was scanned at nine locations, with the scans spaced as three groups of three scans each. Scans within each group were spaced according to the soil’s maximum particle size. Therefore, it may be possible to see the same particle in two adjacent scans. In addition, a single scan of uniform plastic beads was performed as a control specimen for the grain size determination procedure developed in this research. The CT scan image of the plastic beads is shown in Figure 4-7.

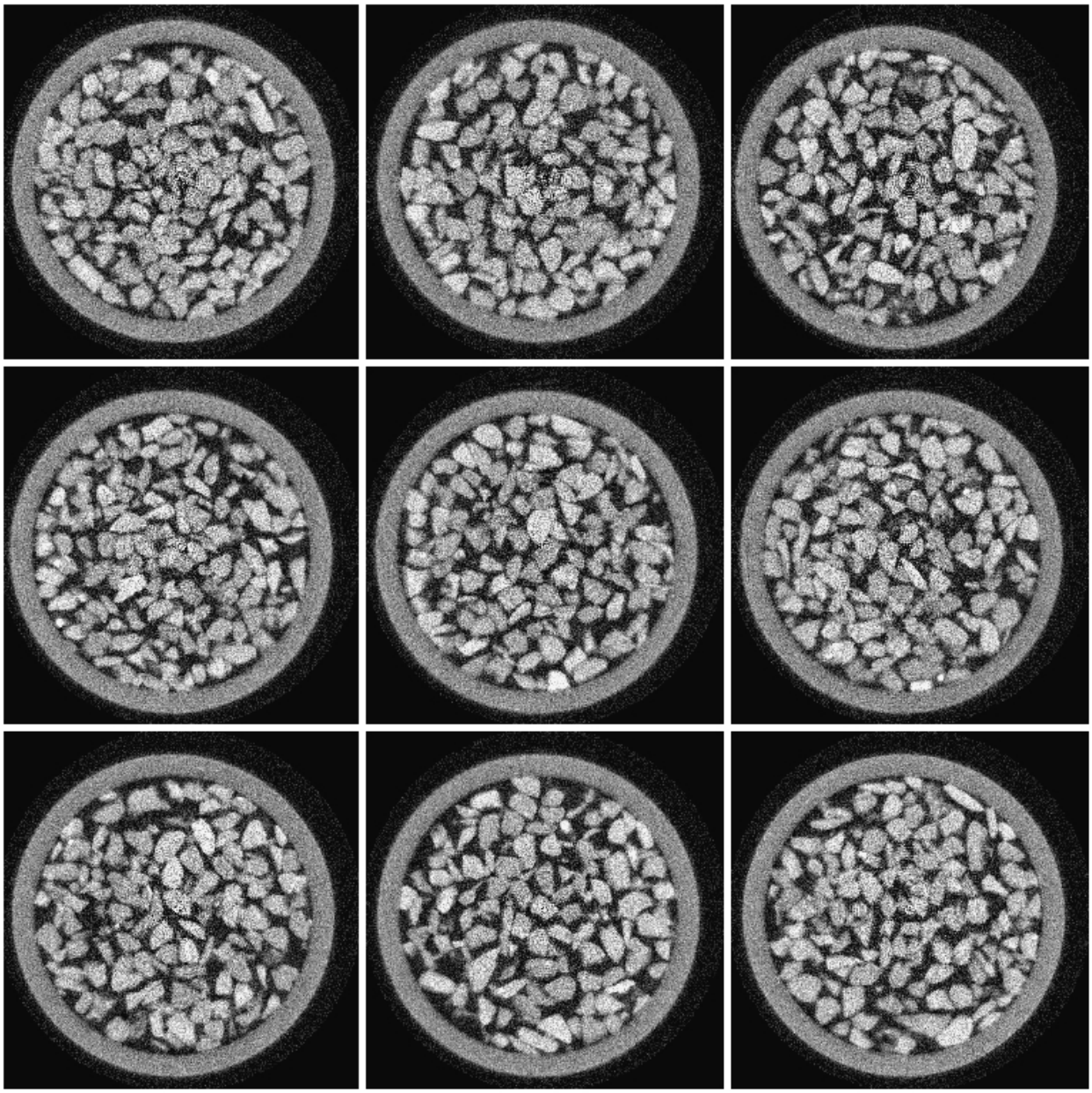

Figure 4-1: Gravel soil CT scans. Row 1: top of sample; Row 2: middle of sample; Row 3: bottom of sample; spacing between scans in each row is 3.0 mm.

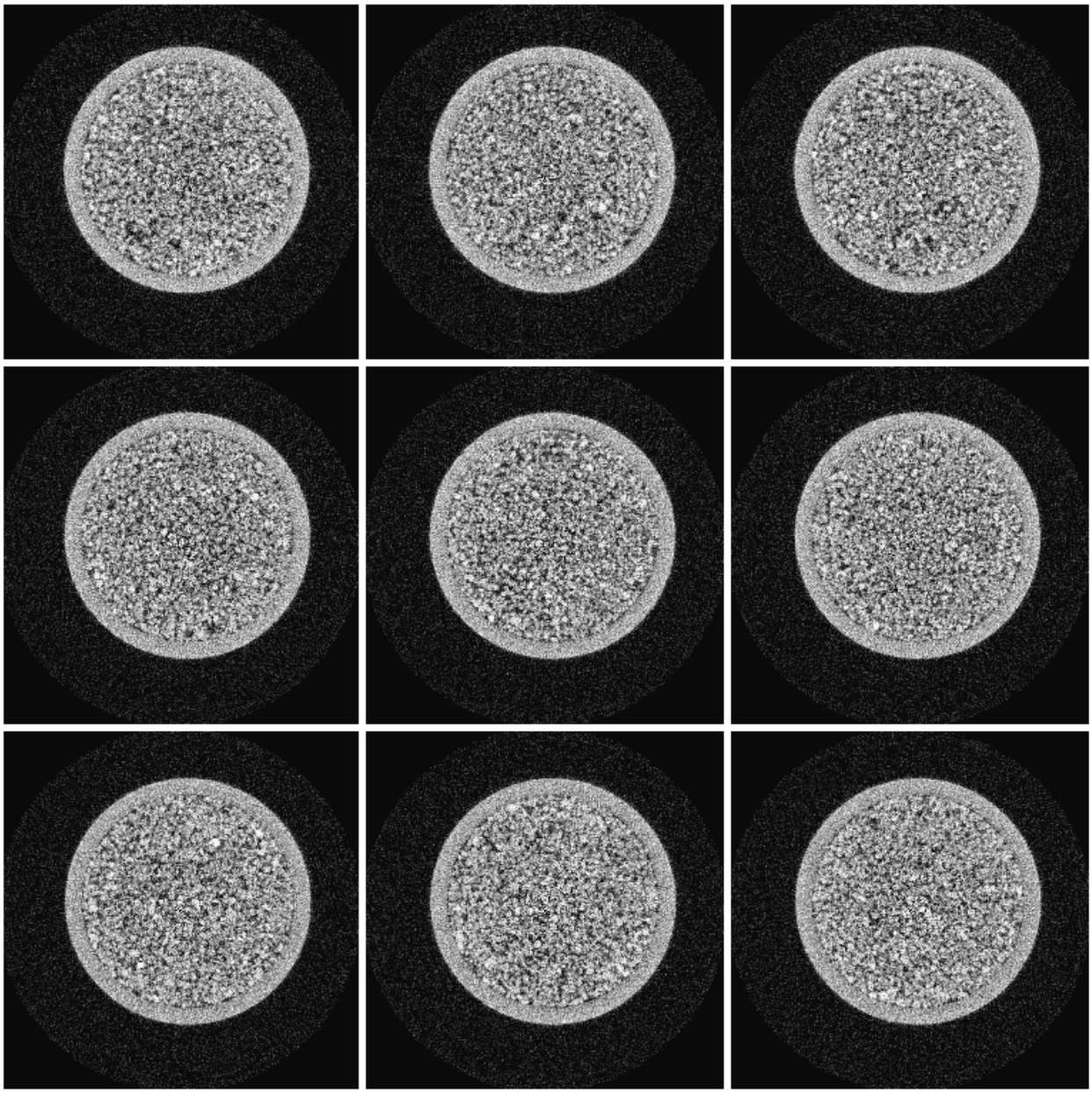

Figure 4-2: Coarse Sand soil CT scans - set #1. Row 1: top of sample; Row 2: middle of sample; Row 3: bottom of sample; spacing between scans in each row is 1.5 mm.

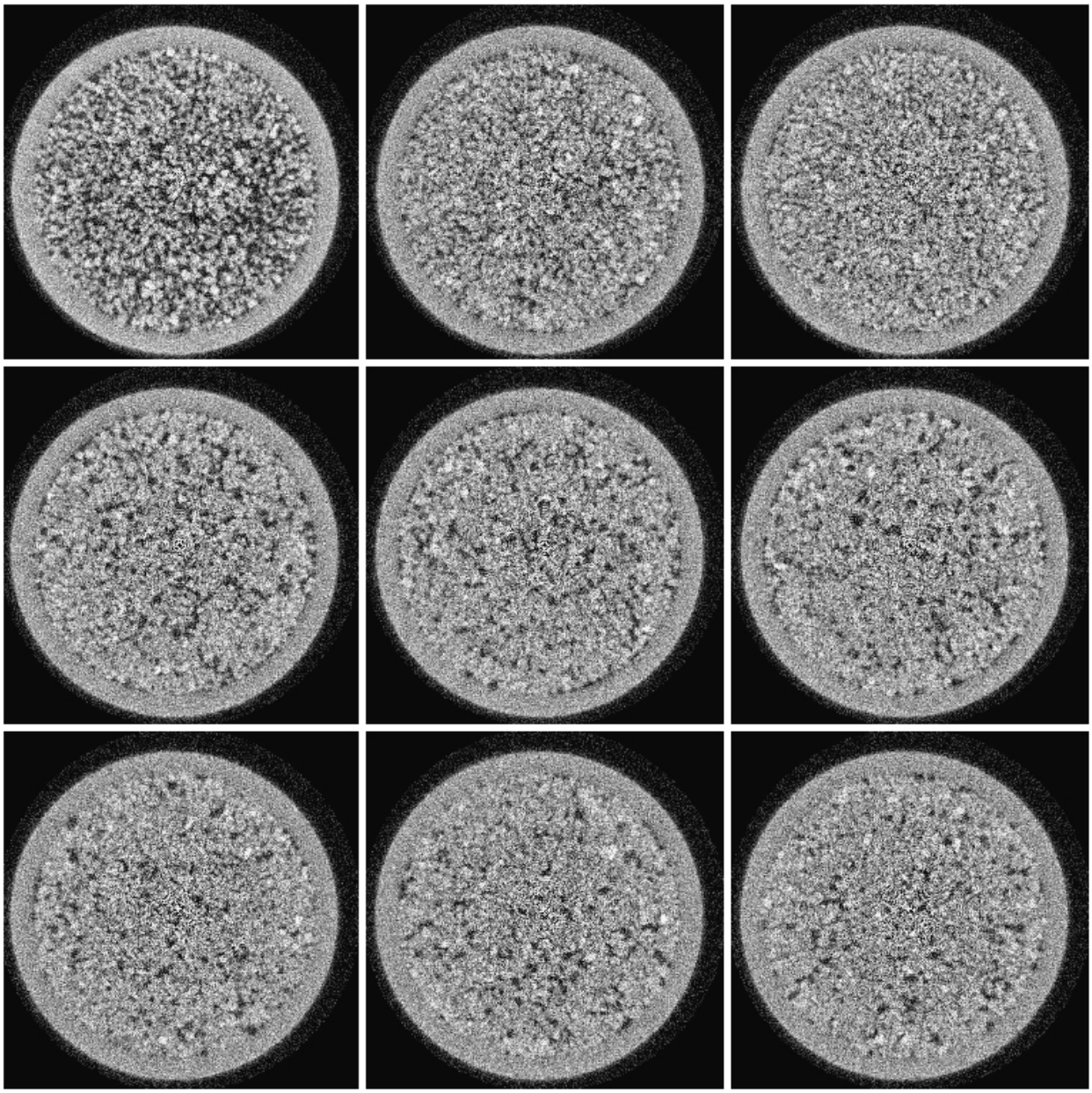

Figure 4-3: Coarse Sand soil CT scans - set #2. Row 1: top of sample; Row 2: middle of sample; Row 3: bottom of sample; spacing between scans in each row is 1.5 mm.

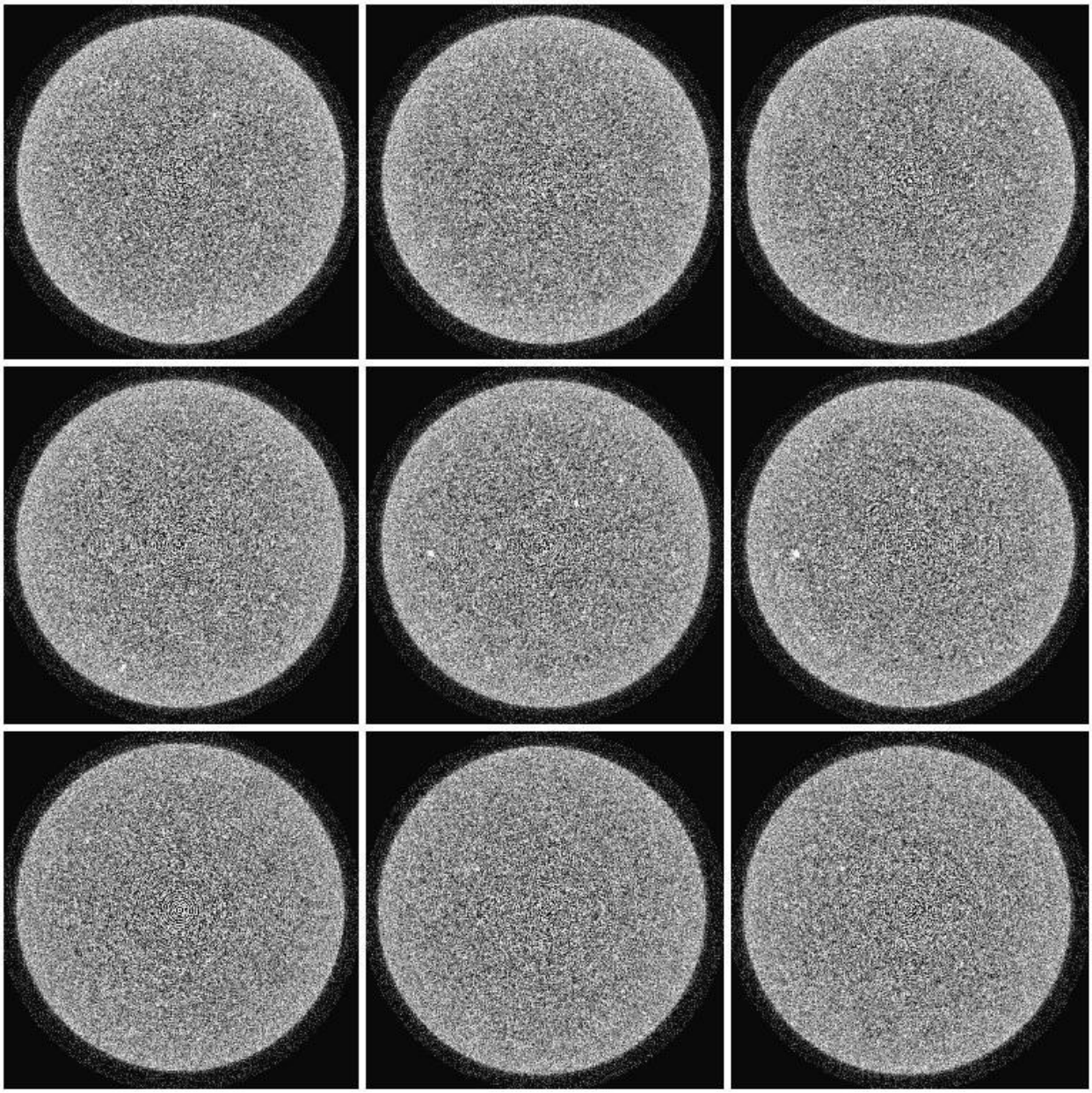

Figure 4-4: Medium Sand soil CT scans. Row 1: top of sample; Row 2: middle of sample; Row 3: bottom of sample; spacing between scans in each row is 0.6 mm.

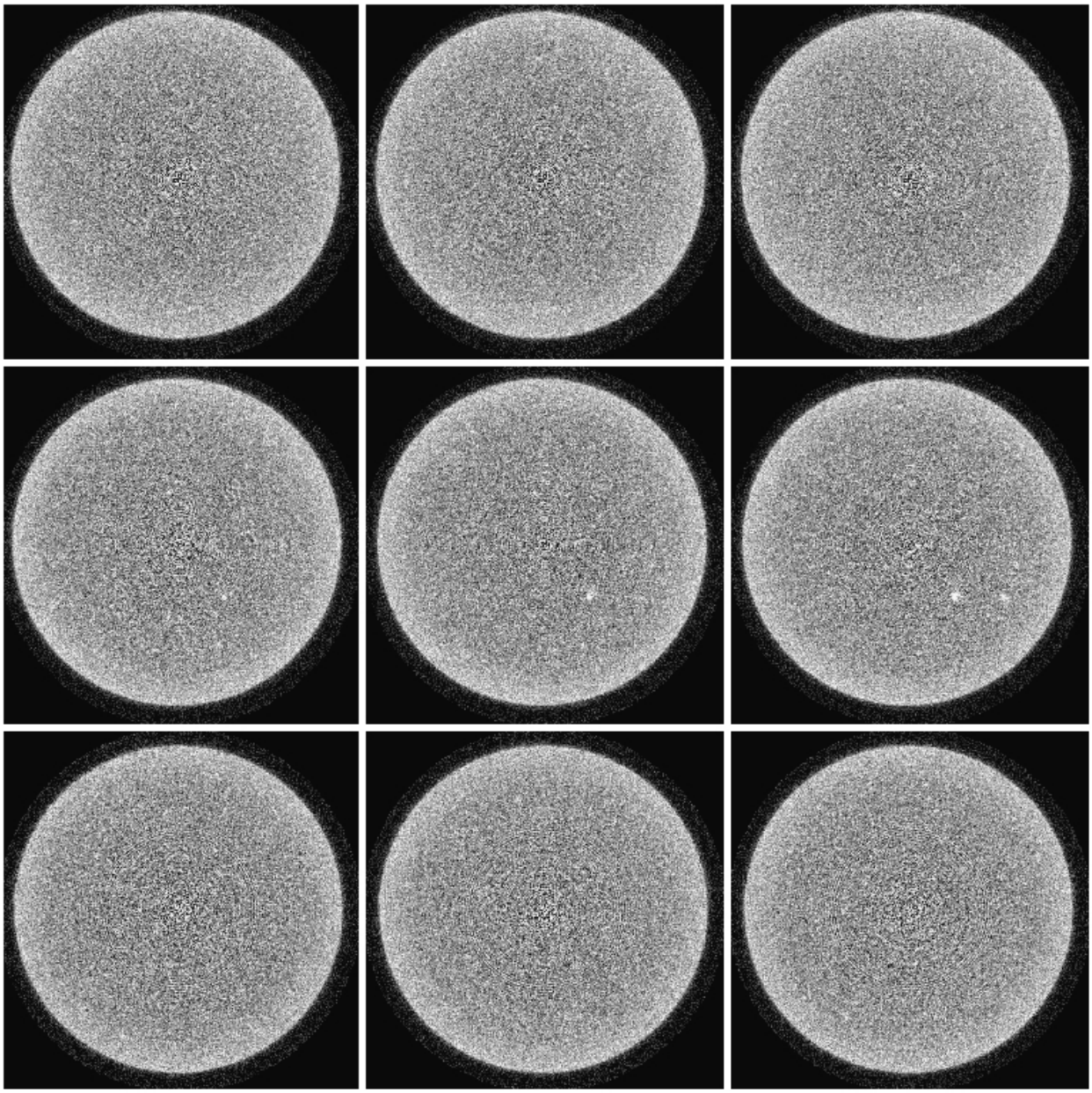

Figure 4-5: Fine Sand soil CT scans. Row 1: top of sample; Row 2: middle of sample; Row 3: bottom of sample; spacing between scans in each row is 0.25 mm.

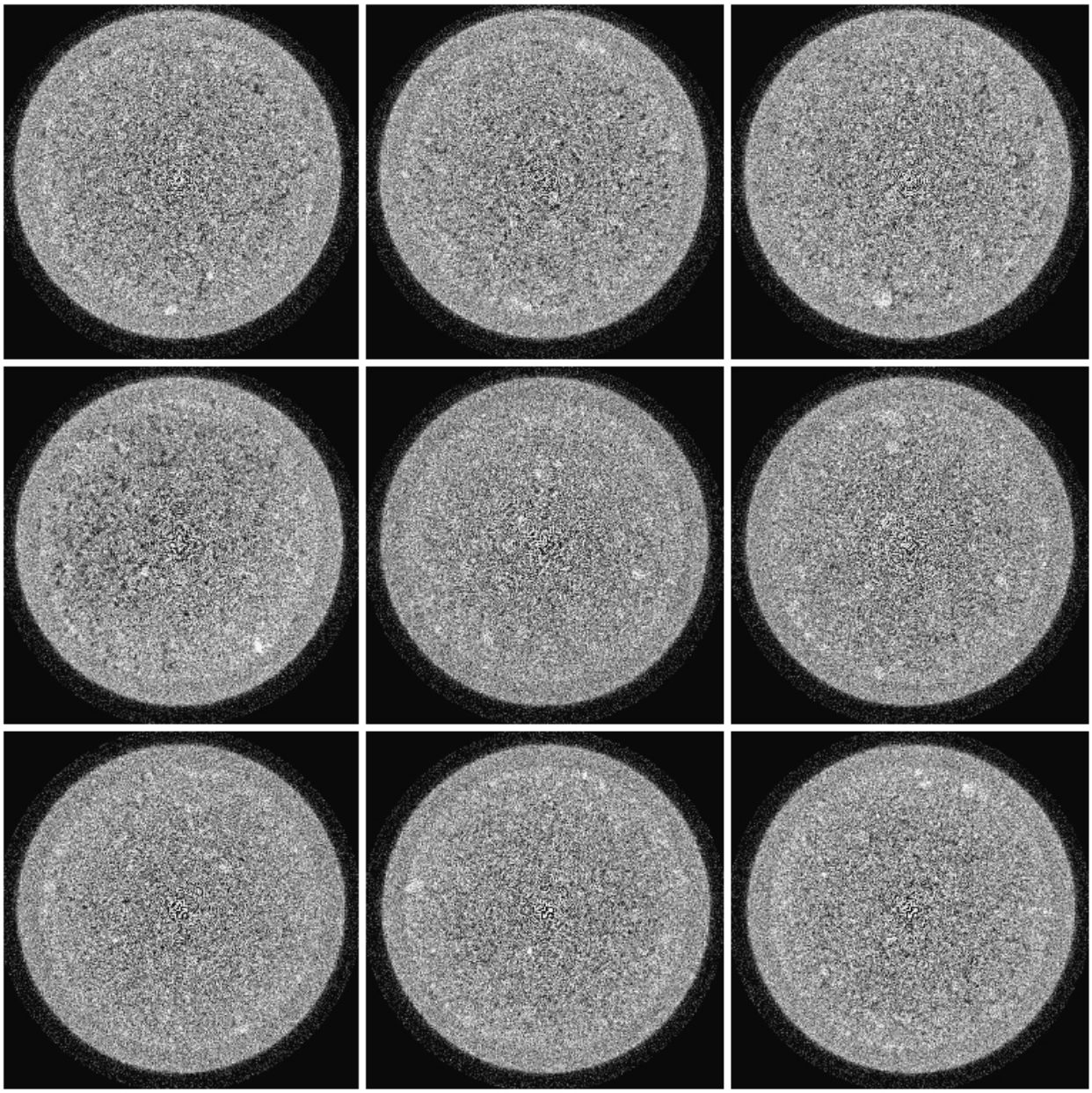

Figure 4-6: Concrete Sand soil CT scans. Row 1: top of sample; Row 2: middle of sample; Row 3: bottom of sample; spacing between scans in each row is 1.5 mm.

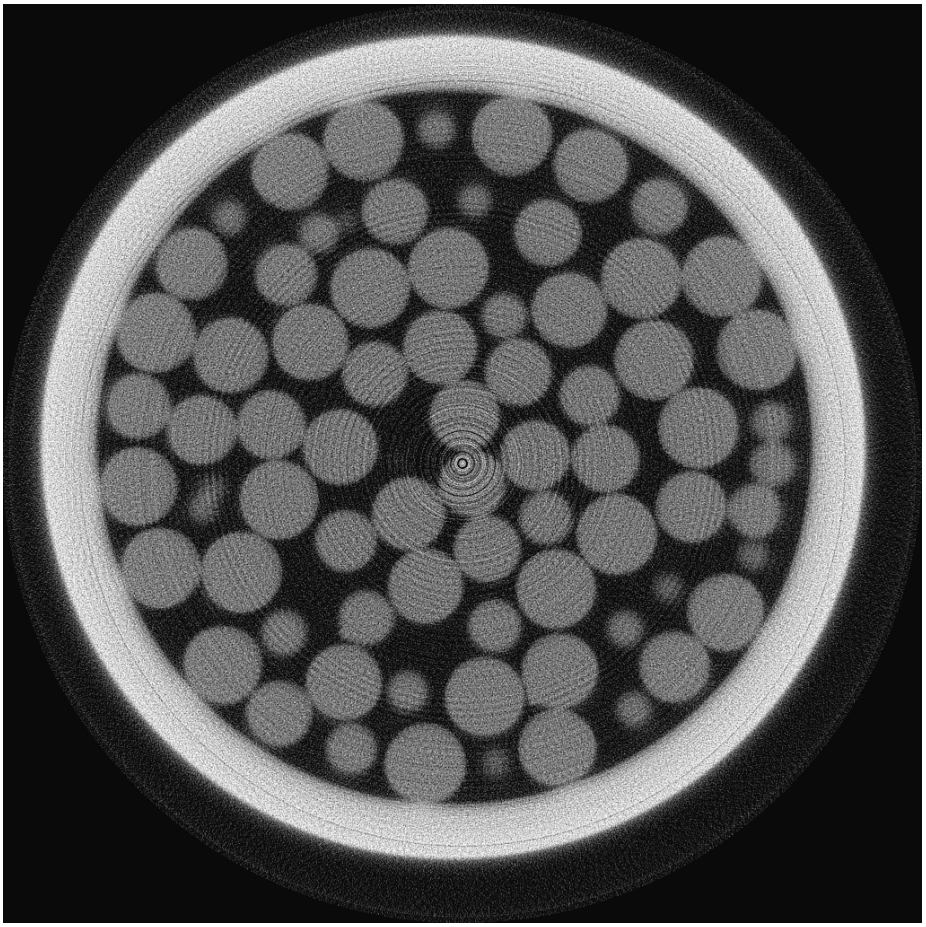

Figure 4-7: CT scan of uniform plastic beads.

The results of this portion of the project show the capabilities of the MSU CT scanner to produce high-quality CT scan images. The CT images of large-particle materials; for example, Figure 4-1 of the Gravel soil and Figure 4-7 of the uniform plastic beads, appear very clear, and individual particles can be distinguished easily. Without changing the container size or the CT camera settings, one can still distinguish individual particle shape in even the finer-grained materials. However, as the particles get smaller; for example, in Figure 4-4 (Medium Sand) and Figure 4-5 (Fine Sand), individual soil particles begin to blend together. This occurs because the CT camera is limited by its digital resolution. The camera can only distinguish between features that are larger than a single pixel. In most of the CT scans completed for this project, the image scale is approximately 0.06 mm per pixel. The Fine Sand material contains soil particles that are as small as 0.177 mm. Particles in this size range begin to "bleed" together in the CT scan images and are not individually distinguishable. The resolution of soil CT scans may be improved in several ways, including using a smaller scan rotation increment, using smaller soil sample containers, and using a high-resolution x-ray converting screen. These options are discussed in more detail in the following paragraphs.

Improving Scan Resolution

A common approach for increasing CT scan resolution is to reduce the scan rotation increment, resulting in more x-ray images which contribute to the final scanned image. The MSU CT scanning software allows scans of 2-, 1-, 1/2-, 1/4-, and 1/8-degree increment scans. This project used 1/4-degree scans, which took approximately two hours each. A

single 1/8-degree scan would take about four hours to complete. This adds significant time requirements to CT scanning, and the improved scan resolution may not be worth the expense. As an experiment, the same soils used here were scanned at lesser scan resolutions, and it was found that the resolution enhancements were generally not significant for rotation increments smaller than 1/2-degree. Thus, it was concluded that the 1/4-degree rotation increment was sufficient for this research, and using the 1/8-degree rotation increment option would likely not dramatically improve the scans.

Effects of Container Size

Another approach for improving the soil CT scan resolution is to use smaller diameter testing containers. The 2-inch PVC containers used in this project were chosen to minimize edge effects and to be representative of standard geotechnical samples that are obtained during subsurface investigations. Edge effects in soil testing occur when the walls of a container impose artificial constraints on particles. A large-diameter container will exert less influence on results than a small-diameter container. In addition to minimizing edge effects, it was desired that the soil samples scanned in this project simulate the samples used in many traditional geotechnical laboratory tests. Split-spoon and thin-walled Shelby tube samplers are the most common methods of retrieving soil samples in the field. Samples obtained during standard penetration tests (split spoon samples) are commonly about 1.5 inches in diameter, and Shelby tubes are available in 2- or 3- inch diameter sizes (Lowe 1975). Using 2-inch diameter soil sample containers for the CT scans was considered adequate to accommodate both desired criteria of reduced edge effects and traditional sampler similarity.

The same size container was used for all the soil scans for consistency in the test procedures and apparatus.

Another method of choosing sample size would be to base the container size on the largest particle diameter in the soil sample. The ratio of container diameter to maximum particle diameter could be set to a constant (or minimum value), and the container sizes would vary between soil types. Large-particle soils would be scanned in large containers, and small-particle soils would use smaller containers. Using smaller containers requires a smaller field of view in the CT process, and the camera could be moved closer to the x-ray converting screen. The camera's digital image size is constant for all fields of view, but the image scale varies as the camera moves. Moving the camera closer would thus improve the resolution of fine-particle soils. However, the camera-moving and focusing procedures in the MSU CT scanner are time-consuming, trial-and-error efforts. Moving and focusing the camera and lens often to accommodate several container sizes would slow the scanning process significantly.

Screen Replacement

A third option that could possibly improve images from the MSU CT scanner would be to use a slower-speed phosphor screen. Slow-speed screens provide higher resolution at the expense of long x-ray exposure times, and so are not used often for most medical x-rays because of the risk of tissue damage from prolonged x-ray exposure. Although not as common as fast screens, slow-speed phosphor screens are manufactured for x-rays of small bones, joints, and other complex body features. Objects scanned in the MSU CT scanner

typically are not affected by long x-ray exposure times, so using a slow screen theoretically poses no problem for the system. However, the company that manufactured and installed the MSU CT scanner had never used screens other than the Trimax4 material that was originally installed with the scanner. The scans for this project were made using a Trimax4-equivalent screen, and at this writing slower screens have not been tested with the MSU CT scanner. At least from a conceptual perspective, using a different screen would be feasible.

Soil Porosity Results

Soil porosity is defined as the ratio of void volume to total volume in a soil sample (Holtz and Kovaks 1981). Using CT scanning to measure a three-dimensional property like porosity assumes that a two-dimensional cross-section of the soil provides an appropriate representation of the complex three-dimensional nature of soils. This practice of determining volumetric parameters from cross-sectional area properties is relatively common and accepted practice for many situations (Russ 2002).

In this study, the porosities of five different soil types were measured using the CT scanning procedure and traditional laboratory methods described earlier. Each soil was measured using three groups of three CT scans each. The scan groups were located near the top, middle, and bottom of the soil samples, and the individual scans within each group were spaced according to the maximum particle size of the soil. The resulting scan images were processed to calculate porosity, and these values were compared to the bulk porosity value measured using traditional mechanical means in the lab. The porosity results are shown in Figure 4-8 and in tabular form in Table 4-1.

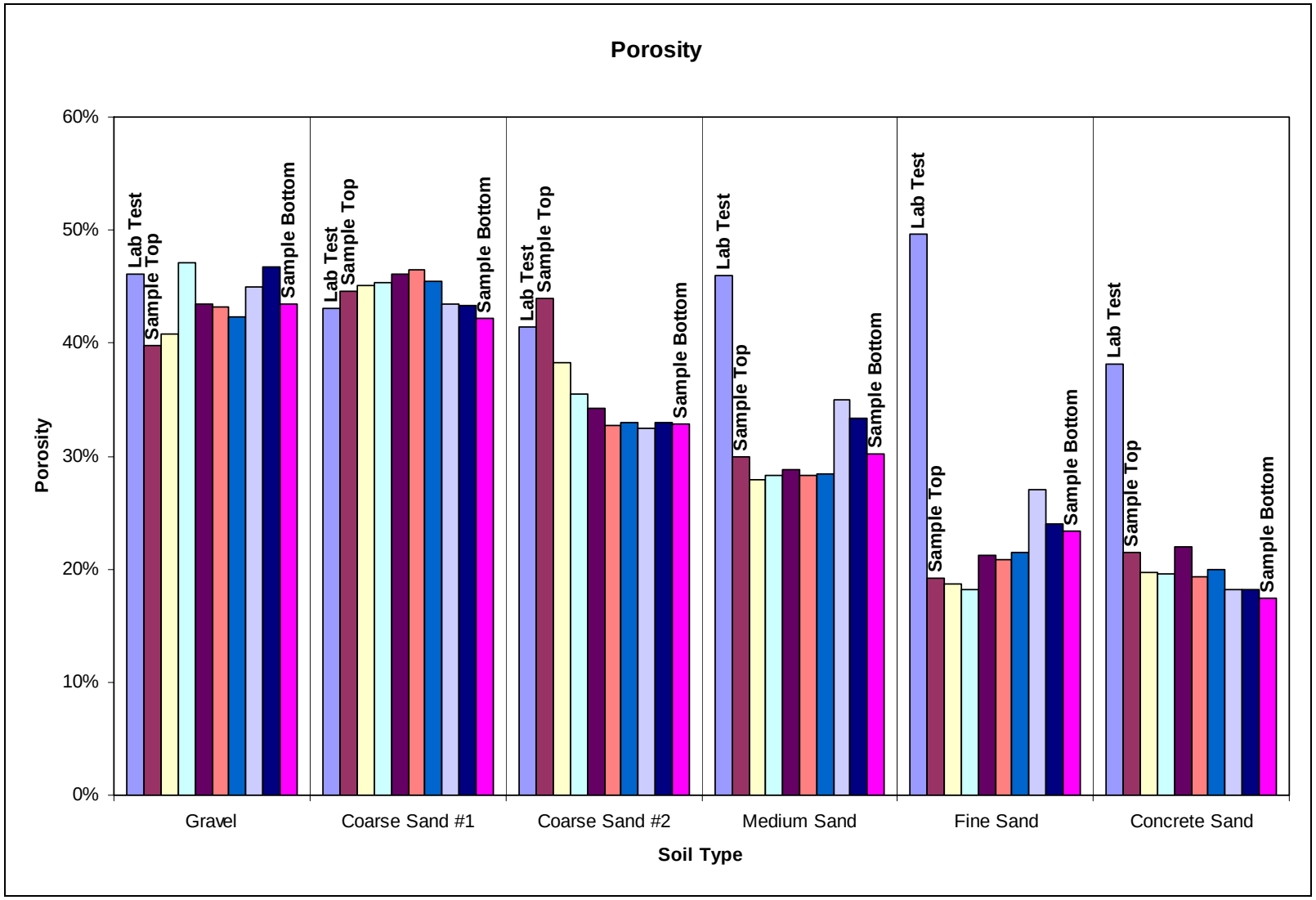

Figure 4-8: Porosity test results comparing CT testing methods with traditional laboratory procedures.

Soil Type	Gravel	Coarse Sand (#1)	Coarse Sand (#2)	Medium Sand	Fine Sand	Concrete Sand
Measured Porosities:						
CT 1-1	39.83%	44.62%	43.91%	29.93%	19.18%	21.48%
CT 1-2	40.80%	45.13%	38.29%	27.97%	18.67%	19.65%
CT 1-3	47.16%	45.30%	35.44%	28.33%	18.13%	19.61%
CT 2-1	43.48%	46.16%	34.23%	28.75%	21.23%	21.95%
CT 2-2	43.25%	46.52%	32.71%	28.28%	20.89%	19.30%
CT 2-3	42.34%	45.43%	33.02%	28.41%	21.48%	19.91%
CT 3-1	44.93%	43.44%	32.41%	35.04%	27.03%	18.14%
CT 3-2	46.75%	43.38%	32.95%	33.38%	23.94%	18.19%
CT 3-3	43.44%	42.21%	32.81%	30.22%	23.35%	17.46%
CT Average	43.55%	44.69%	35.08%	30.03%	21.54%	19.52%
Laboratory Tests:						
Average Specific Gravity	2.69	2.62	2.62	2.63	2.63	2.61
Average Water Content	6.42%	8.10%	12.57%	16.57%	14.82%	19.29%
Bulk Density (g/cm^3)	1.54	1.61	1.72	1.65	1.52	1.93
Bulk Porosity	46.08%	43.05%	41.41%	46.02%	49.61%	38.10%

Table 4-1: Porosity test results comparing the CT-measured results to the laboratory-measured results.

.

The porosity measurements show the effects of the resolution limits of the MSU CT scanner. The porosity values from the Gravel and Coarse Sand soil CT scans are relatively constant across the length of the sample. As shown in Table 4-1, The CT-measured porosity values for the coarser materials are also very close to the measured average porosity of the samples, which helps to verify the image processing methods used. As the soil particles decrease in size, for instance, the Fine Sand and Concrete Sand materials, the distinction between individual particles decreases, the scan images become somewhat blurry, and the calculated image porosity values deviate significantly from the laboratory-measured sample porosities. The sample porosities were determined in the laboratory by using Equation (3-3). Laboratory tests were used to measure specific gravity, bulk density, and water content. The image porosity measurement procedure works well for high-quality images, as shown in the Gravel and Coarse Sand scans. As image quality decreases, so does the accuracy of the porosity calculation. The method for measuring and computing porosity for the more coarse-grained soils works well and agrees with standard techniques. Consequently, improving the quality of CT scan images for fine-grained soils would likely result in more accurate porosity measurements using the image processing method described herein.

Another potential source of error in the image porosity measurements may be the thresholding image processing step, which is used to differentiate between solid and void space in the scan. The thresholding level for each image was chosen as the pixel intensity value that most completely isolated the solid space. Using too high of a threshold value could incorrectly classify additional void space as solid (resulting in lower porosity), and too low of a threshold value could miss-classify some solid space as void (higher porosity). The

selection of a “correct” threshold value is somewhat subjective, but care was taken in this study to consistently use a threshold value that minimized the misinterpretation of solid and void spaces.

Grain Size Distributions

CT scans of the five soil types were also analyzed to determine the size distribution of the soil particles. Two size distribution calculation steps are required in order to develop a grain size distribution from a two-dimensional cross-section image. The first, called granulometry, is an image processing technique used to determine the two-dimensional size distribution of particle cross-sections from a CT scan image. The second procedure, known as stereology, combines topics from geometry and statistics to develop a three-dimensional size distribution from information obtained from cross-section scans. The grain size distributions calculated from CT scans of each soil type were averaged and compared to the distributions determined using laboratory mechanical sieve analysis methods (ASTM D421 and D422). The Gravel, Coarse Sand, Medium Sand, and Fine Sand materials were uniformly-graded soil materials and were manufactured by isolating soil particles whose sizes fell between consecutive sieves. Thus, measuring the exact grain size distribution of the uniformly-graded soils was not possible using standard sieves. Since the largest and smallest possible particles were known for each material, normal distributions were used to approximate equivalent size distributions. The average grain size between consecutive sieves was used as the mean grain size of the uniform-graded soil whose particles fell between the two sieves. The standard deviations of the normal distributions were found with the “three-

sigma rule." That is, in a normal distribution, 99.7 percent of all values lie within three standard deviations on either side of the mean. In this case, the standard deviation of the normal distribution was found by dividing the size range between consecutive sieves by six. For example, the Coarse Grain material consisted of particles between the #10 (2.00 mm) and #20 (0.85 mm). Thus, the Coarse Sand grain size distribution was approximated with a normal size distribution with a mean of 1.43 mm and a standard deviation of 0.192 mm. The grain size distributions calculated by both the CT scanning and the laboratory techniques are shown in Figure 4-9 through Figure 4-14.

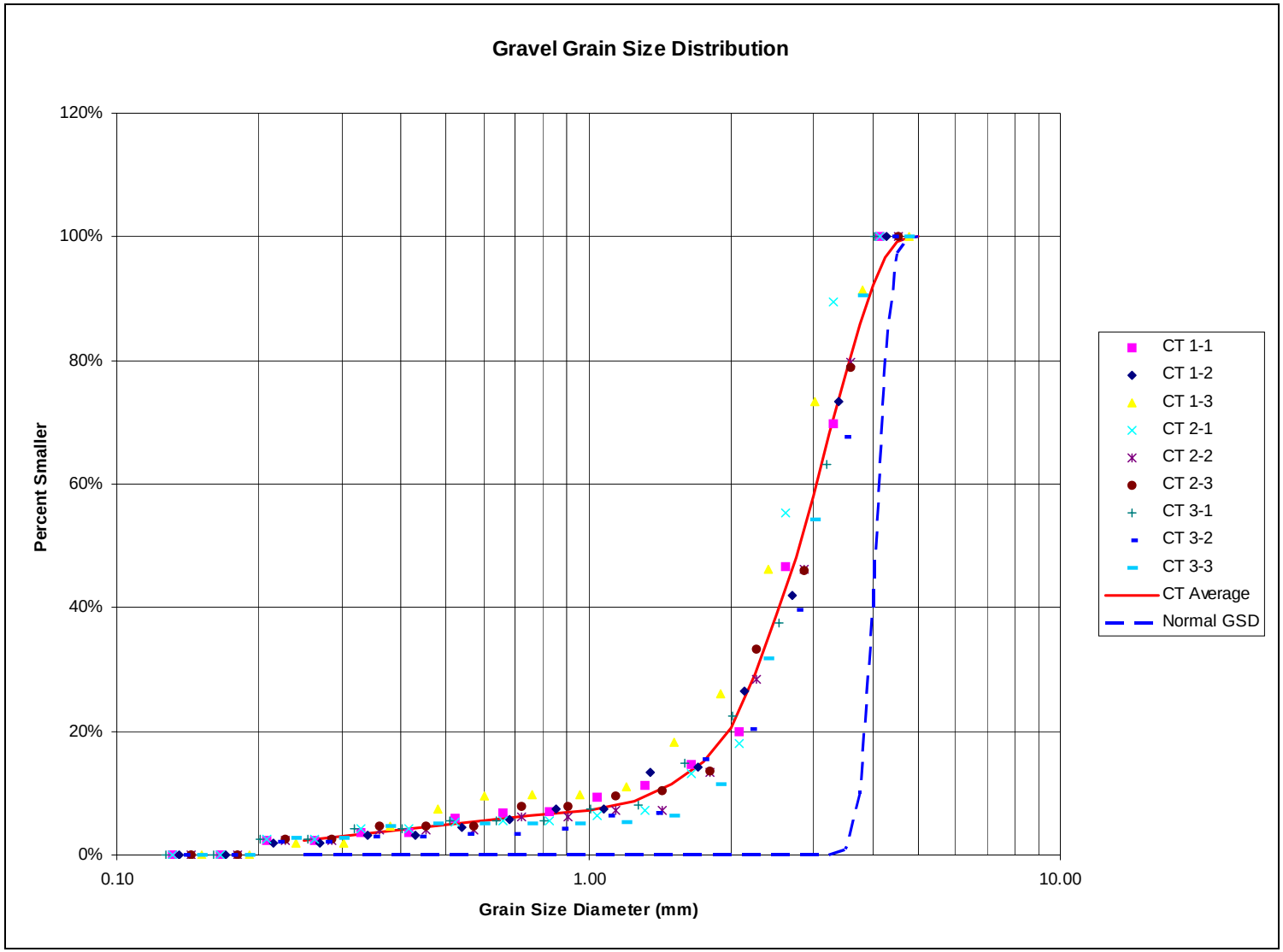

Figure 4-9: Grain size distribution for the Gravel soil.

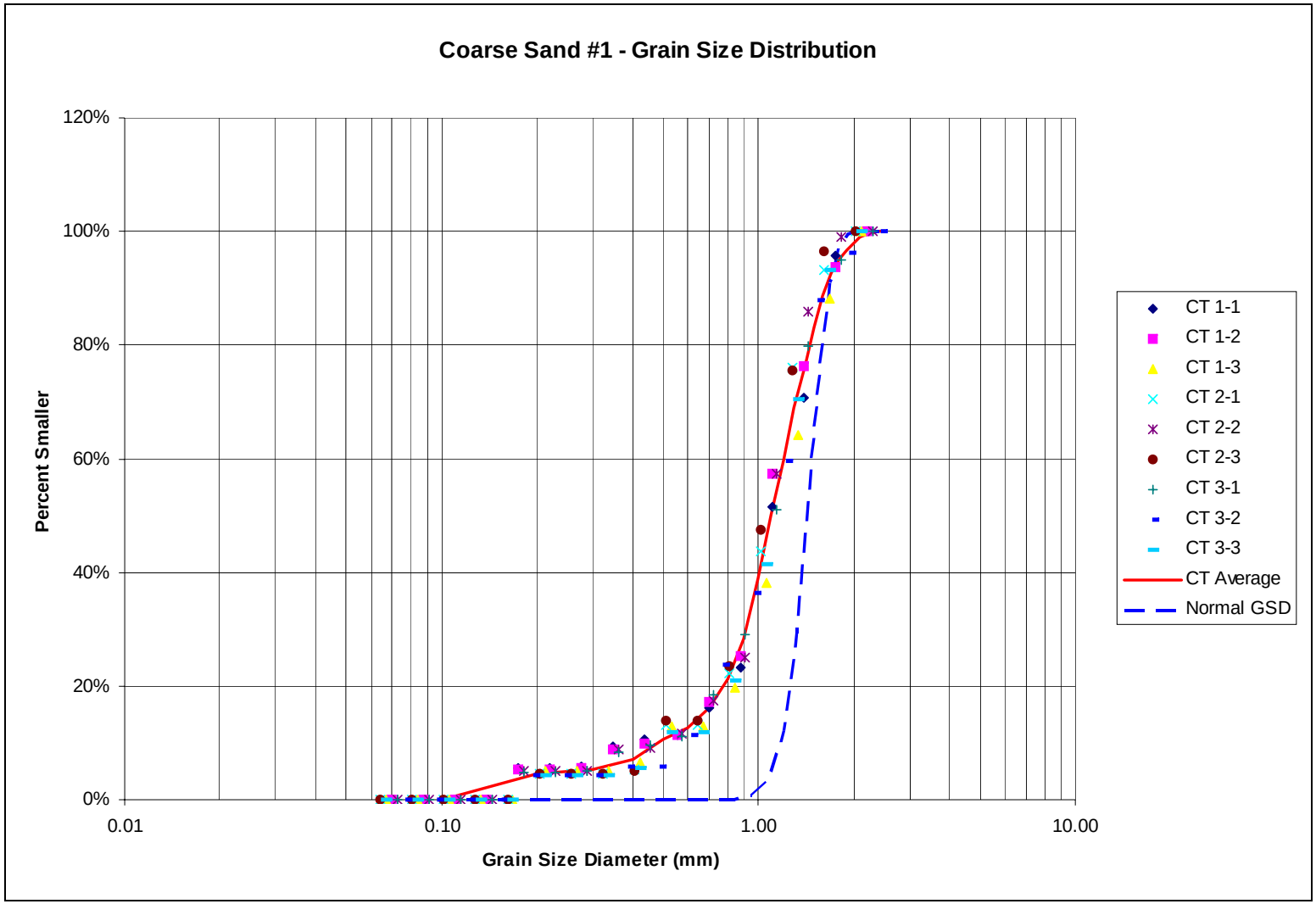

Figure 4-10: Grain size distribution #1 for the Coarse Sand soil.

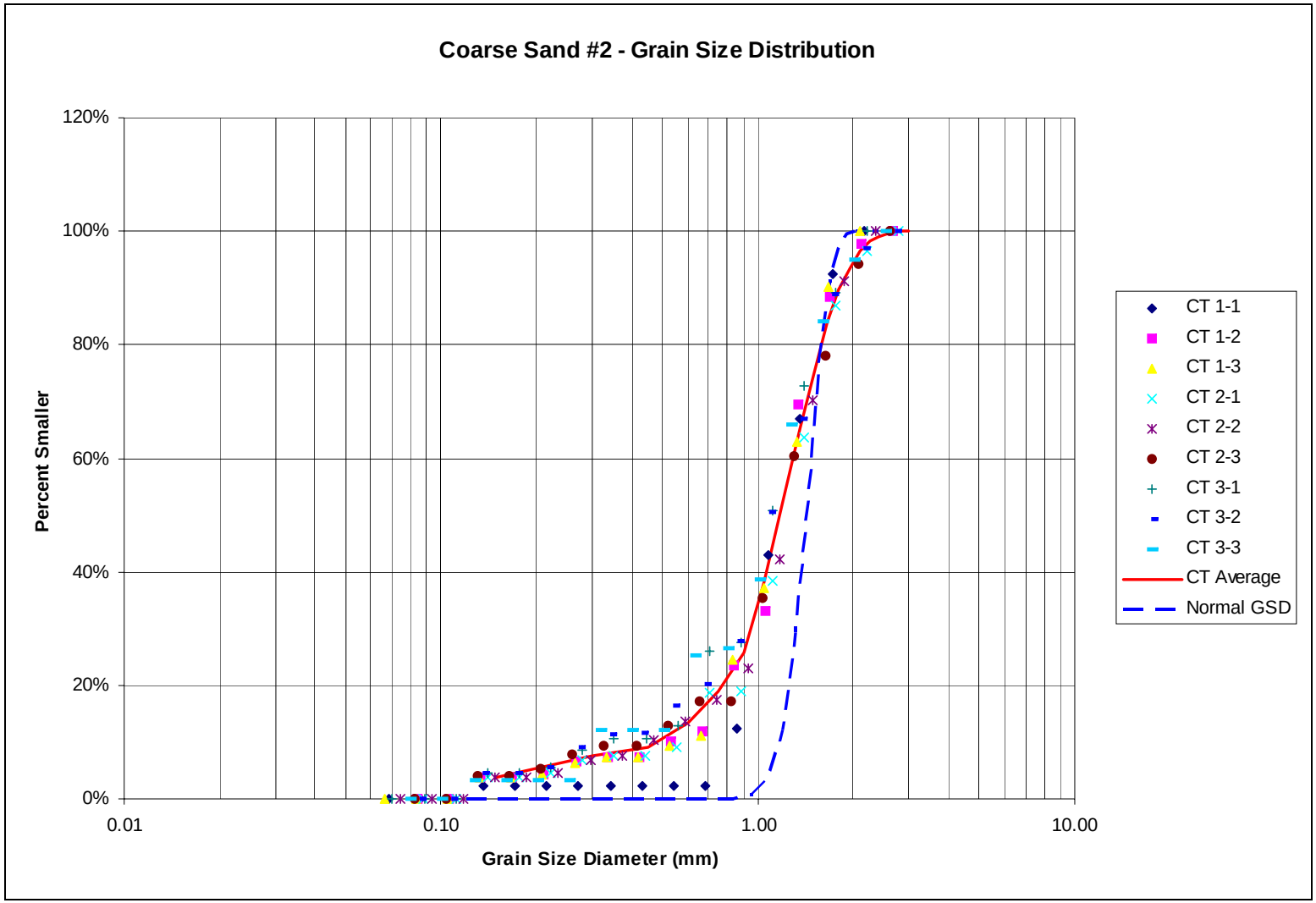

Figure 4-11: Grain size distribution #2 for the Coarse Sand soil.

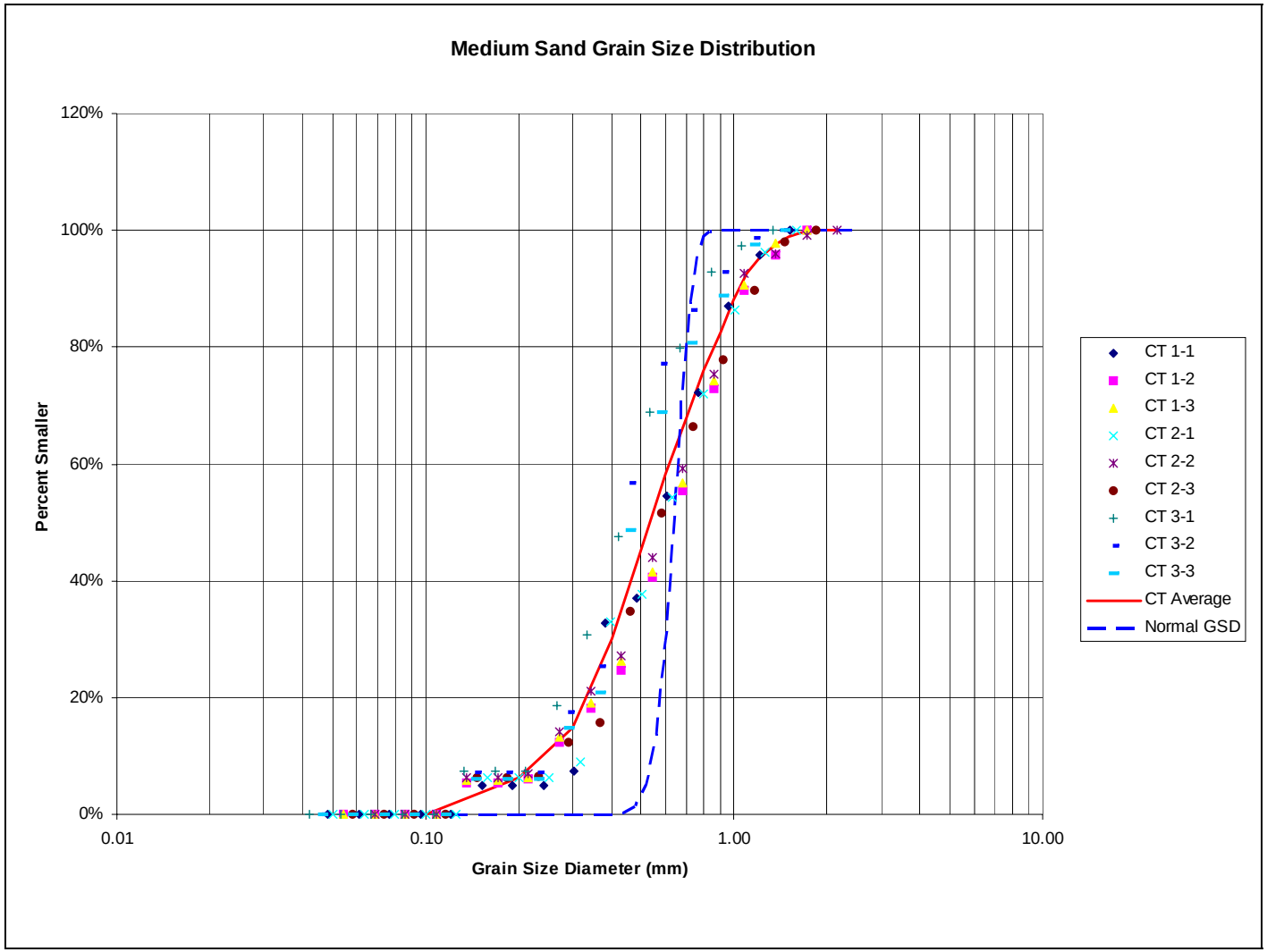

Figure 4-12: Grain size distribution for the Medium Sand soil.

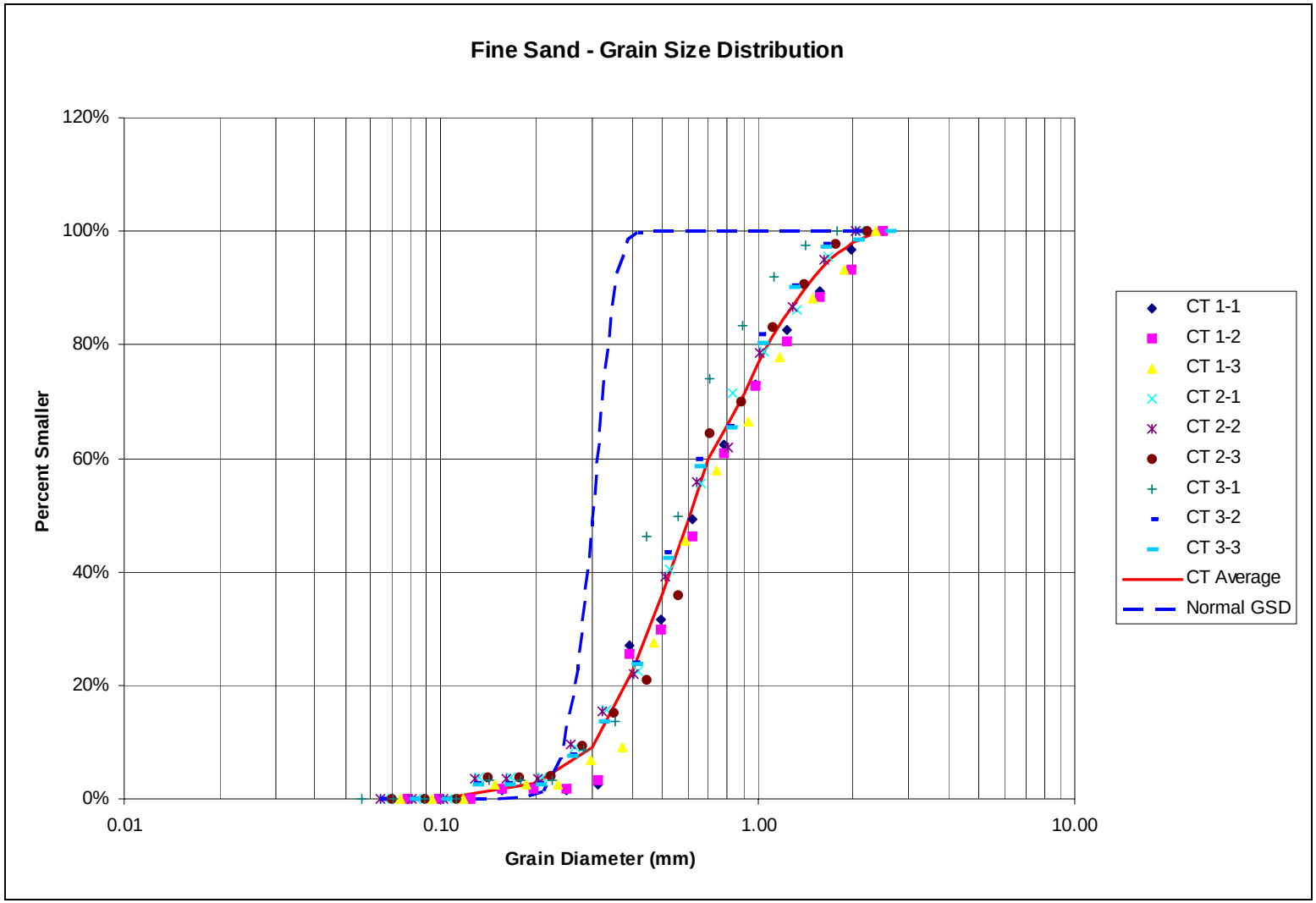

Figure 4-13: Grain size distribution for the Fine Sand soil.

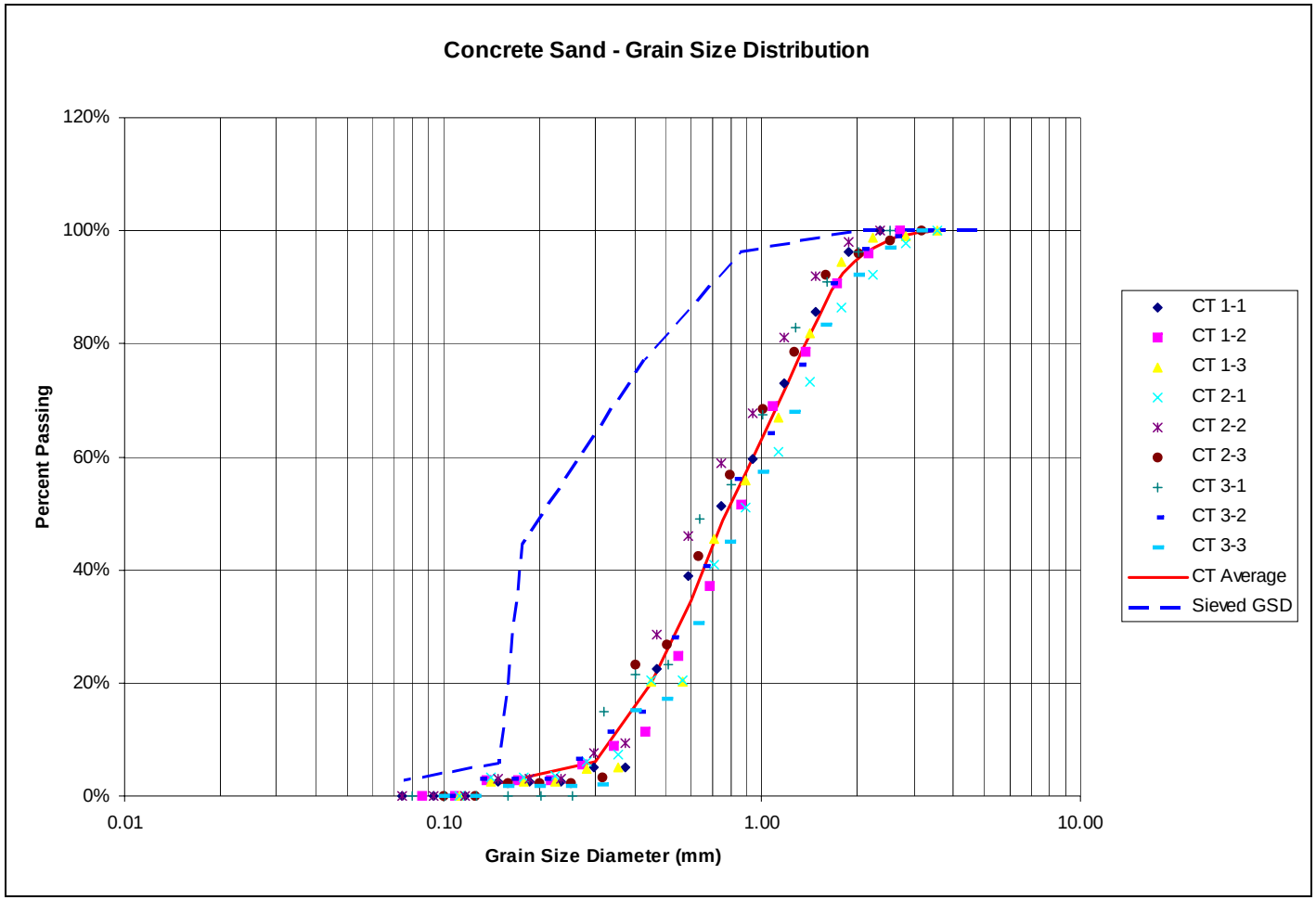

Figure 4-14: Grain size distribution for the Concrete Sand soil.

Similar to the porosity results, the higher resolution images yielded more precise results. Calculated grain sizes determined from CT images of the smaller particle soil samples are generally larger than the sieve-measured grain sizes. This occurs when individual soil particles are indistinguishable in the CT images. In this case, a group of small particles may appear as a single, solid grain. This is particularly evident in the Fine Sand scans, because the outer portions of the scans tended to bleed together and became blurry. During the granulometry step, the blurred sections of the soil cross-section are treated as large homogenous grains; therefore, the computed grain size is inflated in these regions of the cross-section. This erroneous excess of larger particles sizes shifts the cumulative grain size distribution curve to the right. This trend can be observed in the grain size distributions shown in Figure 4-13 (Fine Sand), Figure 4-14 (Concrete Sand), and to some degree, Figure 4-12 (Medium Sand).

Interestingly, the CT measurements of the coarse-grained soils underestimated the actual grain sizes. This is attributed to digital pixel noise and particle shape. Some background pixel noise in the form of either small dots or rings is present in each of the CT scan images. A portion of the small dots are easily removed from digital images with a median filtering process known as despeckling, but ring artifacts are more persistent and difficult to eliminate. Rings are common artifacts in the CT process and are generally caused by abnormal x-ray penetrations that are converted to rings during the reconstruction process. Attempts in this project to reduce the rings were unsuccessful, but some advanced image processing methods to remove them have been developed (Sijbers 2004). The ring artifacts

may divide some of the larger grains into smaller sections, which could be treated as individual small particles in the granulometry steps.

Particle shape may also contribute to some of the particle size discrepancies observed between mechanical sieve analysis and CT scan analysis. The granulometry image processing procedure that was used to estimate particle sizes from a digital image is based on the assumption that the particles in the CT scan images are spherical. Granulometry is a digital image processing procedure consisting of a series of openings. A single opening causes small particles to be removed from the image. An estimate of the image area consisting of small particles can be made by counting how many pixels were removed from the image by the opening. Each successive opening removes larger particles, so a series of openings can describe the size distribution of objects in the digital image. A CT scan image shows cross-sections through a soil sample, so the granulometry process describes the distribution of particle cross-sections contained within the soil sample cross-section. In this study, the particle cross-sections were assumed to be circular during the granulometry procedure. Figure 4-15 shows the effect of the circular granulometry assumption on an elongated particle cross-section.

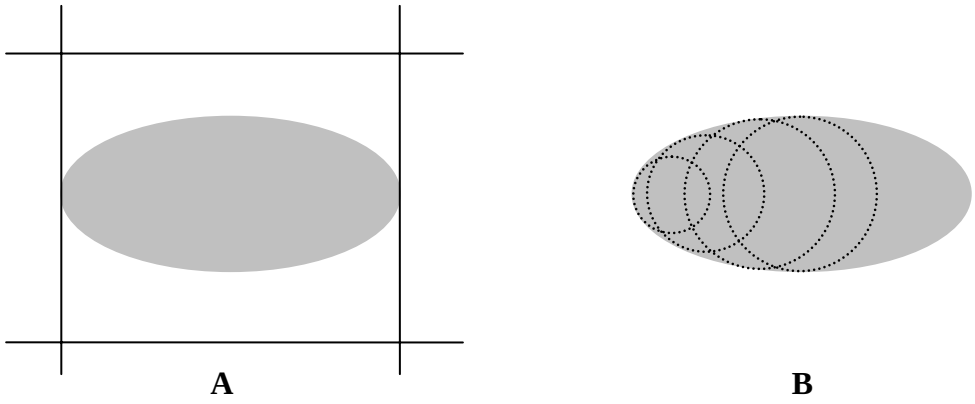

Figure 4-15: Elongated particle size measured in a sieve (A) and by the circular granulometry procedure (B).

The result of the circular assumption is that elongated particles are modeled in the digital image as groups of smaller spherical particles based on their smallest dimension. However, in a laboratory sieve analysis, the same particle would be measured by its longest dimension. Invoking the spherical shape particle assumption shifts the CT-measured grain size distribution curve to the left because non-spherical particles are modeled as groups of smaller particles, as illustrated in Figure 4-15. This effect is evident in the coarser particle size distribution comparisons in Figure 4-9 through Figure 4-11

Uniform plastic beads were used to determine the effect of the spherical particle shape assumption on the granulometry and stereology size determination procedures. The CT scan of a sample of uniform plastic beads is shown in Figure 4-7, and the stereological size distributions calculated from the CT image are shown in Table 4-2. The calculated particle size distribution is shown in the two columns on the right edge of Table 4-2.

Class #	Class Upper Normalized	Class Upper Pixels	Class Lower Normalized	Class Lower Pixels	Transect Prob.	Sphere Alpha	Cross-Section Density	Particle Density	Adj. Particle Density	Cum. Particle Density	Adj. Particle Density	Diam (mm)
1	1.000	89.00	0.794	70.70	60.75%	1.646	74.52%	122.67%	122.67%	122.67%	100.00%	5.69
2	0.794	70.70	0.631	56.16	16.83%	0.456	7.76%	-21.22%	0.00%	0.00%	0.00%	4.52
3	0.631	56.16	0.501	44.61	8.95%	0.116	5.68%	-2.85%	0.00%	0.00%	0.00%	3.59
4	0.501	44.61	0.398	35.43	5.20%	0.041	1.95%	-3.37%	0.00%	0.00%	0.00%	2.85
5	0.398	35.43	0.316	28.14	3.13%	0.017	2.62%	1.15%	0.00%	0.00%	0.00%	2.26
6	0.316	28.14	0.251	22.36	1.93%	0.008	1.36%	-0.13%	0.00%	0.00%	0.00%	1.80
7	0.251	22.36	0.200	17.76	1.20%	0.004	0.96%	0.14%	0.00%	0.00%	0.00%	1.43
8	0.200	17.76	0.158	14.11	0.75%	0.002	0.63%	0.09%	0.00%	0.00%	0.00%	1.13
9	0.158	14.11	0.126	11.20	0.47%	0.001	0.41%	0.06%	0.00%	0.00%	0.00%	0.90
10	0.126	11.20	0.100	8.90	0.29%	0.000	0.98%	1.21%	0.00%	0.00%	0.00%	0.72
11	0.100	8.90	0.079	7.07	0.19%	0.000	0.00%	-0.59%	0.00%	0.00%	0.00%	0.57
12	0.079	7.07	0.063	5.62	0.12%	0.000	0.61%	0.83%	0.00%	0.00%	0.00%	0.45
13	0.063	5.62	0.050	4.46	0.07%	0.000	0.98%	1.27%	0.00%	0.00%	0.00%	0.36
14	0.050	4.46	0.040	3.54	0.05%	0.000	0.00%	-0.55%	0.00%	0.00%	0.00%	0.29
15	0.040	3.54	0.032	2.81	0.03%	0.000	1.54%	2.38%	0.00%	0.00%	0.00%	0.23
16	0.032	2.81	0.025	2.24	0.02%	0.000	0.00%	-0.76%	0.00%	0.00%	0.00%	0.18

Table 4-2: Stereological Size Distribution for the Uniform Plastic Beads CT Scan

As shown in Figure 4-7, the cross-sections of the spherical beads are exactly circles, and the image was much clearer than the fine-grained soil scans. Consequently, the image defects discussed with the porosity results likely did not affect the bead scan image calculations. Also, since the beads were uniform spheres, the shape assumption made for the granulometry size procedure holds true. The stereological particle size distribution from the beads image showed that all the cross-sections in the scan came from particles with sizes between 4.52 mm and 5.69 mm, as shown in the two columns on the right side of Table 4-2.

In addition to developing accurate distributions of particle sizes from the cross-sections, the image processing procedure was able to correctly measure the diameter of the beads. The stereological particle size class containing the bead cross-sections contained particles from 4.52 mm to 5.69 mm. The uniform beads were measured with a caliper, and their diameter was found to be approximately 5.85 mm. This control scan provided a suitable test confirming the validity spherical shape assumption, and it also validated the overall image processing procedures.

Pore Size Distribution

Grain size distribution is easy to measure in the laboratory as compared to pore size distribution. Consequently, it was assumed that if accurate grain size distributions could be developed non-destructively from the CT scans, then the corresponding pore size distributions should be relatively accurate. As shown in the coarser material grain size distribution curves in Figure 4-9 through Figure 4-11, the CT testing methods developed in this study are capable of measuring grain size distributions that compare well with accepted

mechanical laboratory procedures. Therefore, the same CT testing methods were considered adequate for testing pore size distributions as well.

By inverting the black-and-white thresholded CT scan images, the pore space is highlighted instead of the solid space. By using the same granulometry and stereology methods as used for the grain size distributions, pore size distributions from the inverted images can be calculated. As before, the primary assumption in this procedure is that the soil pores are spherical in shape. In reality, pores can have irregular three-dimensional shapes, and because of this quantifying pore size is extremely difficult – if not impossible. A number of approximate methods for quantifying pore size are available, and many of them use the assumption that each pore can be modeled as a bundle of capillary tubes (Duillen 1992). This model is believed applicable because pores commonly consist of a large central portion surrounded by small tapered "pore necks". The small pore necks are modeled as small capillary tubes, and the large central portions of the pores are modeled by large-diameter tubes. Consequently, the spherical-shape assumption required for granulometry and stereology may be reasonable in light of this commonly recognized capillary model for soil pores.

The pore size distributions calculated with the CT scanning method have been compared with a common pore size distribution model. This model, known as the Arya and Paris model, defines an approximate relationship between the measured grain size distribution and a calculated pore size distribution of soils (Arya and Paris 1981). Calculations in the Arya and Paris model are used to determine an approximate number of particles in each fraction of the grain size distribution, and estimate the pores created by

those particles. Pore size distributions for each of the six soil materials were determined using the CT scans and were compared with the calculated pore size distributions from the Arya and Paris method. These pore size results are shown in Figure 4-16 through Figure 4-21.

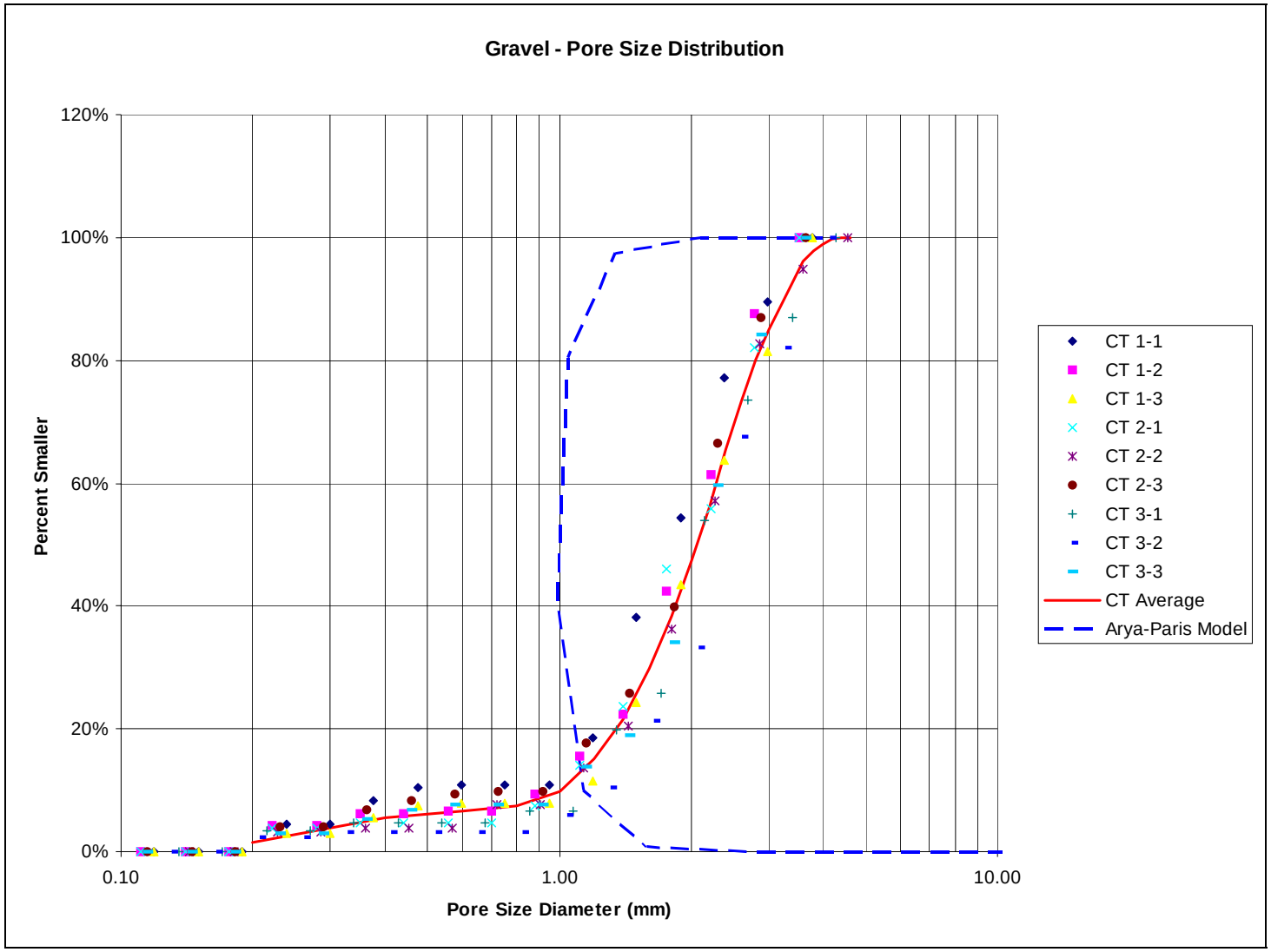

Figure 4-16: Pore size distribution for the Gravel soil.

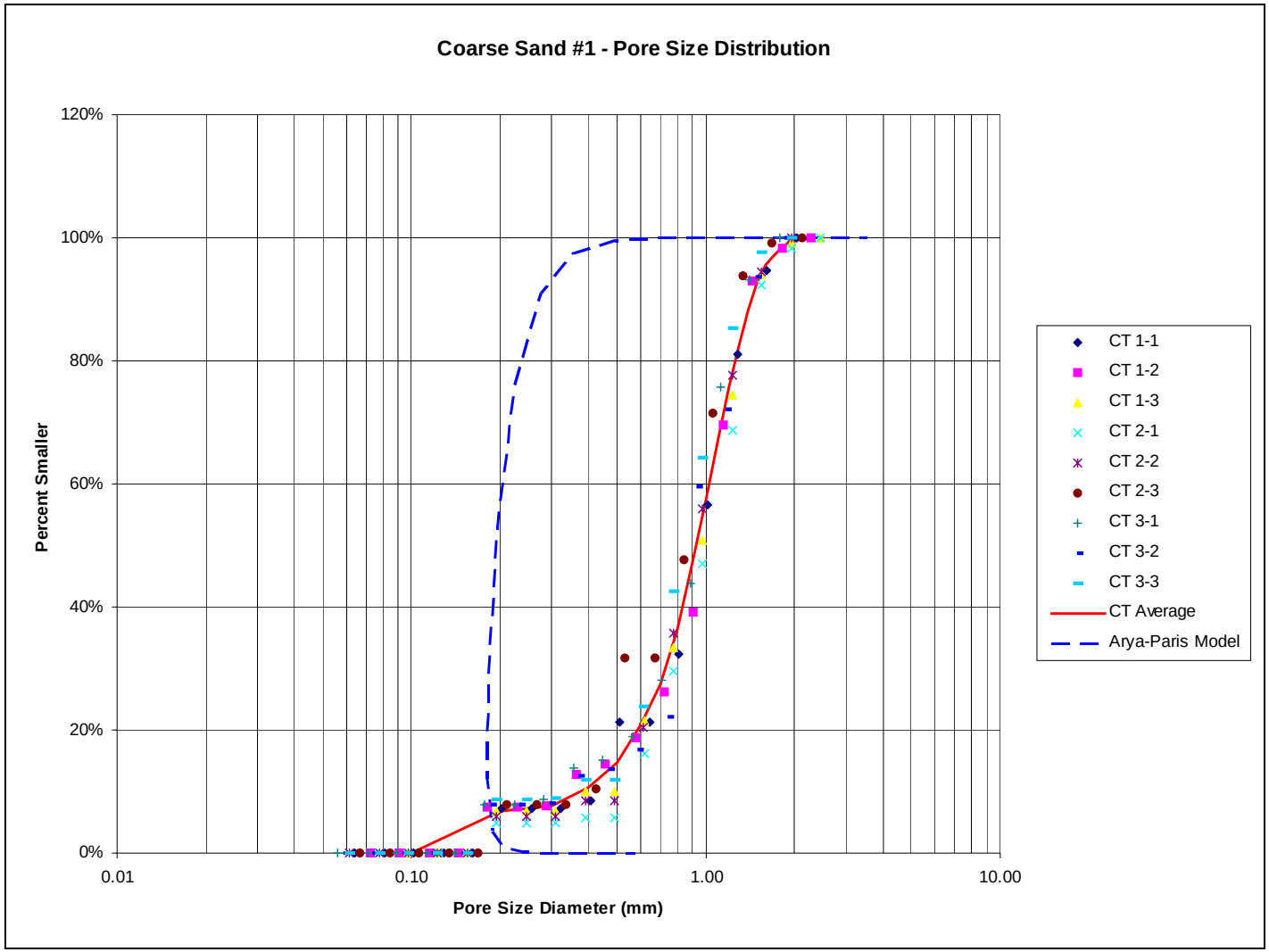

Figure 4-17: Pore size distribution #1 for the Coarse Sand soil.

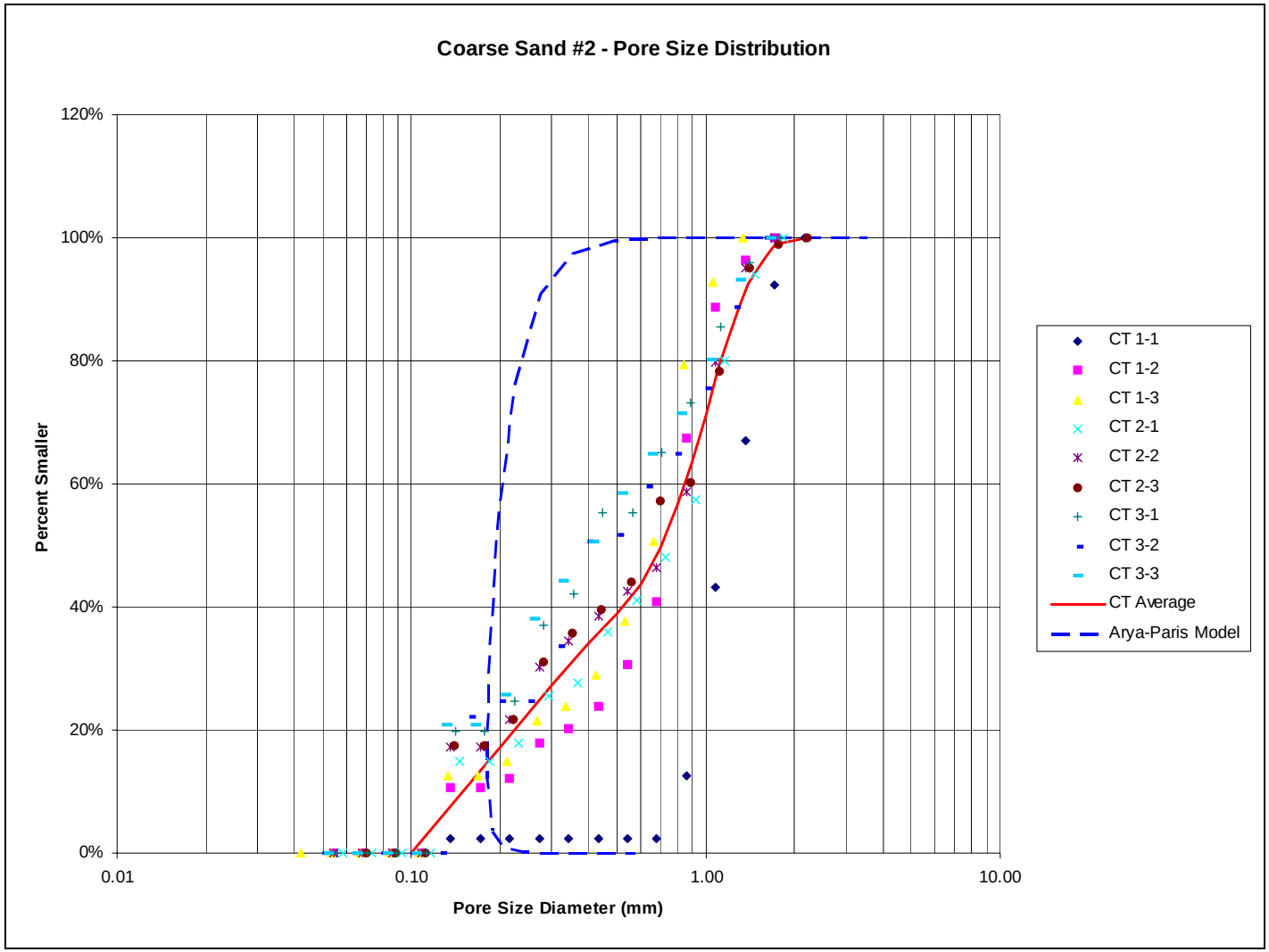

Figure 4-18: Pore size distribution #2 for the Coarse Sand soil.

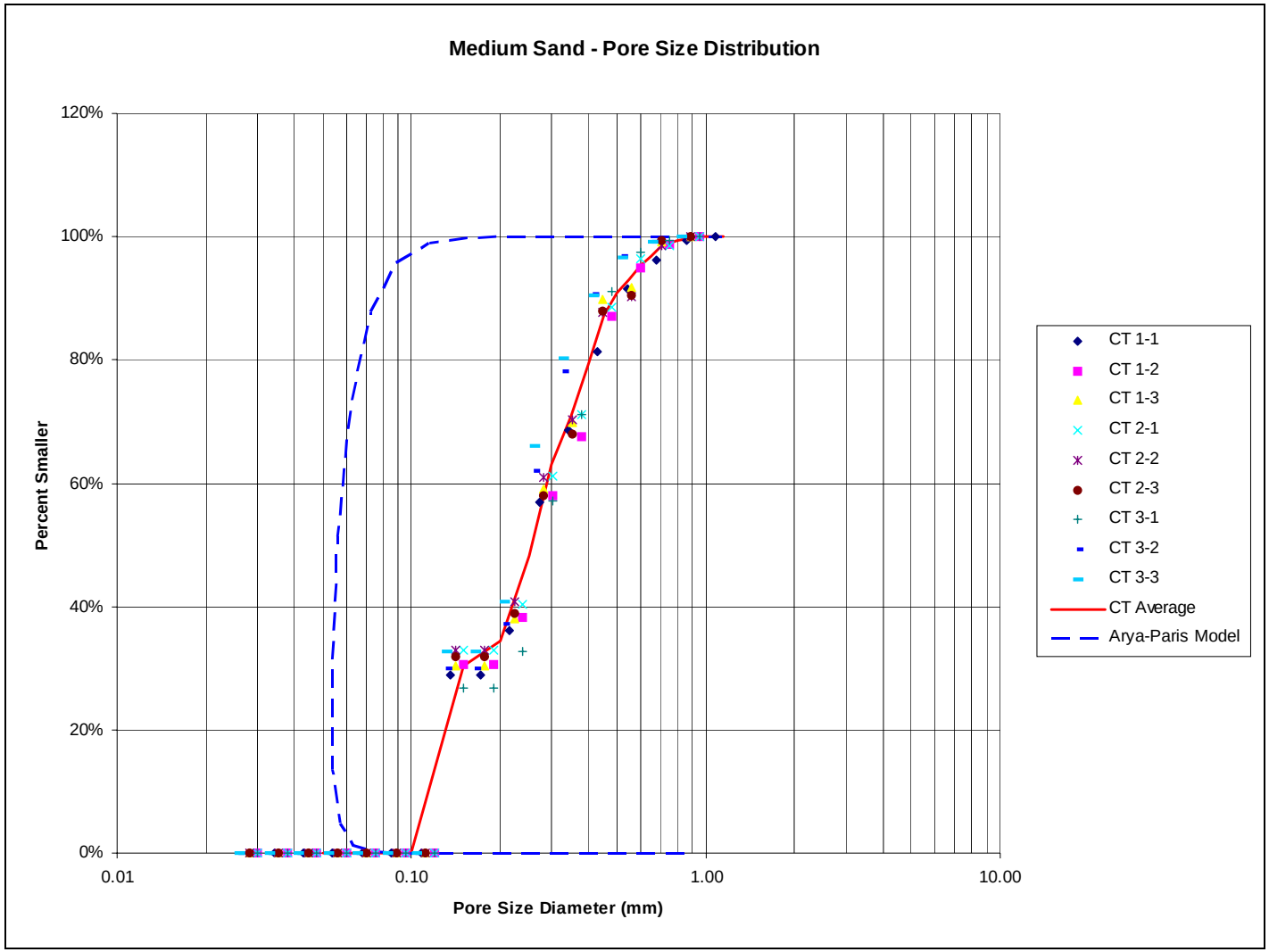

Figure 4-19: Pore size distribution for the Medium Sand soil.

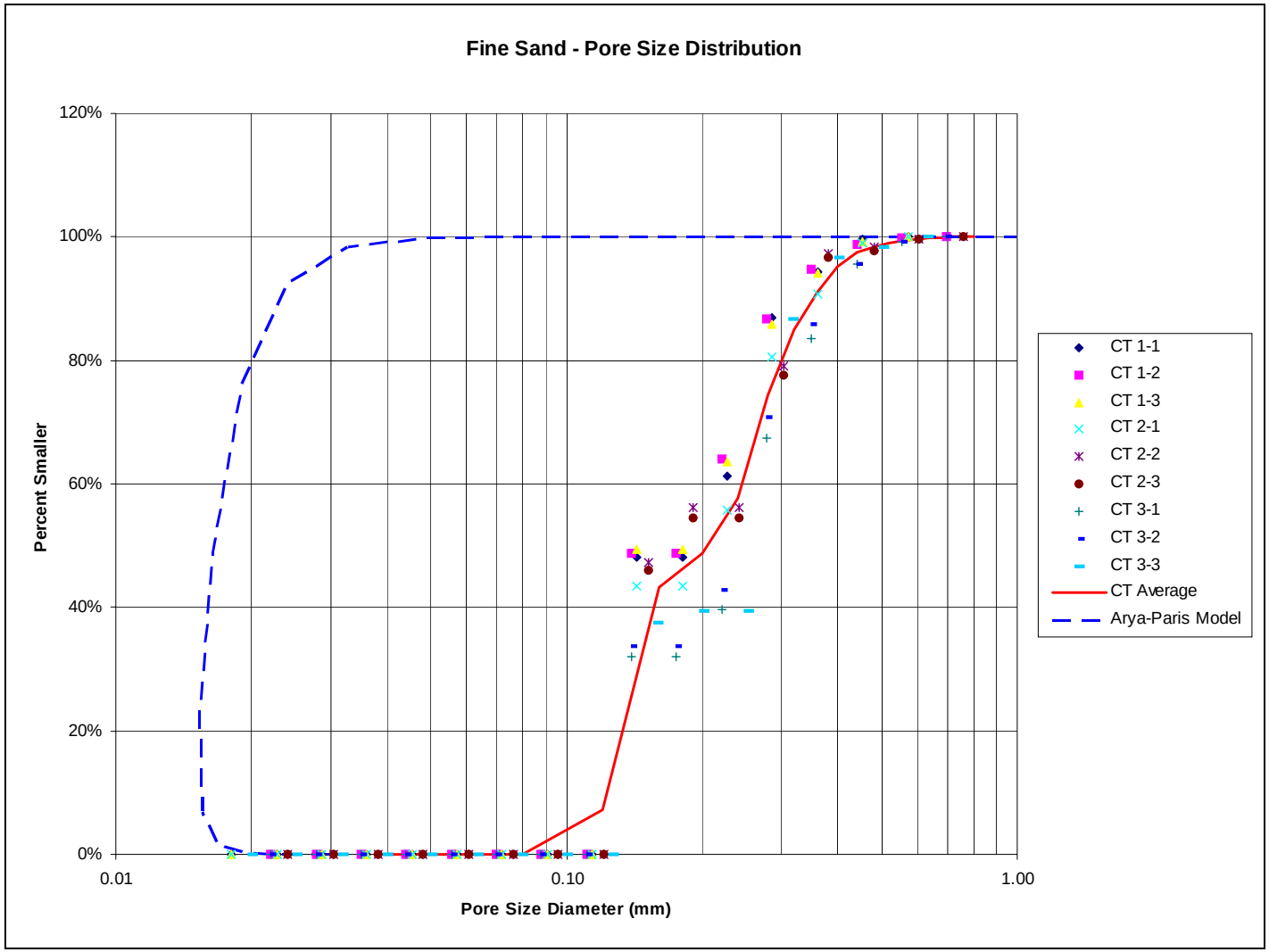

Figure 4-20: Pore size distribution for the Fine Sand soil.

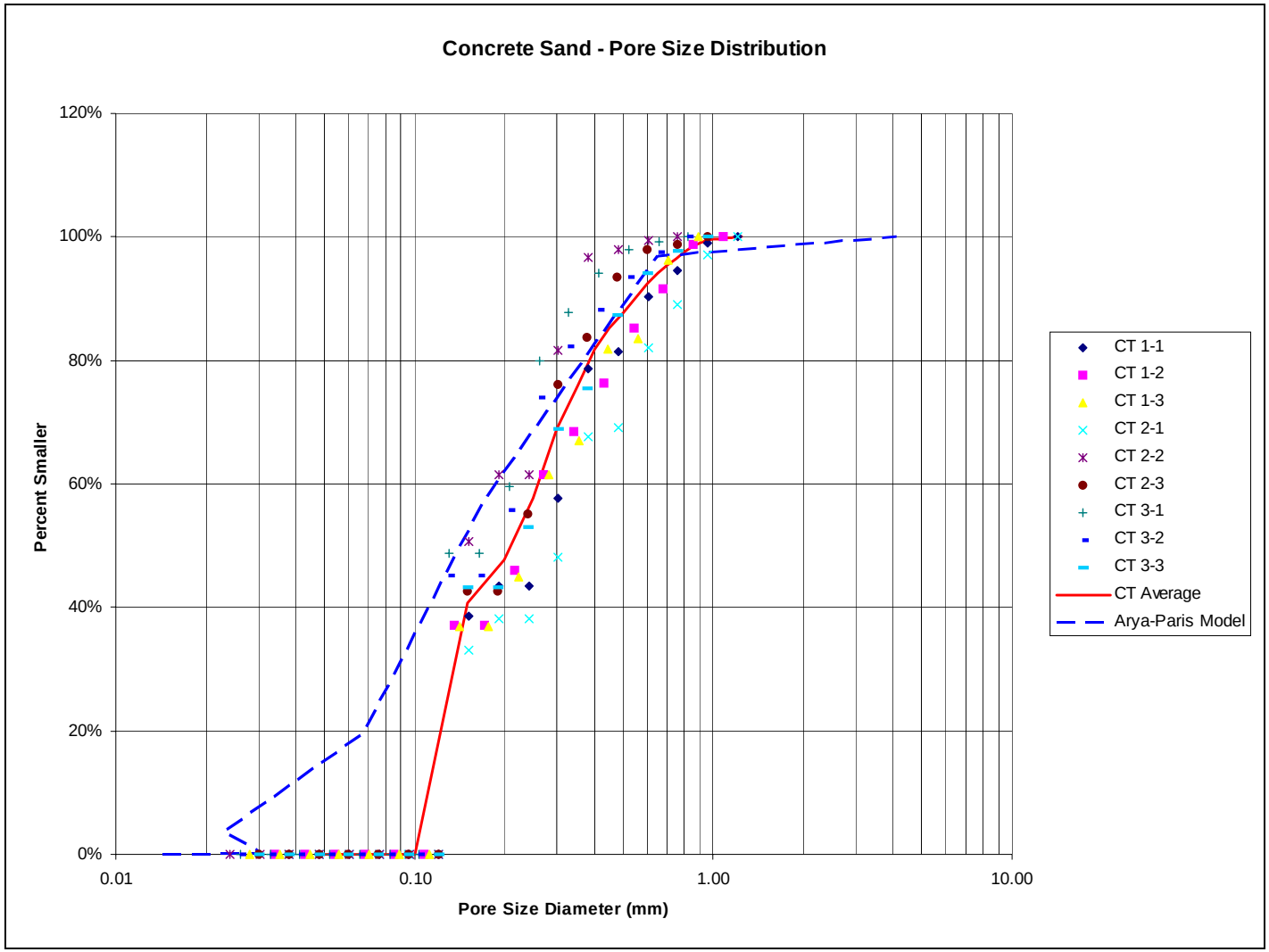

Figure 4-21: Pore size distribution for the Concrete Sand soil.

The first point to make about the pore size results is regarding the applicability of the Arya and Paris pore size distribution model. The model has been recommended for many types of soil, but it was originally developed and confirmed for soils that have a wide variety of particle sizes (well-graded) and a high percentage of fines (Arya and Paris 1981). The authors make no mention of the maximum particle size or the maximum range of particle sizes for which the model is accurate. Since the uniformly graded soils used in this project are not necessarily representative of the soils upon which the Arya and Paris method is based, there is some concern about using the mathematical model for comparison. For example, the model predicts an unreasonable pore size distribution for the Gravel soil used in this study, as shown in Figure 4-16. The Arya and Paris model is based on the hypothesis that the grain size distribution and pore size distribution of a soil share similar shapes, so severe shape deviations from natural grain size distributions are expected to cause inaccuracies in the model. The grain size distributions of the uniformly-graded soils used in this research deviate significantly from common natural soil types, and this is reflected in the unrealistic pore size distributions determined by the model.

The Haverkamp and Parlange (1986) pore size model may be more appropriate, since it is designed for sandy soils. The model was not used in this project because it requires additional soil data to define the wetting and drying water characteristic curves for soils. This data can be determined experimentally or with mathematical approximations. Pore pressure experiments, including laboratory tensiometry, are not applicable for large particle soils such as those used in this study because of the relatively low pore suction in coarse-grained materials (Gaskin 1973). As an experiment, the computational steps of the

Haverkamp and Parlange (1986) model were explored for the soils in this study using the water characteristic curve approximations described by the authors. The water characteristic curve shape approximations are based on the grain size distributions of the soils (Haverkamp and Parlange 1986). However, the approximations led to unsatisfactory results, and the computations could not be completed for the soils in this study.

The CT-measured pore size distribution nearly matches the predicted pore size distribution for the Concrete Sand soil. The Concrete Sand soil is the only soil type used in this project that has a wide variety of grain sizes. Therefore, it may be considered the best candidate of all the soils here for pore size prediction using the Arya and Paris model. The strong pore size distribution comparison between the CT-measured and the Arya and Paris model, in conjunction with the relatively promising grain size distribution comparisons with the mechanical sieve grain size tests for the other soils, provides convincing validity to the non-destructive CT x-ray scanning method described in this thesis. The author believes this approach provides great promise and potential for future application in measuring other difficult to determine parameters such as hydraulic conductivity and thermal conductivity.

CHAPTER 5

CONCLUSIONS AND RECOMMENDATIONS

The goal of this study was to develop non-destructive soil testing procedures using x-ray CT scanning techniques. Traditional soil testing techniques are destructive in nature and may alter the same properties they are designed to measure. Non-destructive tests provide the benefit of not altering the soil structure, so the properties of the unaltered void space may be determined without the risk of introducing systematic errors resulting from soil structure changes during the measurement process.

The first objective of this research was to perform x-ray CT scans of several soil types. The soil types used in this study included four uniformly-graded soils of decreasing particle size that were used to determine the resolution limitations of the CT scanning process, and one soil with a variety of particle sizes used to determine the performance of the CT scanner with materials containing non-uniform particle sizes. Results from this study indicate that the MSU CT scanner is capable of producing high-quality scans of soil materials. Additionally, the results suggest that sample container diameter size plays an important role in the resolution of the CT scans. Smaller diameter containers could allow the CT digital camera to be moved closer to the x-ray converting screen so that small particles could be viewed in more detail. Improving the resolution of the CT scans for finer-grained soils may allow more accurate determination of soil properties from the CT images.

The second objective of this research was to develop image processing techniques to determine soil index properties using CT scan images. Techniques to determine porosity,

grain size distribution, and pore size distribution were developed, and the CT-measured results were compared with results from traditional geotechnical laboratory index test procedures. Mechanical test procedures were not available to experimentally determine pore size distribution for the coarse-grained soils used in this study, so a pore size distribution mathematical model was used for comparison. The Arya and Paris (1981) model approximates the pore size distribution for a soil based on its grain size distribution and bulk density.

Results from the CT-measured porosity test technique suggest that CT scan resolution is an important factor in the accuracy of the image processing techniques. The CT-measured porosity values for soils containing predominantly large particle sizes (1.0 mm to 5.0 mm) compared favorably to the laboratory test results, but the results were less accurate for the finer-grained materials. The small particles appeared to blend together in the CT scans, and the solid and void spaces became difficult to distinguish. The trends observed in this study indicate that the accuracy of porosity measurements from CT scans of small particle soils would improve as the scan resolution is improved.

The CT-measured grain size distribution results agreed well with mechanical grain size distribution tests. Most notably, the grain size distributions determined from the CT scans of the uniform plastic beads and the coarser soils were in satisfactory agreement with the grain size distributions determined from the laboratory procedures. The successes in this portion of the research, particularly with the plastic beads, validated the testing techniques developed in the course of this study. The CT scan resolution was also an important factor in the accuracy of the grain size distribution results. It is expected that if individual particles in

the finer-grained soils were distinguishable, the CT-measured grain size distribution results of the small particle soils would compare more favorably with the laboratory-determined distributions.

The pore size distributions determined from the CT scans show strong promise for the non-destructive test methods developed in this study. The Concrete Sand soil was the only soil of the five used in this study that could be considered a candidate for use in the Arya and Paris (1981) pore size distribution model. The model was originally developed for soils with wide ranges of particle sizes, and the uniformly-graded soils used in this research have very narrow ranges of particle sizes. Pore size distribution has historically been a very difficult soil parameter to determine experimentally. Traditional pore size distribution tests use hardening agents to preserve the soil structure, and thin coupons are made from which pore sizes are determined. The process is time consuming and destructive in nature. The non-destructive CT scanning techniques developed in this research produce similar cross-section views of the soil structure without the possible introduction of systematic errors from impregnating the soil with a hardening agent. The pore size distributions determined from the Concrete Sand CT scans were in good agreement with the estimated pore size distribution from the Arya and Paris model. This favorable result helps to validate the non-destructive testing methods developed in this study, and it indicates that non-destructive CT test methods can produce favorable results without the large time and labor commitment needed for the coupon-preparation process.

This research has demonstrated that non-destructive x-ray CT scanning techniques can be used to determine soil index properties. It is believed that this research has laid the

groundwork for further studies focused on the practical development of standardized non-destructive CT scanning methodologies for soil testing. Since x-ray images show the density of specimens, x-ray CT scanning also lends itself well to bulk density and specific gravity soil testing. This may be achieved by comparing the pixel intensity values of a soil CT scan to the pixels in a benchmark scan of water. Another interesting possibility for x-ray CT scanning is the determination of soil microstructure behavior during the shearing process. Since CT scanning is a non-destructive testing technique, the same soil sample could be measured at various stages in the shearing process to determine the effects of particle shape, alignment, and interaction during shear.

In addition, three-dimensional CT scans may provide interesting qualitative views of the interior structure of soil particles and pores. Hypotheses regarding particle interactions may be developed to validate existing geotechnical theories and to open the door to new and different approaches for quantifying soil behavior. Particularly, three-dimensional CT scans may be used to estimate hydraulic conductivity, as well as pore structure, connectivity, and tortuosity.

BIBLIOGRAPHY

Allen, C. C., A. I. Tsapin, K. Kuebler, L. Haskin, and A. Wang. "Analysis Inside the Box: Studying Rock and Soil in Biological Quarantine." Lunar and Planetary Science Conference XXXIII (2002).

Alshibli, K. A., et al. "Quantifying Void Ratio Variation in Sand Using Computed Tomography." *Geotechnical Measurements - Lab and Field: Proceedings of GeoDenver 2000 Specialty Conference, August 5-8, 2000, Denver 2000*: 30-43.

Arya, L. M., and J. F. Paris. "A Physicoempirical Model to Predict the Soil Moisture Characteristic from Particle-Size Distribution and Bulk Density Data." *Soil Science Society of America Journal* 45 (1981): 1023-1030.

Arya, L. M., F. J. Leij, M. T. van Genuchten, and P. J. Shouse. "Scaling Parameter to Predict the Soil Water Characteristic from Particle-Size Distribution Data." *Soil Science Society of America Journal* 63 (1999): 510-519.

Cassel, D. K., and A. Klute. "Water Potential: Tensiometry." In *Methods of Soil Analysis: Part 1, Physical and Mineralogical Methods, Second Edition*, ed. Arnold Kluke, 563-596. Madison, WI: American Society of Agronomy, Inc., 1986.

"CT Reconstruction (example)." Biomedical Imaging Group. Online: http://bigwww.epfl.ch/demo/ctreconstruction/example.html. Revised February 23, 2000.

Dullien, F. A. L. *Porous Media: Fluid Transport and Pore Structure*, 2nd ed. San Diego, CA: Academic Press, Inc., 1992.

Frost, J. David. "Effect of Boundary Conditions on Volumetric Microstructure Evolution." In proceedings of the FHWA-NSF Workshop on Imaging and Simulation of Concrete Structure, Evanston, IL, July 30-31, 2003.

Gaskin, P. N., and G. P. Raymond. "Pore Size Distribution as a Frost Susceptibility Criterion." *Frost Action on Roads: Proceedings of the Symposium on Frost Action on Roads Held at the Norwegian Road Research Laboratory in Oslo on 1st, 2nd, and 3rd October 1973*: 76-78.

Haverkamp, R., and J.-Y. Parlange. "Predicting the Water-Retention Curve from Particle-Size Distribution: 1. Sandy Soils without Organic Matter." *Soil Science* 142, No. 6 (December 1986): 325-339.

Haverkamp, R., P. Reggiani, and J. R. Nimmo. "Property-Transfer Methods." In *Methods of Soil Analysis – Part 4: Physical Methods*, ed. Jacob H. Dane and G. Clarke Topp, 759-777. Madison, WI: Soil Science Society of America, Inc., 2002.

Holtz, Robert D., and W. D. Kovaks. *An Introduction to Geotechnical Engineering*. Englewood Cliffs, NJ: Prentice-Hall, Inc., 1981.

Jang, D.-J., J. D. Frost, and J.-Y. Park. "Preparation of Epoxy Impregnated Sand Coupons for Image Analysis." *Geotechnical Testing Journal* 22, No. 2 (June 1999): 147-158.

Lowe, John, and Philip F. Zaccheo. "Subsurface Explorations and Sampling." In *Foundation Engineering Handbook*, Winterkorn, H.F. and H.-Y. Fong, 1-86. New York, NY: Van Nostrand Reinhold, Co., 1975.

Phillips, D. H., and J. J. Lannutti. "Measuring Physical Density with X-Ray Computed Tomography." *NDT&E International* 30, No. 6 (December 1997): 339-350.

Russ, John C. *The Image Processing Handbook*, 4th ed. Boca Raton, FL: CRC Press, 2002.

Sahagian, D. L., and A. A. Proussevitch. "3D Particle Size Distributions from 2D Observations: Stereology for Natural Applications." *Journal of Volcanology and Geothermal Research* 84 (1998): 173-196.

Serra, J. *Image Analysis and Mathematical Morphology*. London: Academic Press Inc. (London) Ltd., 1982.

Sijbers, Jan, and Andrei Postnov. "Reduction of Ring Artifacts in High Resolution Micro-CT Reconstructions." *Physics in Medicine and Biology* 49, No. 14 (July 2004): 247-253.

Tollner, E. W., N. D. Melear, L. A. Rodriguez, and M. E. Wright. "Soil Aggregate Size Distributions Using X-Ray Images." *Transactions of the American Society of Agricultural Engineers* 41, No. 4 (July-August 1998): 1207-1215.

Vervoort, R. W., and S. R. Cattle. "Linking Hydraulic Conductivity and Tortuosity Parameters to Pore Space Geometry and Pore-Size Distribution." *Journal of Hydrology* 272 (2003): 36-49.

Yi-Hua Xu, H. C. Pitot. "An Improved Stereologic Method for Three-Dimensional Estimation of Particle Size Distribution from Observations in Two Dimensions and Its Application." *Computer Methods and Programs in Biomedicine* 72 (2003): 1-20.

APPENDICES

APPENDIX A

USING THE MONTANA STATE UNIVERSITY CIVIL ENGINEERING CT SCANNER

This appendix has been written to complement the user's manual and help files supplied with the CT scanner software. This document is intended to be used as a "quick start guide" by new scanner users. The points discussed here are meant to be a summary of the steps required to perform a CT scan. Additional details can be found in the manual and help files provided with the CT scanner software from Synergistic Detector Designs.

Description of the Equipment

The MSU-CE CT scanner is a fully-enclosed system with equipment to acquire, process, and display digital radiography images. The scanner is capable of capturing both single-frame x-ray images (similar to a standard medical x-ray) and reconstructed images of rotated objects (CT scans). All motion of equipment and image acquisition within the x-ray cabinet is computer controlled.

Equipment within the cabinet includes an x-ray tube, a specimen table, and the image acquisition system. The x-ray tube and specimen table are mounted on moveable frames within the cabinet to accommodate various object sizes and scanning needs. The image acquisition system consists of an x-ray converting screen, a 45-degree mirror, a lens, and a digital camera. The x-ray tube is mounted on the right side of the CT scanner cabinet and is directed so that x-rays travel towards the x-ray screen on the left side of the cabinet. The specimen table is located in the center of the cabinet, and the camera assembly is located along the left edge of the cabinet. Figure A- shows the interior layout of the CT cabinet.

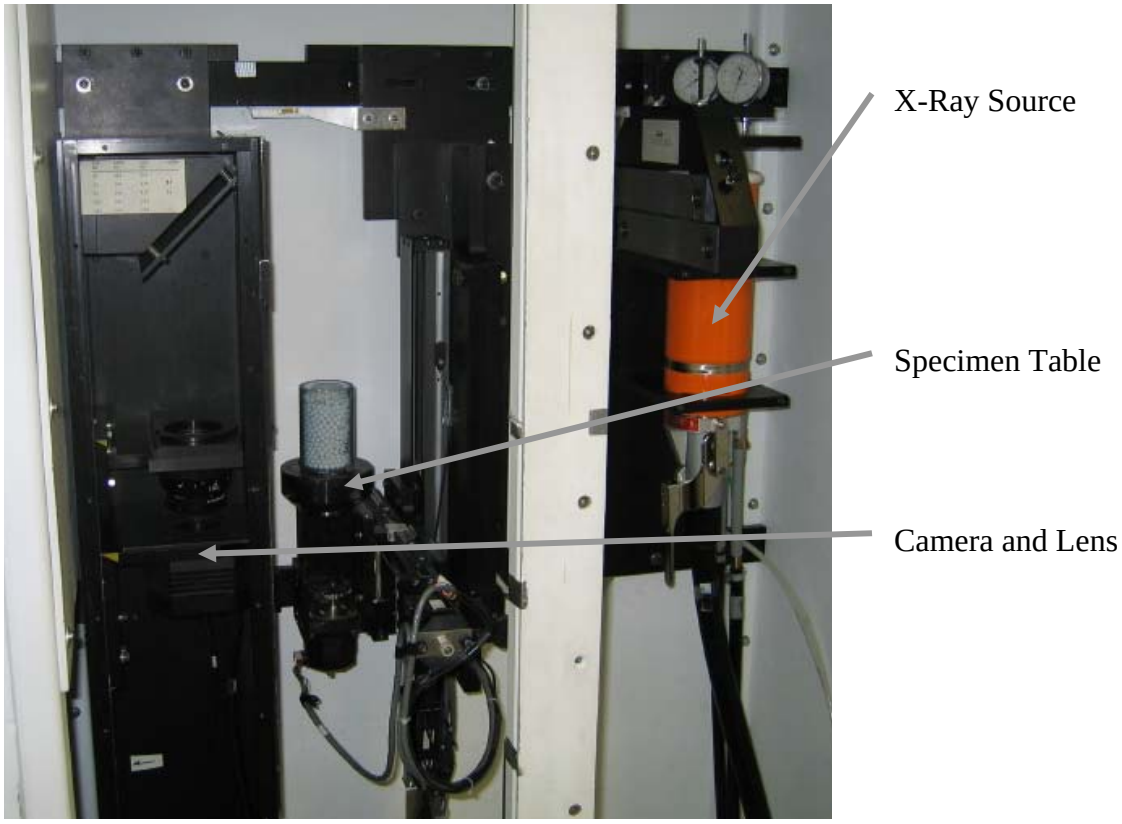

Figure A-1: The interior layout of the CT cabinet.

Adjusting the Scanner

When the CT scanner is set up correctly, it can perform high-quality scans without the need for daily maintenance. The key to producing quality images hinges on proper adjustment of the scanner. Key components of the equipment, which may require adjustments prior to scanning include the camera and lens, the screen, and the specimen table.

Camera and Lens Settings

The images of a CT scan are captured by a digital camera that photographs the pattern of x-rays as they pass through an object. In the MSU CT scanning machine, the image acquisition system consists of a focusing lens and a charge-couple device digital camera. Figure A- shows the optical equipment system within its enclosure on the left side of the CT cabinet.

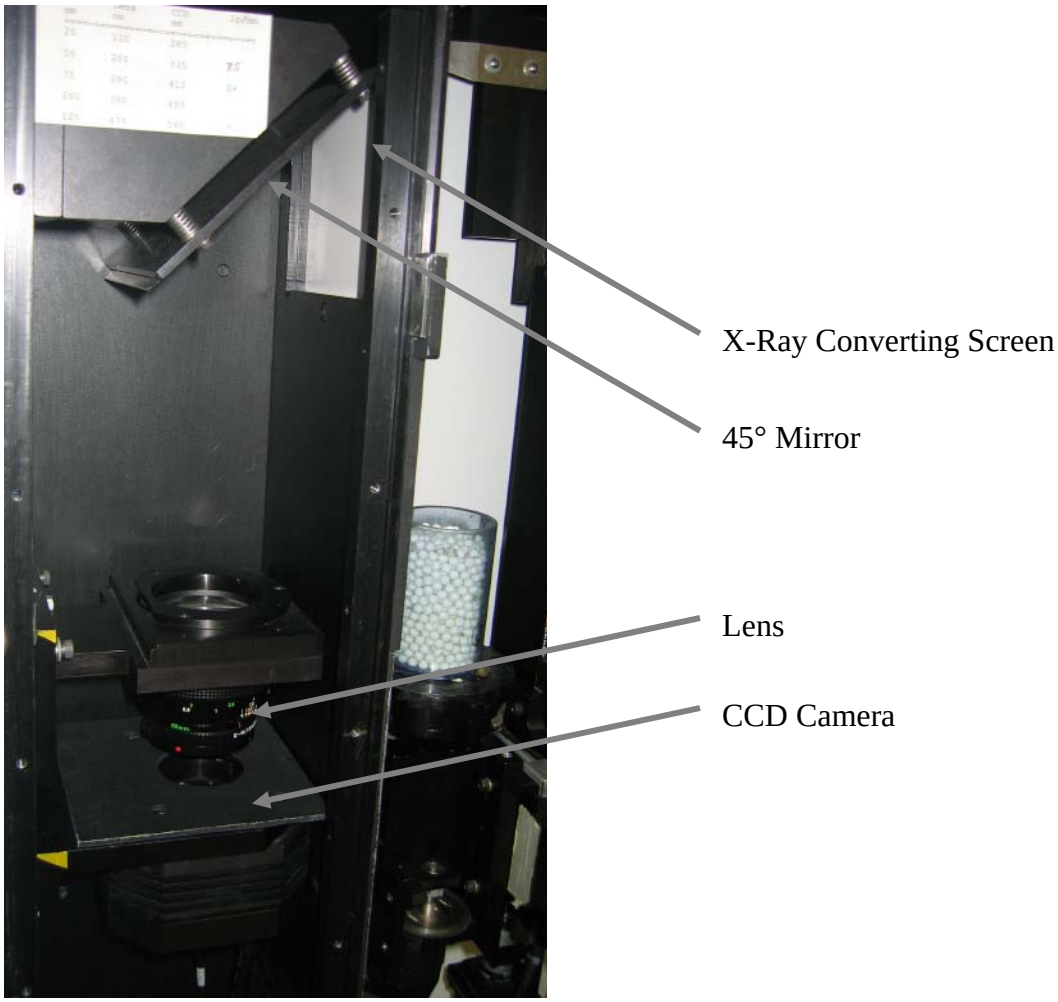

Figure A-2: The MSU CT scanner image acquisition system.

Both the camera and the lens must be positioned and focused correctly in order to accurately capture x-ray images. Their locations are based on the size of the objects being scanned; small objects can be viewed with the camera set close to the mirror, and large objects require the camera to be moved farther away. The width of the camera's view is known as the field of view, and camera and lens locations for four fields of view have been listed on the inside of the camera enclosure. A scale is provided along the left side of the camera enclosure to set the locations of the camera and lens. The camera and lens are affixed in supports that are held in place with hex-head bolts that thread into mounting holes along the left wall of the camera enclosure. The field of view can be chosen by the largest width (diameter) of the objects to be scanned. For example, if the object is approximately 50 mm (2 inches) wide, the camera must be set for a field of view of at least 50 mm. However, some space on either side of the object is required, so the field of view should be slightly wider than the object. Therefore, a field of view of perhaps 65 mm (2.5 inches) might be appropriate. The next largest field of view for which the camera and lens locations have been determined is 75 millimeters (2.95 inches), which is suitable for a two-inch diameter sample.

When the camera and lens have been set based on the required field of view, the lens must be focused. The easiest and quickest way to do this is to start with the x-ray turned off. Remove the x-ray screen cover and screen, and tape a piece of white paper with text over the screen opening. Lightly close the door of the camera exposure (a piece of tape at the top works well), and leave the doors of the cabinet open to allow light into the cabinet. Then, use the Expose control in the Image Window of the control software to expose the camera for

an appropriate time (perhaps 0.1 seconds or less) so that the image shows no saturated pixels (pure black spots in the paper). If the text on the paper is blurry, open the camera enclosure, adjust the lens focus in one direction, close the camera door again, and expose the camera again. If the text got clearer, the adjustment was correct. Continue focusing in the same direction until the text clarity is maximized. If the text gets blurrier, the initial focus adjustment was incorrect. Adjust the focus in the other direction until the image is clear.

To perform small focus adjustments, use a penetrameter with the x-ray turned on. An x-ray penetrameter contains a set of gapped metal wires that converge to a point at one end. After reinstalling the x-ray screen and its cover, tape the penetrameter directly on to the outside of the cover, close the cabinet, turn on the x-ray, and expose the camera (this time, use a longer exposure – perhaps 2 seconds). Now, perform the same iterative focusing process until the resolution of the penetrameter's image is maximized. Note that you have to turn off the x-ray while the cabinet is open and you are adjusting the camera or lens.

Table and X-Ray Locations

It is important to correctly set the locations of the specimen table and x-ray source to achieve high quality scans. The locations of each are mostly dependent on the size and density of the specimen, but no table and x-ray locations have been specified. The table and x-ray should be moved to fit specific scanning needs. The table and x-ray are attached to the stationary frame in the back of the cabinet with moveable supports that attach along top and bottom horizontal beams. They hang on the cabinet frame and can move from side to side as

needed. The moveable frames are secured to the cabinet frame with hex bolts that are threaded into mounting holes along the back beams.

Along the top beam of the fixed black frame is affixed a centimeter scale. This scale measures the distance from the camera's focus point, which is the center of the 45° mirror hanging within the camera enclosure. The distances between the camera and the table, and the camera and the x-ray source are required for the CT scan setup process. The values on the fixed scale correspond to the small metal pointer attached to the table support and the edge of the x-ray support.

Table Leveling

During the CT scanning process, the specimen table rotates around its vertical axis to turn the object through a full rotation. If the table is not completely level, the top of the object will rotate eccentrically and scan quality will diminish. The table can be leveled using two thumb screws that push the bottom of the table support away from the fixed cabinet frame in two dimensions – front to back, and side to side. The leveling process is a similar trial and error process to the lens focusing steps described earlier. A small metal pin is embedded within the plastic table extension included with the CT scan equipment. The pin absorbs more x-rays than the surrounding plastic, so it appears clearly in an x-ray image of the table.

When leveling the table, it is first important to raise the table so the pin is even with the center of the x-ray beam. The leveling procedure explained next actually aligns the table so its top is parallel with respect to the x-ray beams. If a point other than the x-ray center is

used, the table will not be leveled correctly. Unfortunately, the table cannot be leveled by using a bubble level placed on its surface, since the entire x-ray cabinet may not be truly level.

To level the table in the front-to-back direction, raise the table into the x-ray so it is at the height of the x-ray center. This may not correspond to the vertical center of the camera's field of view. Rotate the table so that the pin appears in the center of the image (in the 6 or 12 o'clock position relative to the x-ray beams), and capture an x-ray image of it. In the software, it is helpful to use the Profile tool to mark on the x-ray image the vertical position of the top of the pin in this configuration. Then, rotate the table 180° and capture the x-ray image again. If the table is level in the front-to-back direction, the pin's vertical location will be the same for both rotations. If not, it will move up or down relative to the earlier x-ray. Adjust the front-to-back thumbscrew to tilt the table, and check the pin's vertical position again. Keep adjusting until the pin's vertical location in the x-ray image does not change between front and back positions.

The same process can be used to level the table in the left-to-right position. For this, align the table pin in the 3 and 9 o'clock positions relative to the x-ray beam.

Software and Settings

The software that controls the MSU CT scanner was custom designed by Synergistic Detector Designs. It controls most aspects of the CT system, including the x-ray power, the object table movement, and the camera shutter. The software user interface includes input areas for each of the equipment controls as well as imaging capabilities. Three common

tasks using the software to control the CT scanner will be described here: capturing an x-ray image, running a CT scan, and reconstructing a CT image.

Capturing an X-Ray Image

Capturing an x-ray image is similar to an x-ray technician at a hospital performing an x-ray on a patient's broken bone. The resulting image is a view of an object's internal features, but seen as a two-dimensional image. Internal features may be identified, but their exact location is unknown. The steps to capture an x-ray image using the MSU CT scanner are as follows:

1. Turn on the x-ray console and warm it up, and turn on the power to the CT cabinet.
2. Start the "9621" software from the Windows desktop to control the CT equipment.
3. Click the "Home" button for the table's vertical position to re-zero the table's location.
4. Move the table to an appropriate height so that the feature you wish to view is level with the x-ray converting screen. You can view the table's movement by opening the cabinet and pulling the small switch near the bottom of the center post. Be sure to close the door before turning on the x-ray.
5. Remove the lead collimators from the x-ray and the converting screen to capture a full-screen x-ray image. If the collimators are left on, the image will contain only a thin slice of the object.

6. Using the software, turn on the x-ray power and wait for the red power bar to appear. Any x-ray power up to 160 kV may be used, and the current must be set to 4 mA.
7. Click the “Image” menu to open the image capture software screen, and click “Expose” to control the camera.
8. Type in an exposure time, and uncheck the “Close after data acquisition” option.
9. Click “Expose”, and the x-ray image of the object will appear in the Image window.
10. If the image quality is low, it may be improved by adjusting the table height or rotation, x-ray power, or camera exposure time.

Performing a CT Scan

A CT scan consists of many x-ray images compiled together, so many of the steps to start a CT scan are similar to capturing a single x-ray image. However, the CT scan set up includes many additional parameters unique to the CT process that must be defined. The steps to performing a CT scan are:

1. Turn on the x-ray console and warm it up, and turn on the cabinet power.
2. Start the control software.
3. Install the lead collimators on the x-ray and the screen. They restrict the x-ray beam to a thin band, which helps to reduce unnecessary noise in the CT images.
4. Click the “CT Setup” menu to open the CT control window.

5. Enter appropriate values for each option. For additional information about each parameter, review the CT setup help screens and the CT scanner manual. Note that the x-ray power, x-ray current, and camera exposure must be identical for both the bypass and data acquisition stages.
6. Click “Start” to begin the CT scan. The software will open several image windows as it begins the scan.
7. When the scan starts to capture images for each rotation increment, the “Time Remaining” box will display. You don’t have to watch the scan finish, so use this time as a guide for when you should return.
8. When the CT scan is finished, the software will return the table to its zero position, shut off the x-ray, and display the sinogram of the completed scan.

The software can be unreliable at times when starting a CT scan, and it may cause an error when it starts capturing bypass image data. If this occurs, shut down and restart the software and restart the CT scan. Your previous settings should have been saved, so you should only need to review the scan settings and click “Start.”

A CT scan will not successfully reconstruct if the object moves outside the camera’s field of view. This can be prevented by capturing x-ray images of the object as it rotates through a full rotation before starting the CT scan. Capture an x-ray image of the object using the Expose controls in the Image window in the control software, then rotate the table by several degrees, such as 45°. Capture the new x-ray image, and note the object’s side-to-side movement relative to the camera. If the object moves near or beyond the edge of the image window, turn off the x-ray and move the object closer to the center of the table. The

object should be able to complete a full rotation without moving to the edge of the image. The object does not need to be exactly centered relative to the camera, but it must not move beyond the bounds of the camera's view. When this manual rotation process is finished, start the CT scan. The software will need to be restarted before starting the scan.

Reconstructing a CT Scan

The reconstruction process involves the use of several x-ray views of an object combined to produce a cross-section of the object's interior structure. The software that controls the MSU CT scanner is capable of reconstructing two-dimensional CT scans. The steps for this final step of a CT scan using the Synergistic Detector Designs software are as follows:

1. Complete a CT scan as described in the previous section.
2. Click the "Recon" menu, select "Edit CT Image" to open the CT image editor, and select the CT scan file.
3. Review the settings of a CT scan in the CT image editor window, because some of the parameters may need to be changed. In particular, the Center of Rotation value is important for the reconstructed image. Center of rotation values typically range near 500, but may vary dramatically and depend on the object's location relative to the camera during the scan.
4. Change the Direction of Rotation Flag value from the default (-5) to (5). It is unknown why the default table rotation direction is reverse of the MSU CT scanner's table, but using the default (-5) value will result in poor image quality.
5. Click "Save" to exit the CT Image Editor.

6. Click the “Recon” menu, select “Reconstruct,” and select the CT file used in the previous steps.
7. Type a name for the final image, and click “Save” to begin the reconstruction process.
8. Open the image in the Image Window when the reconstruction is finished.
9. If an incorrect Center of Rotation was used, the objects in the image will appear blurry or will have “halos” around them. If this is the case, return to the CT Image Editor, change the Center of Rotation value, and perform the reconstruction again.

Locating the true center of rotation for an image is a trial-and-error process, and small-increment (high resolution) scans can take several minutes to reconstruct. Therefore, it is recommended that a high-increment (2- or 1-degree) scan be used first to locate the center of rotation before starting a high-resolution scan. The centers of rotation between the low- and high-resolution scans should be similar, as long as the object is not moved on the table between the scans.

Other Maintenance Issues

In general, the MSU CT scanner does not need significant regular maintenance. Barring catastrophic equipment failure, the individual motors and equipment should not need to be removed from the cabinet. Four regular issues that should be addressed include the x-ray converting screen, keeping the camera lens clean, installing a stopper for the table, and power management.

The X-Ray Converting Screen

The x-ray converting screen is one of the most important factors of image quality in the CT scanning process. The digital camera photographs the x-ray pattern as it hits the screen, so a quality screen is required for quality images. If the screen degrades, x-ray image and scan quality will follow. Phosphor screens are common items used in medical x-ray cartridges, and they can be acquired from almost any x-ray supply company. The original screen that was installed by Synergistic Detector Designs was a product known as Trimax 4 made by the 3M corporation. This screen is a green light-emitting, 400-speed phosphor screen, and other manufacturers sell similar products. Lower speed screens typically require longer exposure times but may provide higher resolution than high speed screens. The 400-speed screen used for this project is a compromise between short exposure time and high resolution. In theory, any speed phosphor screen should work in the MSU CT scanner, but phosphor screens other than green-emitting, 400-speed have not been tested.

The screen is held in a small recess in the outside wall of the camera enclosure by a thin metal plate. If necessary, the screen should be trimmed to fit into its recessed frame. Small pieces of tape at the top and bottom of the screen work well to hold it in place while the plate is affixed.

Cleaning the Camera Lens

Bits of material that fall onto the camera lens may obscure the camera's view and cause poor images. This is unlikely to happen, since the lens and camera are enclosed, but dust may accumulate. For loose material, the lens and camera may be cleaned with

compressed air. If fingerprints or sticky materials are on the lens, it may be cleaned with photographic lens cleaner.

Stopping the Table from Falling

Occasionally, the specimen table may move lower than its “home” position when the cabinet power is turned off. If this occurs, the table controller may attempt to move it further down when it is turned on, and the table might move below its bottom position. This can be prevented by placing a small piece of material (stiff foam works well) to act as a stopper when the power is turned off. The foam should be cut so that it just makes contact the with table support when the table is at the home position and should be attached with light adhesive to the black cross-arm of the cabinet frame.

Power Management

The CT scanning equipment is extremely expensive, and many of the parts were custom made and cannot be replaced. Therefore, any way to increase the useable lifetime of the scanner should be encouraged. The power to the cabinet should be turned off when not in use to prevent prolonged use of the motor and camera cooling fans. Additionally, the x-ray power should be turned off when not in use. If the scanner will be used multiple times in a day, it does not need to be shut off between scans, but it is suggested the x-ray power be turned off if it won’t be used for long periods of time. The cabinet power is shut off with a circuit breaker (#8 on the box next to the CT cabinet) and the x-ray power is shut off with the x-ray control panel key.

APPENDIX B

STEREOLOGY CALCULATIONS IN VISUAL BASIC

The first four programs presented here were written as user-defined functions that can be used in a Microsoft Excel spreadsheet. For example, the "alphacalc" function shown below can be used in an Excel spreadsheet cell with the following syntax: "=alphacalc($A$1:$A$17, 10)". The fifth program is a macro that can be started by the user to automatically set up and calculate a spreadsheet for determining the stereological size distribution of cross-sections in a digital image. The only prerequisite step for the setup macro is that the user has copied into Excel the cross-section density vs. radius data calculated using the granulometry procedure. For best results, the granulometry results should be copied to the Excel spreadsheet and sorted by radius, in descending order, before running the setup macro.

Alpha Coefficient Calculation

Required inputs:

1. PRange: The column of cells containing intersection probabilities of each particle class
2. classnum: The number of particle classes (default is 16)

```
Function alphacalc(PRange As Range, classnum As Integer)

    Dim i As Integer, j As Integer
    Dim aRange As Range
    Dim term1 As Double, term2 As Double
    ReDim alpha(classnum + 1) As Double, P(classnum + 1) As Double

    'Set up a new 1-D array with the intersection probabilities for each particle class
    For i = 1 To classnum
    P(i) = PRange(i).Value
    Next i

    'Calculate the first two alpha values
    alpha(1) = 1 / P(1)
```

```
alpha(2) = alpha(1) * P(2) / P(1)

   Calculate the remaining alpha values
   For i = 3 To classnum
   term1 = alpha(1) * P(i)
   term2 = 0
   For j = 1 To i - 2
   term2 = term2 + alpha(j + 1) * P(i - j)
   Next j
   alpha(i) = 1 / P(1) * (term1 - term2)
   Next i

   Output the new alpha values into the Excel spreadsheet
   alphacalc = alpha(classnum)

End Function
```

Transferring 2D Cross-Section Distribution from Linear Classes to Geometric Classes

Required inputs:

1. linclassrange: the column of cells containing the normalized diameters of each linear class
2. geomclassrange: the column of cells containing the normalized upper bounds the geometric classes
3. lindensityrange: the column of cells containing the probability density of the linear classes as calculated by the granulometry procedure
4. classnum: the number of the geometric class being calculated

---

```
Function NAr(linclassrange As Range, geomclassrange As Range, lindensityrange As Range,
classnum As Integer)

   Dimension all variables
   Dim i As Integer, j As Integer, k As Integer
   ReDim NArea(geomclassrange.Rows.Count) As Double

   j = 1
   k = 1
   For i = 1 To geomclassrange.Rows.Count
   Last geometric class has zero cross-sectional area
   If i = geomclassrange.Rows.Count Then
```

```
   NArea(i) = 0
   GoTo loopout
   End If

   Distribute the area from linear classes to geometric classes
   While linclassrange(k, 1).Value >= geomclassrange(i + 1, 1).Value
   k = k + 1
   Wend
   k = k - 1
   NArea(i) = 0
   For j = j To k
   NArea(i) = NArea(i) + lindensityrange(j, 1).Value
   Next j
   j = k + 1

   If on last geometric class, skip to here
loopout:
   NAr = NArea(classnum)
   Next i

End Function
```

Stereological Particle Density Calculation

Required inputs:

1. areadensityrange: the column of cells containing the 2-D cross-section densities for the geometric classes as calculated by the previous VB function (NAr)
2. alpharange: the column of cells containing the alpha values for each geometric class, as calculated by the "alphacalc" VB function
3. H: the projected height of the assumed particle shape (1.00 for spheres)
4. classnum: the number of the geometric class being calculated

---

```
Function volume(areadensityrange As Range, alpharange As Range, H As Double, classnum
As Integer)

   Dimension all variables
   Dim i As Integer, j As Integer
   Dim term1 As Double, term2 As Double

   Create an empty 1-D array for the density values
   ReDim vol(classnum + 1) As Double
```

```
    Calculate the density for the first class
    vol(1) = 1 / H * alpharange(1).Value * areadensityrange(1).Value

    Calculate the remaining classes
    For i = 2 To classnum
    term1 = alpharange(1) * areadensityrange(i).Value
    term2 = 0
    For j = 1 To i - 1
    term2 = term2 + alpharange(j + 1).Value * areadensityrange(i - j).Value
    Next j
    vol(i) = 1 / H * (term1 - term2)
    Next i

    Output the density array to the spreadsheet
    volume = vol(classnum)

End Function
```

Adjusting for Negative Values in the Particle Size Distribution

Note: this Visual Basic code has been adapted from Yi-Hua Xu's example (2003).

Required inputs:

1. volrange: the column of cells containing the stereological particle density as calculated by the "volume" VB function
2. classnum: the number of the geometric class being calculated

---

```
Function negadjust(volrange As Range, classnum As Integer)

    Dimension all variables
    Dim i As Integer, adj As Double, MC As Double
    ReDim volout(classnum) As Double

    Start the "minus collector" variable at zero
    MC = 0
    For i = 1 To classnum
    adj = MC + volrange(i, 1).Value
    Use this command for positive density values
    If adj >= 0 Then
    GoTo Calc1
    Use this command for negative density values
    Else: MC = adj
```

```
   adj = 0
   GoTo Calc2
   End If

Calc1:
   MC = 0
   Reset the minus collector variable to zero before going on to the next class

Calc2:
   volout(i) = adj
   If negative values are found, they are set to zero and accumulated in the next class

   Next i

   Output the adjusted density values for each class
   negadjust = volout(classnum)

End Function
```

Set Up and Calculate the Stereology Calculation Spreadsheet

This program is used as a user-run macro and utilizes each of the above user-defined functions in Excel to set up the stereology calculation spreadsheet. Only one command is required by the user to perform the entire stereology procedure.

Required inputs (these are inputted by the user through the use of pop-up dialog boxes):

1. newtable: the location of the top-left corner cell of the new table location
2. tablename: the name of the soil used in a particular scan
3. radmax: the largest radius (in pixels) of the cross-sections in the scan, as given by the granulometry procedure
4. radint: the interval between consecutive cross-section radii
5. roiscale: the diameter (in pixels) of the region of interest in the digital image of the scan, used to scale the final results to millimeters

---

```
Sub setup()

   Dimension all variables
   Dim newtable As Range, tablename As String, i As Integer, j As Integer
   Dim radmax As Double, radint As Double, radnum As Integer, roiscale As Integer,
geomnum As Integer
```

```
    'Collect information about the soil granulometry data from the user to be placed in the
spreadsheet
    Set newtable = Application.InputBox("Select the top-left cell for the new table location",
"Name Cell", Type:=8)
    tablename = Application.InputBox("What is the name of the new soil?", "Soil Name",
Type:= 2)
    radmax = Application.InputBox("What is the largest opening radius in the granulometry
data?", "Maximum Radius", Type:=1)
    radint = Application.InputBox("What is the radius interval between consecutive
openings?", "Radius Interval", Type:= 1)
    radnum = radmax / radint + 1
    roiscale = Application.InputBox("What is the diameter (in pixels) of the ROI in the
original image", "ROI Scale", Type:=1)
    geomnum = 16
    ReDim newtab(radnum + geomnum, 22) As Variant

    Set up title cells along top row
    newtable(1, 1).Value = tablename
    i = 2
    newtable(i, 1).Value = "Radius"
    newtable(i, 2).Value = "Diam (pix)"
    newtable(i, 3).Value = "Diam (mm)"
    newtable(i, 4).Value = "Normalized Diam"
    newtable(i, 5).Value = "Area * Mean"
    newtable(i, 6).Value = "Sum of Pixels"
    newtable(i, 7).Value = "Density"
    newtable(i, 8).Value = "Cum. Density"

    newtable(i, 10).Value = "Class #"
    newtable(i, 11).Value = "Class Upper"
    newtable(i, 13).Value = "Class Lower"
    newtable(i, 15).Value = "Sphere Prob"
    newtable(i, 16).Value = "Sphere Alpha"
    newtable(i, 17).Value = "Class Area Density"
    newtable(i, 18).Value = "Class Volume Density"
    newtable(i, 19).Value = "Adj. Vol. Density"
    newtable(i, 20).Value = "Cum. Vol. Density"
    newtable(i, 21).Value = "Adj. Cum. Vol. Density"
    newtable(i, 22).Value = "Diam (mm)"

    Set up image scale section
    newtable(4 + geomnum, 11).Value = "Sphere H:"
    newtable(4 + geomnum, 12).Value = 1#
```

```
    newtable(6 + geomnum, 11).Value = "Scale:"
    newtable(6 + geomnum, 12).Value = "2 in ="
    newtable(6 + geomnum, 13).Value = roiscale
    newtable(6 + geomnum, 14).Value = "pix"
    newtable(7 + geomnum, 12).Value = "1 pix ="
    newtable(7 + geomnum, 13).Formula = "=2 / " & newtable(6 + geomnum,
13).Address(rowabsolute:=False, columnabsolute:=False) & " * 25.4"
    newtable(7 + geomnum, 14).Value = "mm"
```

Stop code to allow user to input Radius, Area*Mean, Sum of Pixels, and Density data from granulometry results (sorted by radius, high to low)

```
    Stop
```

Set up "Diam" through "Cum. Density" Columns

```
    For i = 3 To radnum + 2
```

Diam column

```
    newtab(i, 2) = "=" & newtable(i, 1).Address(rowabsolute:=False, columnabsolute:=False)
& "*2+1"
```

Diam (mm) column

```
    newtab(i, 3) = "=" & newtable(i, 2).Address(rowabsolute:=False, columnabsolute:=False)
& "*" & newtable(7 + geomnum, 13).Address & ""
```

Normalized Diam column

```
    newtab(i, 4) = "=" & newtable(i, 2).Address(rowabsolute:=False, columnabsolute:=False)
& "/" & newtable(3, 2).Address & ""
```

Cum. Density column

```
    newtab(i, 8) = "=1 - " & newtable(i, 6).Address(rowabsolute:=False,
columnabsolute:=False) & " / " & newtable(2 + radnum, 6).Address & ""
    Next i

    For i = 3 To radnum + 2
    newtable(i, 2).Formula = newtab(i, 2)
    newtable(i, 3).Formula = newtab(i, 3)
    newtable(i, 4).Formula = newtab(i, 4)
    newtable(i, 8).Formula = newtab(i, 8)
    Next i
```

Set up geometric classes

```
    For i = 3 To 2 + geomnum
```

Geometric class labels

```
    newtab(i, 10) = "=" & i & " - 2"
```

Geometric class lower bounds

```
    newtab(i, 13) = "=10 ^ (-1 * " & newtable(i, 10).Address(rowabsolute:=False,
columnabsolute:=False) & " / 10)"
```

```
    Geometric class upper bounds
    If i = 3 Then
    newtab(i, 11) = "=1"
    Else: newtab(i, 11) = "=" & newtable(i - 1, 13).Address(rowabsolute:=False,
columnabsolute:=False) & ""
    End If
    Geometric class upper bounds - pixels
    newtab(i, 12) = "=" & newtable(i, 11).Address(rowabsolute:=False,
columnabsolute:=False) & " * " & newtable(3, 2).Address & ""
    Geometric class lower bounds - pixels
    newtab(i, 14) = "=" & newtable(i, 13).Address(rowabsolute:=False,
columnabsolute:=False) & " * " & newtable(3, 2).Address & ""

    Set up distribution calculations - these commands input formulas
    Sphere transect probabilities
    newtab(i, 15) = "=1 / " & newtable(3, 11).Address & " * (Sqrt(" & newtable(3,
11).Address & " ^ 2 - " & newtable(i, 13).Address(rowabsolute:=False,
columnabsolute:=False) & " ^ 2)- Sqrt(" & newtable(3, 11).Address & " ^ 2 - " & newtable(i,
11).Address(rowabsolute:=False, columnabsolute:=False) & " ^ 2))"
    Alpha values
    newtab(i, 16) = "=alphacalc(" & Range(newtable(3, 15), newtable(2 + geomnum,
15)).Address & "," & newtable(i, 10).Address(rowabsolute:=False, columnabsolute:=False)
& ")"
    Convert cross-section density from linear classes to geometric classes
    newtab(i, 17) = "=NAr(" & Range(newtable(3, 4), newtable(2 + radnum, 4)).Address & ","
& Range(newtable(3, 11), newtable(2 + geomnum, 11)).Address & "," & Range(newtable(3,
7), newtable(2 + radnum, 7)).Address & "," & newtable(i, 10).Address(rowabsolute:=False,
columnabsolute:=False) & ")"
    Calculate the stereological particle density
    newtab(i, 18) = "=volume(" & Range(newtable(3, 17), newtable(2 + geomnum,
17)).Address & "," & Range(newtable(3, 16), newtable(2 + geomnum, 16)).Address & "," &
newtable(4 + geomnum, 12).Address & "," & newtable(i, 10).Address(rowabsolute:=False,
columnabsolute:=False) & ")"
    Adjust for negative values
    newtab(i, 19) = "=negadjust(" & Range(newtable(3, 18), newtable(2 + geomnum,
18)).Address & "," & newtable(i, 10).Address(rowabsolute:=False, columnabsolute:=False)
& ")"
    Accumulate adjusted density values
    newtab(i, 20) = "= " & newtable(i, 19).Address(rowabsolute:=False,
columnabsolute:=False) & "+" & newtable(i + 1, 20).Address(rowabsolute:=False,
columnabsolute:=False) & ""
    Normalize the cumulative distribution to 100%
```

```
    newtab(i, 21) = "= " & newtable(i, 20).Address(rowabsolute:=False,
columnabsolute:=False) & "*1/" & newtable(3, 20).Address & ""
    Scale the pixels to millimeters
    newtab(i, 22) = "= " & newtable(i, 12).Address(rowabsolute:=False,
columnabsolute:=False) & "*" & newtable(7 + geomnum, 13).Address & ""
    Next i

    Output the formulas into the spreadsheet
    For j = 10 To 22
    For i = 3 To 2 + geomnum
    newtable(i, j).Formula = newtab(i, j)
    Next i
    Next j

    Format the entire table
    Range(newtable(3, 1), newtable(2 + radnum, 1)).NumberFormat = "0.0"
    Range(newtable(3, 2), newtable(2 + radnum, 2)).NumberFormat = "0"
    Range(newtable(3, 3), newtable(2 + radnum, 3)).NumberFormat = "0.00"
    Range(newtable(3, 4), newtable(2 + radnum, 4)).NumberFormat = "0.000"
    Range(newtable(3, 5), newtable(2 + radnum, 5)).NumberFormat = "0.0"
    Range(newtable(3, 6), newtable(2 + radnum, 6)).NumberFormat = "0"
    Range(newtable(3, 7), newtable(2 + radnum, 7)).NumberFormat = "0.00%"
    Range(newtable(3, 8), newtable(2 + radnum, 8)).NumberFormat = "0.00%"
    Range(newtable(3, 10), newtable(2 + geomnum, 10)).NumberFormat = "0"
    Range(newtable(3, 11), newtable(2 + geomnum, 11)).NumberFormat = "0.000"
    Range(newtable(3, 12), newtable(2 + geomnum, 12)).NumberFormat = "0.00"
    Range(newtable(3, 13), newtable(2 + geomnum, 13)).NumberFormat = "0.000"
    Range(newtable(3, 14), newtable(2 + geomnum, 14)).NumberFormat = "0.00"
    Range(newtable(3, 15), newtable(2 + geomnum, 15)).NumberFormat = "0.00%"
    Range(newtable(3, 16), newtable(2 + geomnum, 16)).NumberFormat = "0.000"
    Range(newtable(3, 17), newtable(2 + geomnum, 17)).NumberFormat = "0.00%"
    Range(newtable(3, 18), newtable(2 + geomnum, 18)).NumberFormat = "0.00%"
    Range(newtable(3, 19), newtable(2 + geomnum, 19)).NumberFormat = "0.00%"
    Range(newtable(3, 20), newtable(2 + geomnum, 20)).NumberFormat = "0.00%"
    Range(newtable(3, 21), newtable(2 + geomnum, 21)).NumberFormat = "0.00%"
    Range(newtable(3, 22), newtable(2 + geomnum, 22)).NumberFormat = "0.00"
    newtable(4 + geomnum, 12).NumberFormat = "0.000"
    newtable(6 + geomnum, 13).NumberFormat = "0"
    newtable(7 + geomnum, 13).NumberFormat = "0.000"

End Sub
```